



BRNO UNIVERSITY OF TECHNOLOGY

VYSOKÉ UČENÍ TECHNICKÉ V BRNĚ

FACULTY OF MECHANICAL ENGINEERING

FAKULTA STROJNÍHO INŽENÝRSTVÍ

INSTITUTE OF AEROSPACE ENGINEERING

LETECKÝ ÚSTAV

WING FATIGUE SAFE LIFE INVESTIGATION OF SINGLE-ENGINE MULTIPURPOSE AIRCRAFT

VYŠETŘOVÁNÍ BEZPEČNÉHO ÚNAVOVÉHO ŽIVOTA KŘÍDLA VÍCEÚČELOVÉHO JEDNOMOTOROVÉHO TURBOVRTULOVÉHO LETOUNU

MASTER'S THESIS

DIPLOMOVÁ PRÁCE

AUTHOR

AUTOR PRÁCE

Bc. Jan Hubáček

SUPERVISOR

VEDOUCÍ PRÁCE

Ing. Ladislav Chybík

BRNO 2020

Assignment Master's Thesis

Institut: Institute of Aerospace Engineering
Student: **Bc. Jan Hubáček**
Degree program: Mechanical Engineering
Branch: Aircraft Design
Supervisor: **Ing. Ladislav Chybík**
Academic year: 2020/21

As provided for by the Act No. 111/98 Coll. on higher education institutions and the BUT Study and Examination Regulations, the director of the Institute hereby assigns the following topic of Master's Thesis:

Wing fatigue safe life investigation of single-engine multipurpose aircraft

Brief Description:

Thesis deals with critical wing cross section fatigue safe life estimation of single-engine multipurpose turboprop aircraft with STOL performance. Aircraft is supposed to be all-metal truss monoplane with high-wing configuration. Aircraft shall be certified according to FAR 23 regulation. Wing safe life estimation will be done according to methods listed in FAR 23 and advisory circular AC 23-13A.

Master's Thesis goals:

- standards, advisory materials and fatigue approach research
- V-n diagram calculation
- Mission profile estimation
- Load spectra estimation
- Wing load distribution
- Critical cross section stress analysis
- Cumulative damage fatigue life analysis (Palmgren-Miner)

Recommended bibliography:

NIU, M. Ch.-Y. Airframe structural design. 2nd ed. Hong Kong: Hong Kong Conmililit Press Ltd. ISBN 962-7128-09-0.

PILKEY, W. D., PILKEY, D. F., BI, Z. Peterson's stress concentration factors. John Wiley & Sons, 2020.

PÍŠTĚK, A. Pevnost a životnost letadel. 1. vyd. Brno: Vysoké učení technické, 1988.

RŮŽIČKA, M., HANKE, M., ROST, M. Dynamická pevnost a životnost. ČVUT, 1992.

Deadline for submission Master's Thesis is given by the Schedule of the Academic year 2020/21

In Brno,

L. S.

doc. Ing. Jaroslav Juračka, Ph.D.
Director of the Institute

doc. Ing. Jaroslav Katolický, Ph.D.
FME dean

Abstract

The Diploma Thesis deals with fatigue safe-life estimation of critical wing cross-section of an aircraft. The aircraft type is specified as all-metal high-wing strut monoplane. Aircraft is certified under FAR 23 Amendment 23-46 regulations. Wing safe-life estimation is evaluated in respect to methods listed in FAR 23 and its advisory circulars.

The theoretical part of diploma thesis reviews the project bases and literature. It briefly introduces project background, reasons for fatigue life calculation and aircraft subjected to fatigue analysis. Subsequently literature review was focused on requirements of standards, advisory circular documents and research in field of fatigue life.

Second part of the thesis is focused on a computational analysis and a software development. First sub-part of computational analysis includes preparation of input data, including V-n diagram calculation, mission profile estimation, wing load distribution, critical cross-section stress analysis. Then detail analysis of fatigue was evaluated in respect to fatigue characteristics estimation, cumulative damage and fatigue life calculation with defined mission profile, wing safe life estimation.

Abstrakt

Práce se zabývá stanovením bezpečné únavové životnosti křídla. Letadlo, které bylo podrobeno analýze, je vzpěrový hornoplošník celokovové konstrukce. Letadlo je certifikováno na základě předpisu FAR 23 Amendment 23-46. Výpočet bezpečné únavové životnosti musí být proveden v souladu s požadavky předpisu FAR 23 a jeho poradními oběžníky.

Teoretická část práce je věnována hlavně přehledu literatury a představení projektu, kde byla stručně shrnuta jeho historie vzniku. Část přehledu projektu také pojednává o podstatě požadavku na posouzení bezpečné únavové životnosti zadavatelem. V další části byl rovněž proveden rozbor literatury týkající se únavy. Jednalo se zejména o rozbor předpisu FAR 23, jeho poradních oběžníků a obecně literatury vztahující se k únavě jak v letectví, tak v obecném strojírenství.

Druhá část diplomové práce byla zaměřena zejména na výpočetní analýzu a vývoj specializovaného software. Výpočetní část obsahovala zejména přípravu vstupů, včetně obálek zatížení, stanovení typického letu, výpočet zatížení křídla a napjatostní analýza ve vybraných řezech křídla. Z výstupů prvotní analýzy se následně provedl výpočet poškození a životnosti pro daný typový let.

Rozšířený abstrakt

Výpočet bezpečné únavové životnosti křídla je spojen s projektem firmy Praga Avia. Tento projekt byl zaměřen na modernizaci a transfer TC (Type Certificate) Maďarského letounu SMG-92 Turbine Finist. Tento typ letadla konstrukčně vychází z ruského letounu SM-92T. Firma Praga Avia je nyní držitelem TC (Typového certifikátu). Marketingová studie zadavatele ukázala, že zákazníci mají zájem o tento letoun zejména pro provoz zaměřený na seskoky padákem. Na takovém typovém letu však ještě bezpečná únavová životnost nebyla prokazována. Díky tomu vznikl požadavek na její výpočet.

K tomu, aby analýza mohla být provedena, bylo zapotřebí udělat rešerši dostupných materiálů. Rešerše byla rozdělena na tři oblasti. První oblast byla samotná certifikační báze FAR 23 Amendment 23-46 jakožto předpis, podle kterého bylo původní letadlo certifikováno. Tento předpis specifikuje obecné požadavky na únavovou analýzu pro různé části draku a různé přístupy k únavě. Mimo jiné také specifikuje možnost použití přístupu konstrukce s bezpečnou životností (safe-life) pro konstrukci křídla. Tento předpis rovněž doporučuje, pro detailnější požadavky a metodiku posuzování únavové životnosti, oběžník AC23-13A. Oběžník obsahuje mimo jiné spektra pro 8 kategorií letounů, doporučení pro volbu součinitele spolehlivosti a požadavky na výpočet poryvového násobku. Navíc je možné v tomto poradním oběžníku nalézt odkaz na výpočetní program ACE100 s detailně popsanou metodikou výpočtu.

Rozbor literatury pokračoval základním uvedením do problematiky únavy. Byly zde zmíněny základní pojmy jako je popis únavového cyklu, analytický popis Wöhlerových křivek, vliv středních napětí a koncepce lokálních/nominálních napětí. Poté je rozbor literatury zaměřen na oblast únavy v letectví. Zde byly představeny a porovnány běžné únavové přístupy používané k vyhodnocování únavy v letectví (Safe-life, Damage tolerance, Fail-safe). Poté zde byly rozebrány důležité aspekty týkající se analýzy bezpečného únavového života. Zejména aspekty týkající se práce se spektry zatěžování a z nich následné určování poškození.

Výpočet bezpečné únavové životnosti byl rozdělen do několika sekcí. První část byla příprava vstupních dat pro výpočet únavové životnosti. Mezi tato data patří typový let, který byl sestaven dle letové příručky pro návrhový profil provozu pro výsadky parašutistů. Typický let byl rozdělen do 5 fází letu, ve kterých byly stanoveny požadované charakteristiky (výška, rychlost, hmotnost...).

V další části je provedena napjatostní analýza. Nejdříve bylo vypočteno zatížení křídla a jeho průběhy. V této fázi bylo přijato zjednodušení týkající se zanedbání tečných sil, tečných ohybových momentů a kroutícího momentu. Pro tyto složky nebylo možno získat aerodynamická data (nebyla poskytnuta zadavatelem pro účely práce, kvůli utajení). Z provedené analýzy byl přijat předpoklad, že namáhání od ohybu je dominantní složkou namáhání křídla. Dle kritéria maximálního tahového napětí byly zvoleny 4 řezy na křídle. Nakonec byl vybrán, dle dříve zmíněných kritérií, řez u vnitřního konce frézovaného dílu vyztužujícího spoj vzpěry a křídla. Zde bylo analyzováno nejvyšší napětí pro případ 1g zatěžování. K tomuto napětí bylo vypočteno i napětí od pozemního zatížení, jakožto nutný vstup do výpočtu.

Další část práce se věnovala přípravě nástrojů pro výpočet poškození. Z důvodů limitovaných výpočtových možností v stávajícího programu ACE 100 bylo nutné připravit si vlastní výpočtový nástroj. Hlavním důvodem pro vytvoření vlastního software byla možnost rozdělit let do 5 fází, což má za následek přiblížení výsledků realitě. Tento soft-

ware byl zpětně validován programem ACE100. Pro validaci byl použit vzorový příklad uvedený v dokumentaci programu. Vývoj výpočetního software byl proveden v prostředí Excel a Python. Po validaci programu bylo možné let rozdělit do 5 fází, což bylo provedeno s daty jejichž vážený průměr byl stejný jako vzorové hodnoty pro ukázkový příklad v ACE100. Díky tomu mohlo být toto vylepšení verifikováno.

Po všech těchto přípravách bylo možné vypočítat bezpečnou únavovou životnost v kritickém řezu. Na základě vstupních dat byl typový let doplněn o manévrové a poryvové násobky v každé fázi. Data poté byla dosazena do výpočetního software a stanovena bezpečná únavová životnost. Jako pokračování projektu se počítá s provedením únavové zkoušky. Změnou součinitele spolehlivosti (jako součinitel pro zkoušky) proto byla odhadnuta doba trvání zkoušky pro tento typový let.

Keywords

fatigue, safe-life, wing, strut, turboprop, FAR 23, AC23-13A, ACE100, AFS-120-73-2, damage calculation, spectra, SMG-92, Finist

Klíčová slova

únava, bezpečná únavová životnost, křídlo, vzpěra, turbovrtulový, FAR 23, AC23-13A, ACE100, AFS-120-73-2, výpočet poškození, spektra zatížení, SMG-92, Finist

Bibliography

HUBÁČEK, Jan. *Vyšetřování bezpečného únavového života křídla víceúčelového jednomotorového turbovrtulového letounu*. Brno, 2021. Dostupné také z: Available: <https://www.vutbr.cz/studenti/zav-prace/detail/132090>. Diplomová práce. Vysoké učení technické v Brně, Fakulta strojního inženýrství, Letecký ústav. Vedoucí práce Ladislav Chybík.

Declaration of authenticity

I declare that I have elaborated my master's thesis on the theme of "Wing fatigue safe-life investigation of single-engine multipurpose aircraft" independently with the use of technical literature and other sources of information which are all quoted in the thesis and detailed in the list of literature at the end of the thesis.

In Brno on May 21, 2021

Jan Hubáček

Acknowledgement

I would like to thank my family for the support. I would like to express special thanks to my supervisor Ing. Ladislav Chybík for his guidance and support, Ing. Petr Augustýn PhD. and Ing. Tomáš Bělohradský for their assistance.

TABLE OF CONTENTS

1	Introduction	14
1.1	About plane	14
1.2	TCDS transfer	16
1.3	Plane parameters	16
2	Requirements of standards	18
2.1	FAR PART 23, Amendment 23-46	18
2.2	AC23-13A	19
2.2.1	Load spectra estimation and classification	19
2.2.2	Stress analysis	19
2.2.3	Fatigue analysis	20
2.2.4	Outputs of fatigue analysis	20
2.2.5	Links to the supplementary material	20
2.3	ACE100	20
3	Fatigue theory	21
3.1	Stress cycle parameters	21
3.2	S-N curves	22
3.2.1	Analytic description of S-N curves	23
3.3	Factors influencing fatigue life	24
3.3.1	Mean stress	24
3.3.2	Zones according to the notch quantity	27
3.3.3	Surface treatment influence	29
3.3.4	The part design influence	30
3.4	Palmgren-Miner rule	31
3.5	Fatigue life analysis approaches according to notch stress factor evaluation	34
3.5.1	Concept of nominal stresses	34
3.5.2	Net cross-section stress	35
3.5.3	Gross cross-section stress	36
3.5.4	Concept of local stresses	37
4	Fatigue in aerospace engineering	39
4.1	Important aerospace fatigue terms	39
4.2	Fatigue life analysis approaches according to damage evaluation	40
4.2.1	Safe-life concept	41
4.2.2	Damage tolerant concept	41
4.2.3	Fail safe concept	41
4.3	Safe-life workflow	43
4.4	Load spectra	43
4.4.1	Classification according to load type	44
5	Inputs for fatigue calculation	50
5.1	Mission profile	50
5.1.1	Parachutist dropping	50
5.2	V-n diagram calculation	52
5.2.1	Design speeds	53
5.2.2	Limit maneuvering load factors	54
5.2.3	Gust load factors	54

5.2.4	Service load envelope	56
5.3	Stress analysis	58
5.3.1	Wing freebody diagram	58
5.3.2	Load case 1: Flight loads 1g	59
5.3.3	Load case 2: Ground loads	64
5.3.4	Critical cross-section choice	64
5.3.5	Critical cross-section 1	66
5.3.6	Critical cross-section 2	68
5.3.7	Critical cross-section 3	69
5.3.8	Critical cross-section 4	70
5.3.9	Stress analysis conclusion	70
6	Damage calculation software development	72
6.1	Used spectra	72
6.2	Used S-N curves	73
6.2.1	Data Sheet E.02.01 S-N curve	73
6.2.2	Oding S-N curves	73
6.3	First iteration	74
6.3.1	Spectra interpolation	74
6.3.2	Gust and Maneuver	75
6.3.3	Taxi	79
6.3.4	Impact and rebound	80
6.3.5	GAG cycle	82
6.3.6	Damage calculation	84
6.4	Second iteration	85
6.4.1	Gusts and Manoeuvres	88
6.4.2	Taxi, landing impact and rebound	89
6.4.3	GAG cycle	89
6.4.4	Damage calculation	92
7	SMG-92 Safe-life estimation	93
7.1	Gust load factor	93
7.2	Mission profile completion	93
7.3	Damage calculation	94
8	Conclusion	97
9	List of shortcuts and symbols	102
	List of shortcuts and symbols	102
	List of Figures	103
	List of Tables	106

1 Introduction

Assignment of fatigue life investigation came out from project of SMG-92 Turbine Finist Type Certificate transfer. New TC holder is planning to start modernisation of plane, therefore one of partial goals in this project is to determine safe-life of plane. The project will be introduced by brief history. Details about project will be also mentioned.

1.1 About plane

SM-92 Finist was designed by Russian company Technoavia in 1992 by chief designer V. P. Kondratev, manufactured and first prototype flew on 28th of December 1993. Main concern of the whole project was to design simple and technologically uncomplicated plane. This plane should replace retiring Antonov An-2. Perspective plane was quickly outperformed due to low power of M-14P (265 kW) nine-cylinder radial engine.

Engine was the main reason for decision to begin modernisation of the plane. Modernisation included most important upgrade from M-14P radial engine to M601F turboprop engine. This model was called SM-92T, modernised plane can be seen in fig. 1.2.



Figure 1.1: Military version of SM-92 with radial engine [29]



Figure 1.2: SM-92T in cargo version[33]

SM-92T is suitable for operation from almost any runway. This plane can carry enough payload and hangar is not required. It has also descent operating range of 1600 km (in flight level 3000 m). The plane can be reorganised for several roles, namely:

- Ski version
- Ski version with wheels
- Float version
- Para version
- Reconnaissance aircraft
- Agricultural version
- Medical version
- Cargo version
- Glider towing version
- Forest rescue version

On the basis of SM-92T was built and certified aircraft called SMG-92 Turbine Finist in Hungary. This plane is subject of next analysis. Therefore is important to give some overview of history of this project.

1.2 TCDS transfer

The Type Certificate of SMG-92 Turbine Finist as well as project documentation and intellectual properties was purchased by Czech company Praga Avia, located in Hradec Kralove. The first step of the new TC holder is to get EASA certificate important for the project future. Praga Avia company (TC holder) recognises large potential in modernisation of such a plane, because the planes of this category should be replaced with newer planes like SMG-92 Turbine Finist with low maintenance costs.[33]

Hungarian SMG-92 Turbine Finist was designed and certified under FAR-23 right before EASA association was founded. Hungarian version was equipped with M601D powerplant in difference with Russian version (M601F). Certification of plane in EU (European union) makes the plane especially suitable for TCDS transfer. Therefore it is possible to apply for "grandfathered" design approval which covers all planes certified European countries before EASA foundation.[37] Modernisation Goals are in terms of powerplant unit replacement, avionics replacement meeting current standards. New TC holder recognises a large potential in use of this aircraft in role of parachute dropping. For this type of mission profile was not yet determined safe-life. Therefore it is necessary to determine fatigue safe-life of parachutist dropping operation. Seats are rearranged into configuration for 10 parachutists on board in this configuration. Mission profile is characterised with short duration which has significant impact to plane safe-life. Radical mass change (770 kg) causes plane to be more vulnerable to the gust loads and contributes to decrease in safe-life of plane.



Figure 1.3: Para version of SMG-92 in operation [36]

1.3 Plane parameters

SMG-92 Turbine Finist was designed as high-wing monoplane with taildragger landing gear configuration. Large tires enables plane to launch from various types of runways. Special attention is paid to the simplicity of plane construction for reason of maintenance. Plane is all-metal construction with majority of aluminium alloys. Plane is equipped with advanced flight navigation equipment, Glass cockpit. Could be equipped with anti-icing system and aircraft oxygen system etc. SMG-92 Turbine Finist with its rectangular wing

is also designed to be fault tolerant, with favourable stall characteristics. As multipurpose aircraft it could serve in large variety of flight missions in large variety of climates practically in non-stop regime.

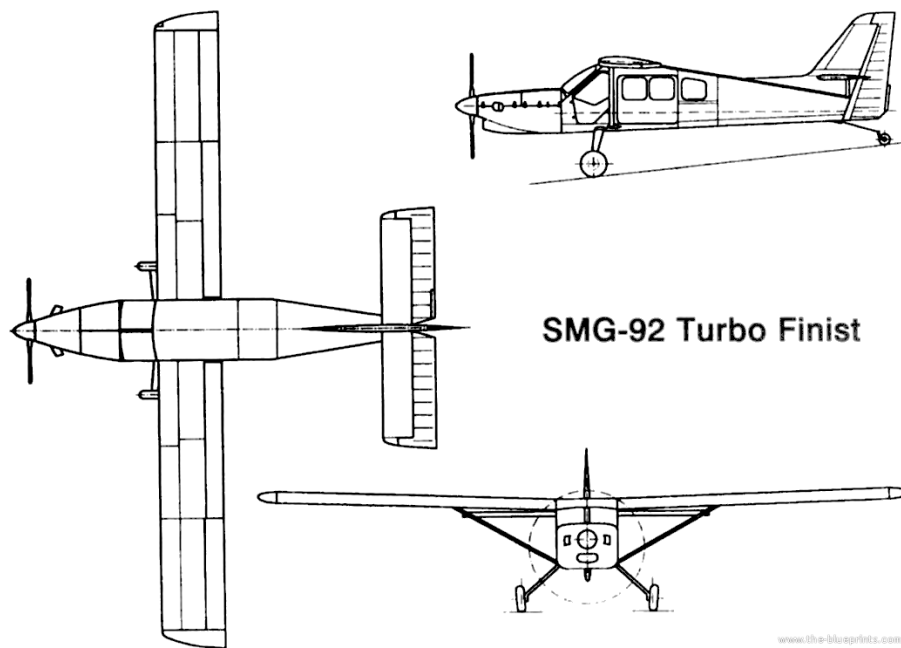


Figure 1.4: 3 view drawing of SMG-92 Turbine Finist [34]

Table 1.1: Technical data [24]

Airworthiness Category:	-	Normal, Utility
Airworthiness Requirements:	-	FAR Part 23 Amdt. 23-46
Power plant	-	M601D
Propeller	-	AVIA V508D
Aircraft length	m	9.974
Wingspan	m	14.96
Wing area	m ²	20
Max. takeoff weight	kg	2700
Max. fuel capacity	l/kg	1220/976
Max. cruise speed in level 3000 m	km/h	315
Number of passengers	-	10
Climb (at sea level)	m/s	8
Stall speed (MTOW, landing configuration)	km/h	105
Fuel consumption in 3000 m at cruise speed	kg/km	0.43
Range in level 3000 m at cruise speed (220-230 km/h)	km	1600
Range in level 3000 m at cruise speed (315 km/h)	km	1100
Max. range in level 6000 m	km	2100
Max. endurance	h	7.5
Max. airport level	m	2000
Service ceiling	m	8000
Standard conditions landing run	m	350
MTOW landing run	m	500

2 Requirements of standards

Analysed aircraft has FAR Part 23 Amendment 23-46 certification base. Fatigue analysis and its procedures are briefly concluded in:

2.1 FAR PART 23, Amendment 23-46

Direct citations will be applied in chapters below for reason of precise certification requirements formulation. Sections with this citations will be written with italic script. In [28] is fatigue evaluation policy mentioned in parts:

1. **Sec. 23.571 Metallic pressurised cabin structures**

Certified aircraft has not cabin pressurisation and fuselage was not defined as objective of fatigue analysis. Requirement is therefore not applicable.

2. **Sec. 23.572 Metallic wing, empennage and associated structures**

This part is key part for purposes of thesis. Such structure can be certified with approaches:

- *fatigue strength investigation by tests or analysis supported by test evidence*
- *fail-safe strength with loads multiplied with factor of 1.15*
- *damage tolerance evaluation*
- *include load spectra*
- *account for any significant effects due to the mutual influence of aerodynamic surfaces*
- *consider slipstream propeller effects, slipstream loading and buffet from vortex impingements.*

3. **Sec. 23.573 Damage tolerance and fatigue evaluation of structure**

This section is not so important, because analysed wing structure is not made of composites and does not require damage tolerant analysis required. Therefore it will be followed only with brief list of referenced topics:

- damage tolerant methods for testing of composite structures with specified critical structural elements location on airframe
- damage tolerant methods for testing of metallic airframe components

4. **Sec. 23.574 Metallic damage tolerance and fatigue evaluation of commuter category aeroplanes**

This section is also not applicable, because analysed plane is certified only in Normal and Utility category.

5. **Sec. 23.575 Inspections and other procedures**

This chapter specifies means of inspection methods required by Sec. 23.571, 23.572, 23.573 or 23.574.

6. **Sec. 23.627 - Fatigue strength.**

The structure must be designed, as far as practicable, to avoid points of stress concentration where variable stresses above the fatigue limit are likely to occur in normal

service.

This section represents ideal model of fatigue proof structure. Every airplane will have spots with higher stress concentration, in practise we can only reduce number of stress concentrators critical for reaching desired life of structure.

FAR regulation includes links to advisory circular in sections:

1. A fatigue strength evaluation, more commonly known as a safe-life evaluation. See § 23.571(a) for pressurized cabin and § 23.572(a)(1) for wing, empennage, and associated structure. (49/29/05 AC 23-13A)
2. A fail-safe strength evaluation. See § 23.571(b) for pressurized cabin and § 23.572(a)(2) for wing, empennage, and associated structure.
3. A damage tolerance evaluation. See § 23.573(b) and § 23.571(c) for pressurized cabin and § 23.572(a)(3) for wing, empennage, and associated structure.

2.2 AC23-13A

Advisory circular [30] provides information about fatigue evaluation of metallic structures for normal, utility and commuter category airplanes. It covers also small airplane fatigue regulations, safe-life fatigue evaluation, fail-safe design rotorburst requirements flight with known cracks and damage tolerance which also includes links to FAR 25 regulations. Further direct citations of [30] are written in *italic*. This advisory circular also defines most of methods for FAR 23 plane fatigue certification, mainly methods listed below.

2.2.1 Load spectra estimation and classification

Load spectra are sequence of loading, which are measured in real flight conditions and processed by some statistical methods (Rainflow counting, Level crossing counting). Evaluated flight conditions consists mainly of:

- *operational loads*
- *gust loads*
- *landing impact loads*
- *taxi loads*
- *GAG cycle loads*
- *vibrations*
- *propeller slipstream effect etc.*

2.2.2 Stress analysis

Which should include:

- *Complete structural analysis with consideration and evaluation (K_t concept) of stress concentrations based on gross stress levels.*
- *Analysis should be especially focused on joints, fittings (eccentrically loads, bearing, bypass stress), corrosion and extreme thermal environments*

2.2.3 Fatigue analysis

Analysis is supported by $S - N$ data and component testing with ensured similarity of structure. In this phase is calculated damage from the load spectra.

2.2.4 Outputs of fatigue analysis

Determination of safe replacement times this part includes reliability estimation with scatter factor concept.

Guide for maintenance which concerns inspection intervals, inspection thresholds and methods. [30]

2.2.5 Links to the supplementary material

1. FAA Report No. ACE-100-01, Fatigue Evaluation of Empennage, Forward Wing and Winglets/Tip Fins on Part 23 Airplanes, dated February 15, 1994.
This report is especially useful for fatigue damage calculation. It includes detailed calculation description guide to ACE100 computer program listed below.
2. User's Instructions for Computer Program to Calculate Fatigue Safe-Life (Unfactored) for Small Airplanes, dated March 1996.

2.3 ACE100

Advisory circular [30] recommends ACE 100 software. Program was developed by FAA in Fortran language in MS-DOS environment to accelerate design and manufacture process. ACE 100 was used as a reference to verify results obtained in calculation of safe-life in this thesis. Output is in structured tables format, see in fig 2.1. Output format is relatively simple to plot and verify along with custom calculated values. Program is supplied with guidance materials ACE100-1 which are perfect guide for calculation procedure.

```

0.65      .155E+00
0.675 3051. -4520. .126E+00 .133E+10 .954E-10
0.70      .285E-01
0.725 3277. -4520. .235E-01 .927E+09 .253E-10
0.75      .500E-02

TAXI DAMAGE .... .718E-06/1000 landings
<0x0c>

GUST DAMAGE CALCULATION

Date: 23-12-2021

a(n)/    a(n)/    Cum Freq    Cum Freq    a(n)/    Freq per    Freq Per
a(n)LLF  a(n)LLF  Per n.m.   Per n.m.   a(n)LLF  n.m.        Hour
(+)      (+)      (+)        (-)        (-)      (n)
(Ave)

0.01      .327E+01
0.030     .218E+01  0.030     .181E+01   .269E+03
0.05      .146E+01  .878E+00  0.071     .926E+00   .138E+03
0.075     .530E+00  .322E+00  0.123     .335E+00   .497E+02
0.10      .195E+00  .119E+00  0.164     .123E+00   .183E+02
0.125     .119E+00  0.164     .123E+00   .183E+02
0.15      .119E+00  0.164     .123E+00   .183E+02
0.175     .119E+00  0.164     .123E+00   .183E+02

```

Figure 2.1: Example of ACE100 calculation output

3 Fatigue theory

To satisfy requirements of standards it is important to understand theory and approaches used in fatigue calculations. Fatigue is a time depended process of material degradation under the cyclic load exposure.[7] This process can be further described with following parameters below, life influencing factors and generally used fatigue life calculation approaches.

3.1 Stress cycle parameters

Stress cycle is basic characteristics of fatigue loading. It is supposed that the stress cycle has harmonic character(see in fig. 3.1). Stress cycle is described with following parameters.[16] According to fatigue ratio stress cycles can be sorted into categories presented in fig. 3.2.

Stress amplitude

$$\sigma_a = \frac{\sigma_{max} - \sigma_{min}}{2}$$

Mean Stress

$$\sigma_m = \frac{\sigma_{max} + \sigma_{min}}{2}$$

Fatigue ratio

$$R = \frac{\sigma_{min}}{\sigma_{max}}$$

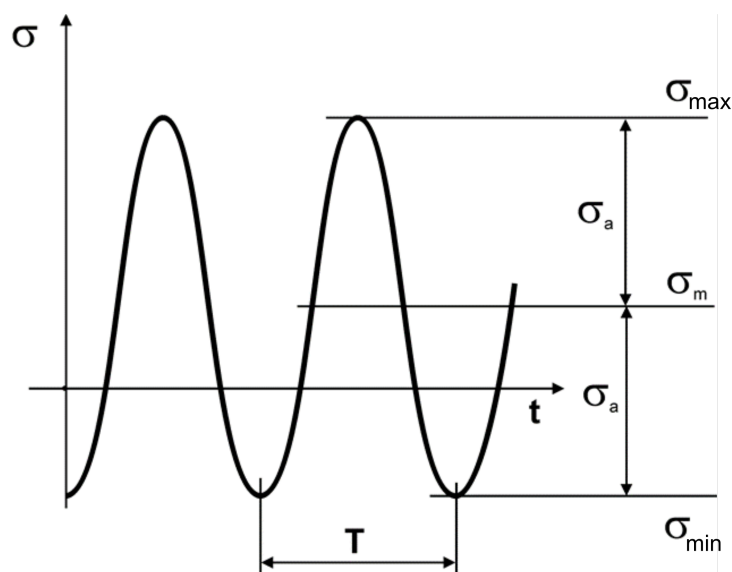


Figure 3.1: Shape of stress cycle[1]

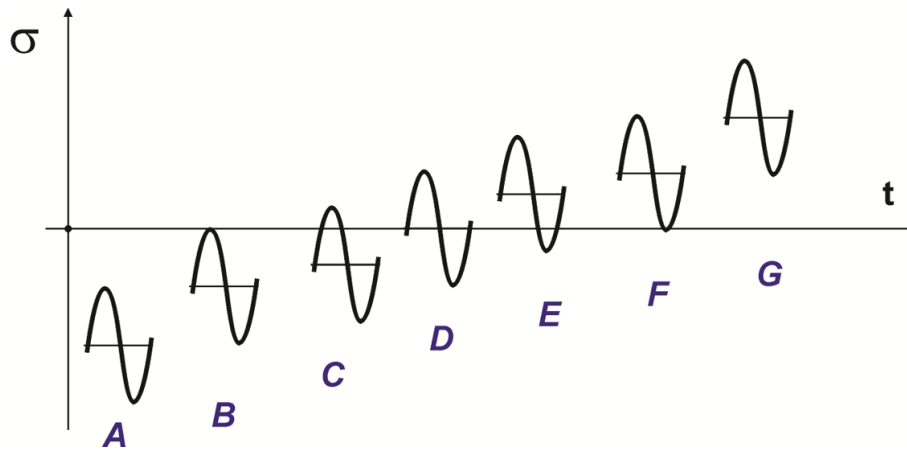


Figure 3.2: Cycles sorted according to fatigue ration

Where:

$R \in (1, -\infty)$ Compression-Compression

$R = -\infty$ Pulsating in compression

$R \in (-\infty, -1)$ Asymmetric alternating (mean stress in compression)

$R = -1$ Alternating symmetric

$R \in (-1, 0)$ Asymmetric alternating (mean stress in tension)

$R = 0$ Pulsating in tension

$R \in (0, 1)$ Tension-Tension

3.2 S-N curves

S-N curve (dependence of stress amplitude S on number of cycle to failure N) is characteristic of material in terms of fatigue strength. Main parameters of this dependence are endurance limit and stages of fatigue life Low cycle fatigue, High cycle fatigue, Finite and Infinite life [12] as shown in fig. 3.3.

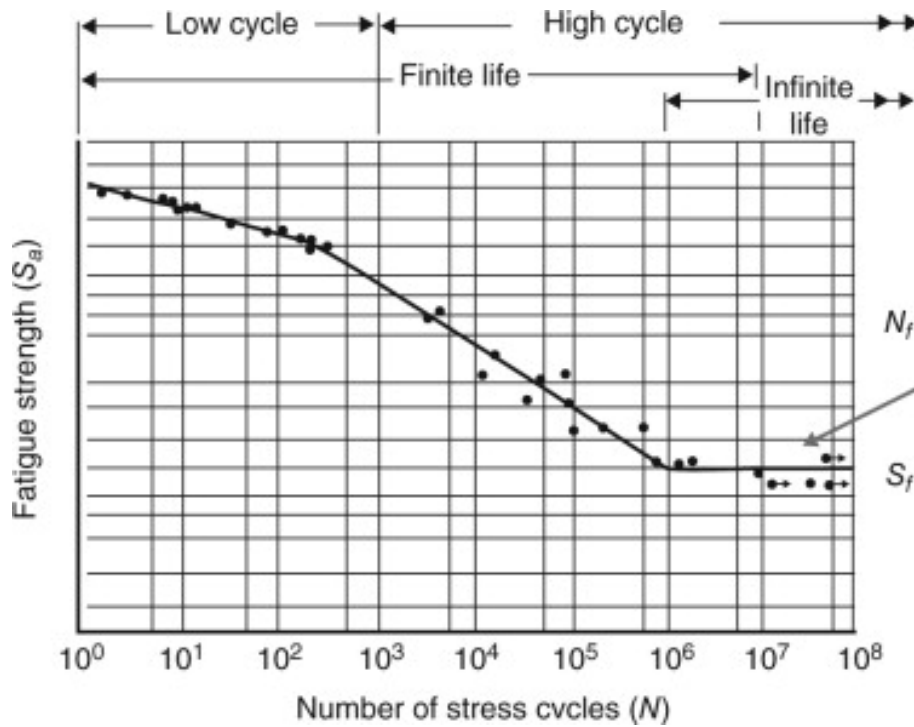


Figure 3.3: Steel S-N curve in semi-log coordinates [12]

Materials such as steels are characterised for its clearly visible endurance limit. On the other hand aluminum alloys, frequently used in aerospace, has no endurance limit, see in fig. 3.4.[20]

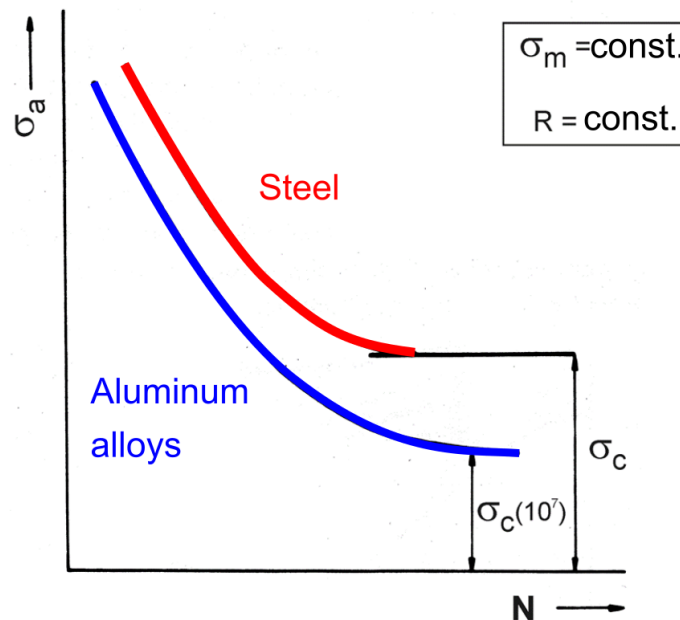


Figure 3.4: Comparison between aluminum alloys and steel S-N curve in cartesian coordinates[1]

3.2.1 Analytic description of S-N curves

S-N curve are usually plotted in semi-log scale. Due to semi-log scale is possible to obtain S-N curve piecewise linear description (in semi-log coordinates). Analytic description of curve is obtained by regression of experimental data, curve for low cycle fatigue is then

described as follows in eqn. (3.1).[20]

$$\sigma_a^w \cdot N = C \quad (3.1)$$

Where:

σ_a Stress amplitude[MPa]

w and C Constants describing curve [-]

N Number of cycles [-]

Another more exact description of curve is then:

$$(\sigma_a - \sigma_c)^b \cdot (N - A) = C \quad (3.2)$$

A,b,C, σ_c Constants describing curve [-]

Another usual description of S-N curve could be expressed in number of half cycles to failure:

$$\sigma_a = \sigma'_f \cdot (2 \cdot N)^2 \quad (3.3)$$

Where:

σ'_f Fatigue strength coefficient [-]

b Fatigue curve parameter [-]

3.3 Factors influencing fatigue life

Parts which are subjected to fatigue will always have some kind of imperfections (surface roughness, notches etc.). It is practically impossible to manufacture a part without such imperfections. Similarly, the character of part loading is not always precisely describable, therefore there are methods compensating uncertainty in load description.

3.3.1 Mean stress

Most of fatigue curves are represented by $\sigma_a = f(N)$. This is valid only for constant mean stress. If the curve is used for different mean stress values, interaction between mean stress and stress amplitude have to be quantified and values have to be corrected. In practice with increasing mean stress value, stress amplitude decreases, which results in same number of cycles to failure. Several criteria are available for taking the influence into account. [16]

Haigh's diagram

Haigh's diagram is one of the most popular ways of visualising the impact of mean stress on fatigue life. Dependence between stress amplitude and mean stress values is shown in Haigh's diagram, see fig. 3.5. Load paths are visualised as red lines with slope equal to Fatigue ratio (fatigue ratio magnitude is noted in fig. 3.5). Loading criteria are plotted as blue and black lines which limits the green loading envelope. Criteria could be also ellipse or a parabola in fig. 3.8.[21] For construction of such a diagram more than 300 specimen results have to be used to ensure rigorous results for such. That is for the entire aerospace construction nearly impossible.

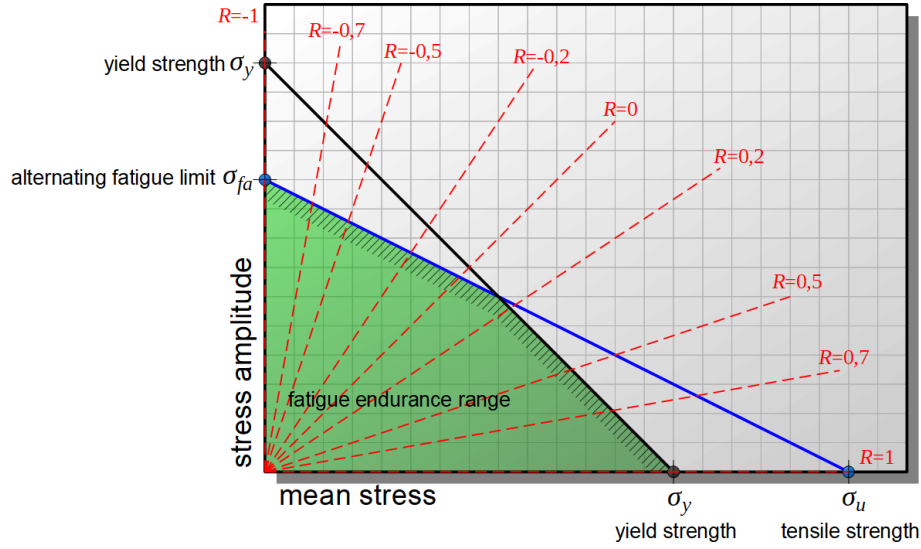


Figure 3.5: Haigh diagram [26]

There are several criteria mentioned below:

1. **R.A.E. correction** - this correction was developed in connection with R.A.E. measured S-N curves which is described with equation:

$$\sigma_a = 10,3 \cdot \left(1 + \frac{1000}{\sqrt{N+B}}\right) \quad (3.4)$$

$$\text{where } B = \left(\frac{1000}{\frac{\sigma_p - \sigma_m}{10,3} - 1}\right)^2$$

These curves are measured with mean stress $\sigma_m = 90 \text{ MPa}$. Number of cycles to the failure can be corrected as:

$$N_m = N \cdot \frac{90}{\sigma_m} \quad (3.5)$$

2. **Oding correction** - this type of correction is more universal. It assumes every cycle to be converted into pulsating cycle with following formulas:

- (a) For values $\sigma_m \geq 0$

$$\sigma_{puls} = \sqrt{2 \cdot \sigma_a \cdot (\sigma_a + \sigma_m)} \quad (3.6)$$

- (b) For values $\sigma_m \in \langle 0, -2.857 \sigma_a \rangle$

$$\sigma_{puls} = \sqrt{2 \cdot \sigma'_a \cdot (\sigma'_a + |\sigma_m|)} \quad (3.7)$$

Where σ'_a is:

$$\sigma'_a = \sigma_a - |0.35 \cdot \sigma_m| \quad (3.8)$$

- (c) For values $\sigma_m < -2.857 \cdot \sigma_a$

$$\sigma_{puls} = 0 \quad (3.9)$$

Criterion is commonly used with S-N curves from [16] in shape eg.:

$$\sigma_{puls}^4 \cdot N = 8,157 \cdot 10^{13} \quad (3.10)$$

This type of S-N curve can be seen in fig. 3.6

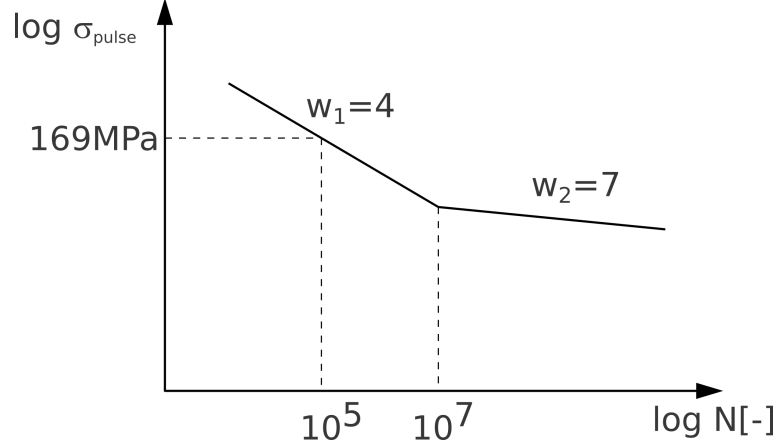


Figure 3.6: Example curve material for D16 TC [16]

3. **Goodman criterion** - is commonly used criterion. It is advantageous for its simplicity of construction and easy feedback control. This criterion is defined with linear dependence curve.

$$\sigma_a = \left(1 - \frac{\sigma_m}{R_m}\right) \cdot \sigma_{a,0} \quad (3.11)$$

The limit criterion is defined by endurance limit and ultimate strength which can be seen in fig. 3.8

4. **Gerber criterion** - is represented with quadratic dependence between mean stress and stress amplitude. Quadratic dependence is used for better correlation with sample test results. Gerber criterion is given in form of parabolic dependence.

$$\sigma_a = \left(1 - \frac{\sigma_m}{R_m}\right)^2 \cdot \sigma_{a,0} \quad (3.12)$$

Graphical representation in Haigh's diagram can be seen in fig. 3.8.

5. **Solderberg criterion** - is one of the most conservative criterion due limitation with respect to yield strength as one of the limit points of limit line. Similarly to Gerber line (resp. criterion) Solderberg criterion is simply represented with line:

$$\sigma_a = \left(1 - \frac{\sigma_m}{R_e}\right) \cdot \sigma_{a,0} \quad (3.13)$$

Where:

R_e Yield strength

R_m Ultimate strength

σ_a Stress amplitude

$\sigma_{a,0}$ Stress amplitude of cycle where $\sigma_m = 0$

R_e Yield strength
 R_m Ultimate strength

Transformation from $\sigma_{a,0} \rightarrow \sigma_a$ is shown in fig. 3.7.

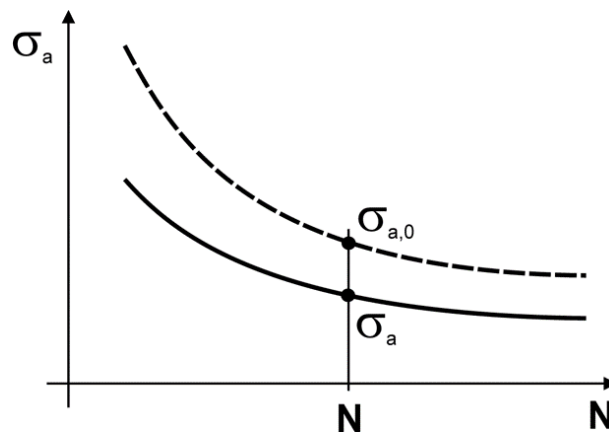


Figure 3.7: Transformation $\sigma_{a,0} \rightarrow \sigma_a$ [1]

fig. 3.8 shows Oding, Goodman, Gerber, Solderberg criteria for both negative and positive mean stress values. [1]

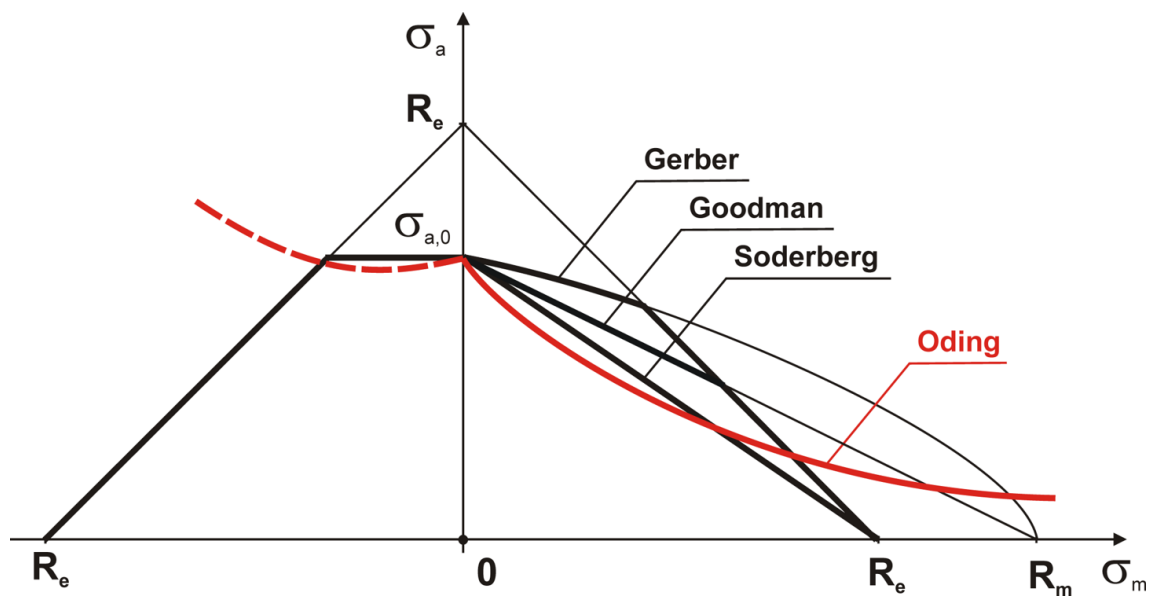


Figure 3.8: Previously mentioned criteria in negative mean stress values[1]

3.3.2 Zones according to the notch quantity

According to [16] three types of notch quality are chosen for easier determination of critical cross-section. Important nomenclature is:

Regular zone - with fatigue crack sources that couldn't be eliminated (e.g. skin contacts with load distributing parts in longitudinal direction).

Nonregular zone - parts with transverse contacts and skin cutouts.

- **Zone I**

This zone includes spot welded, riveted or free stringers and flanges. Only load in normal direction is permitted.

- **Zone II**

Skin regular zones with stringers including connected ribs, bulkheads and places see fig 3.9 in construction with stringers connected to the skin with screws see fig 3.10.

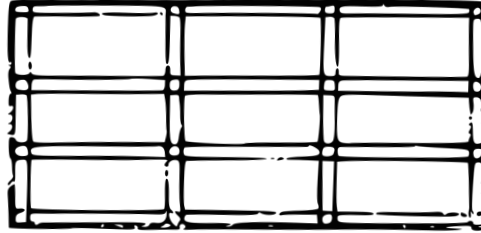


Figure 3.9: Regular zone

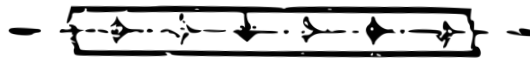


Figure 3.10: Free holes concentration

- **Zone III**

- Skin sheets connection
- Flange connection, see fig. 3.11
- places which are distributing greater torsion or lumped loads (engine nacelles, landing gear etc.) to the regular zones
- openings in skin, possible openings in skin with reinforcement see fig. 3.12

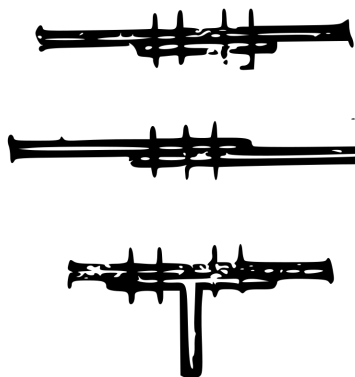


Figure 3.11: Skin connections

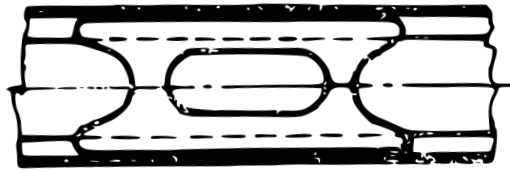


Figure 3.12: Non-regular zone with reinforcement

3.3.3 Surface treatment influence

Shot peening is mechanical surface treatment process. It is based on shooting of metal balls against treated surface. The technology leads to significant increase of endurance limit. It is usable for parts with complex geometry. The influence can be seen in fig. 3.13

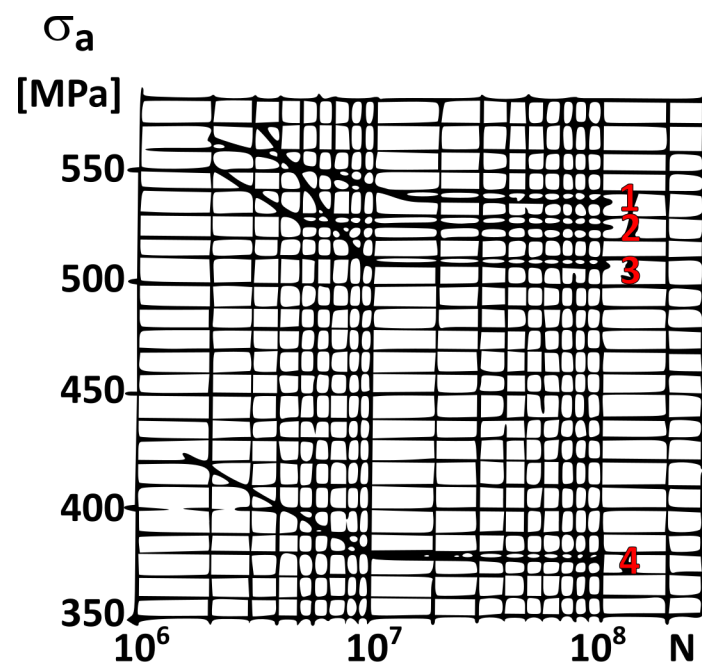


Figure 3.13: Influence of shot peening on part made out of 30CHGSNA steel (Curves represent: 1. polishing+shot peening, 2. machining finishing pass, 3. polishing, 4. machining finishing pass)[8]

Deep rolling mechanical surface treatment method of introducing residual compression stresses into material and increase fatigue life.

Cementation leads to significant decrease in endurance limit inspite of increase in static strength.

Nitriding has beneficial influence on fatigue life, process leads to increase of compression surface stresses in order of 1000 MPa. In case of high carbon steels nitriding leads to reduction endurance limit.

Galvanization especially chrome, cadmium and nickel coating reduces endurance limit up to 40 %

Anodizing of any kind has unfavourable influence on fatigue life of part. It leads to reduction of endurance limit as can be seen in fig. 3.14 [8]

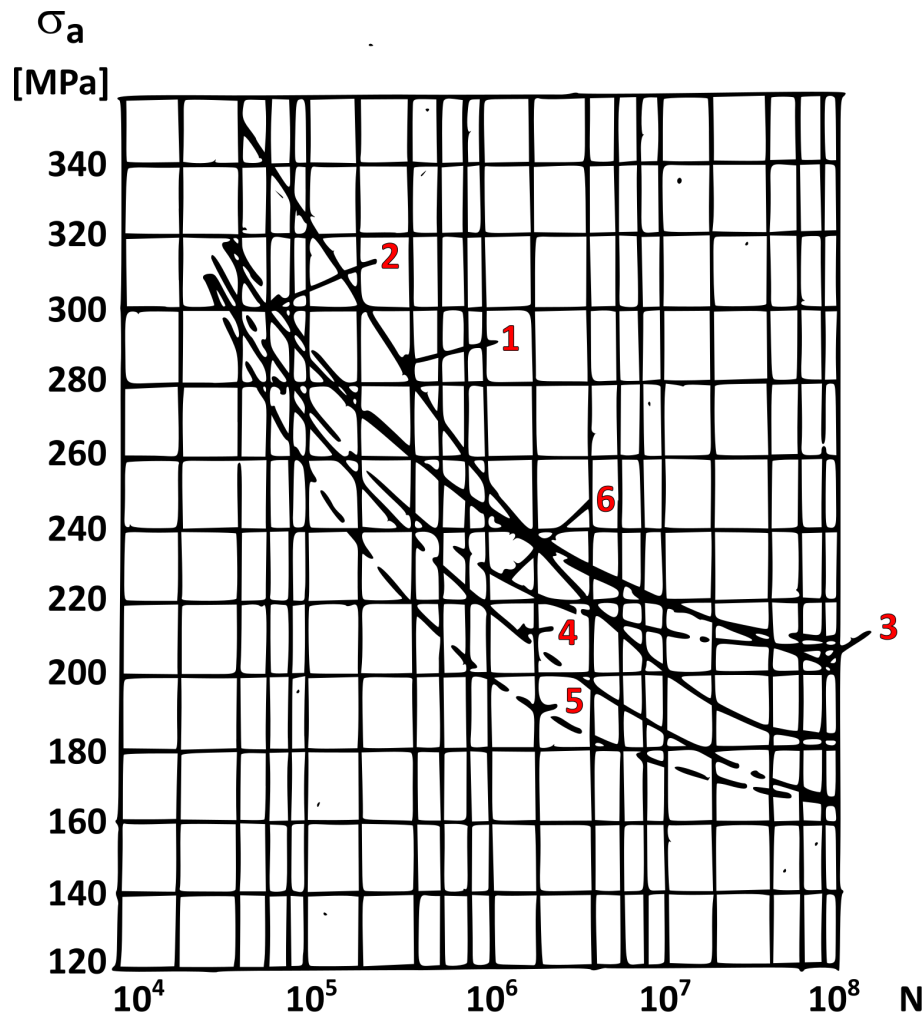


Figure 3.14: Influence of anodizing on endurance limit. (Curves represent: 1. machining and polishing 2. 10%NaOH anodisation, 3. $H_2SO_4 + HF$ anodisation, 4. $H_2SO_4 + NaF$ anodisation, 5. $H_3PO_4 + HF$ anodisation, 6. 20%NaOH anodisation)[8]

3.3.4 The part design influence

For the aircraft structure design it is postulate to get avoid of notches, refer to [28]. It is not possible to completely fulfil this criterion, on the other hand it is important to adapt design to reduce damage caused by notch. [28]

One of many ways to reduce damage caused by notch is to prevent superposition of stress concentrations, example can be seen in fig. 3.15.

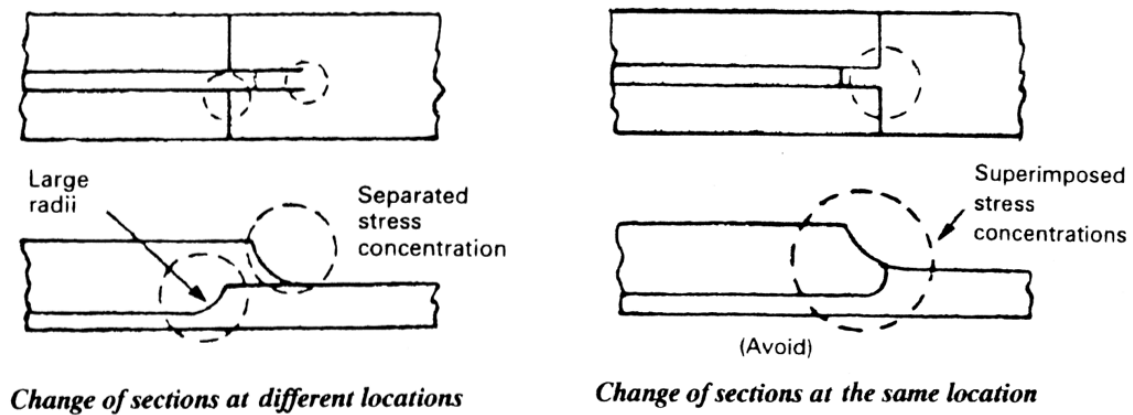


Figure 3.15: Difference of notch concentration[15]

Other possible way of stress concentration reduction is to enlarge notch radius. Comparison of stress distribution can be seen in fig. 3.16.

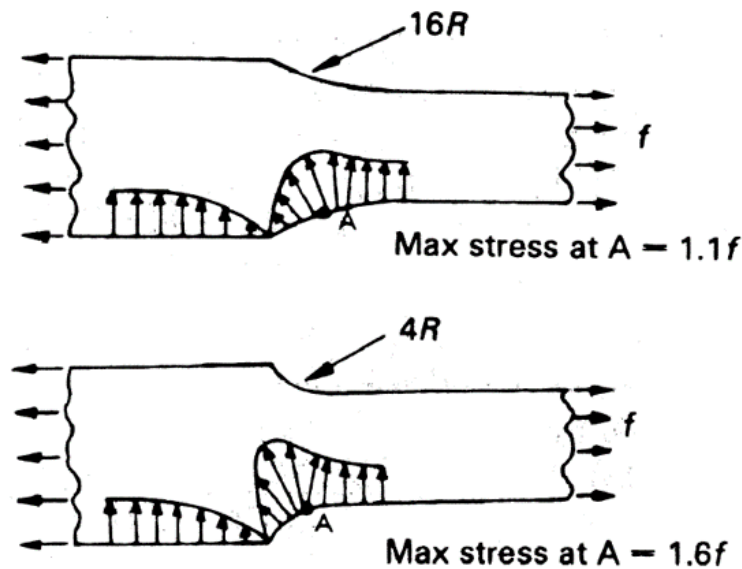


Figure 3.16: Influence of notch radius on stress concentration[15]

3.4 Palmgren-Miner rule

Palmgren-Miner rule is a simplest way to calculate cumulative damage (damage caused by several different stress levels). Particular damage is defined as:

$$d = \frac{n_i}{N_i} \quad (3.14)$$

d particular damage

n_i number of cycles on certain stress level

N_i Number of cycles to failure

Cumulative damage caused by operational loads could be expressed as sum of discrete damages:

$$D = \sum_{i=1}^n \frac{n_i}{N_i} \quad (3.15)$$

D cumulative damage

n_i number of cycles on certain stress level

N_i Number of cycles to failure

Palmgren-Miner rule is the easiest but not the most reliable rule used in damage level determination. Problem is in particular multiple stress level damage calculation and nonlinearities included in cumulative damage summation, nonlinearities can be seen in fig. 3.17.[20]

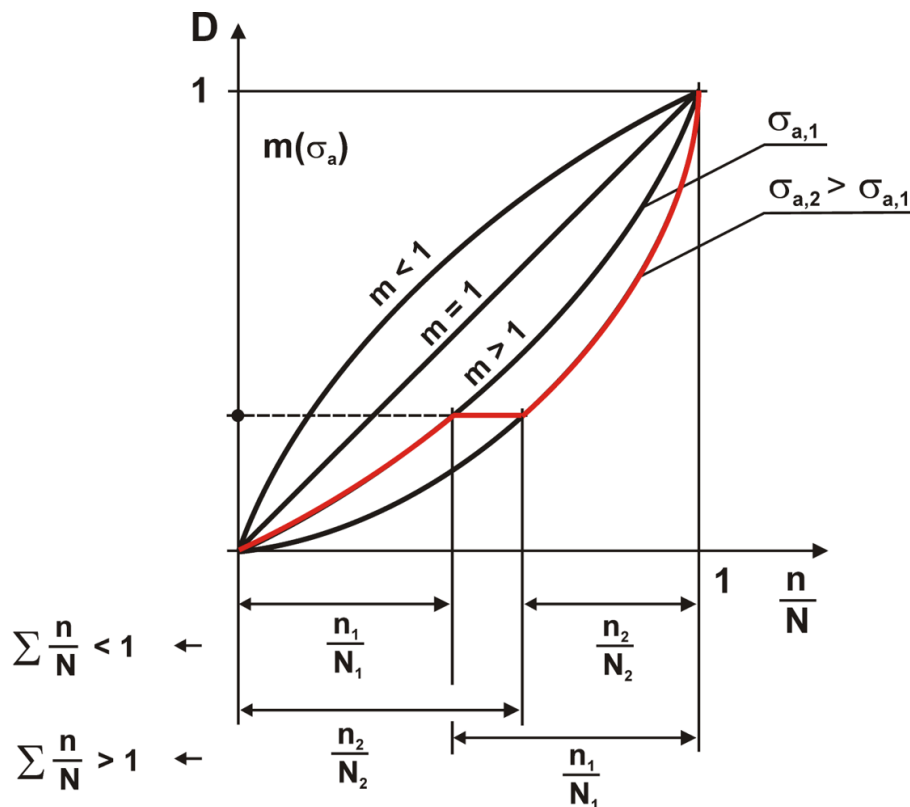


Figure 3.17: Nonlinearities included in cumulative damage summation [1]

Mean fatigue life is then calculated as:

$$L_S = \frac{1}{D_{1 \text{ hour}}} \quad (3.16)$$

Where:

$D_{1 \text{ hour}}$ Cumulative damage per 1 flight hour

Method is also inherently conservative, because of ignoring consecution of loading history, that could impact damage results in several ways:

1. Influence of sequence of high and low stress blocks in loading history.

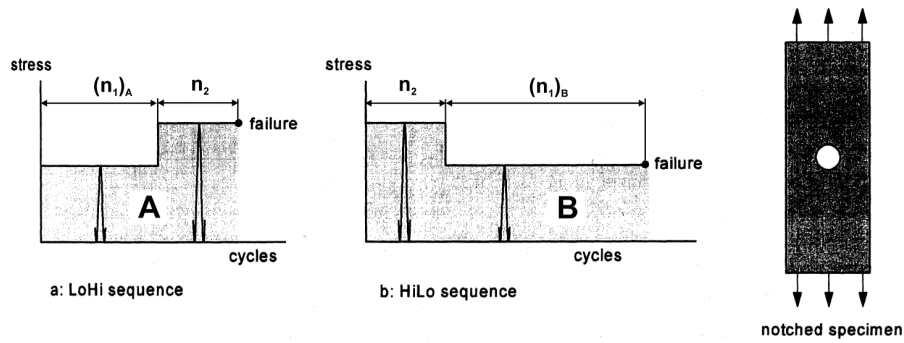


Figure 3.18: HiLo and LoHi stress sequence influence [22]

2. Damage difference is caused by plastic stresses at the root of the notch, stress distribution difference is shown in fig. 3.19.

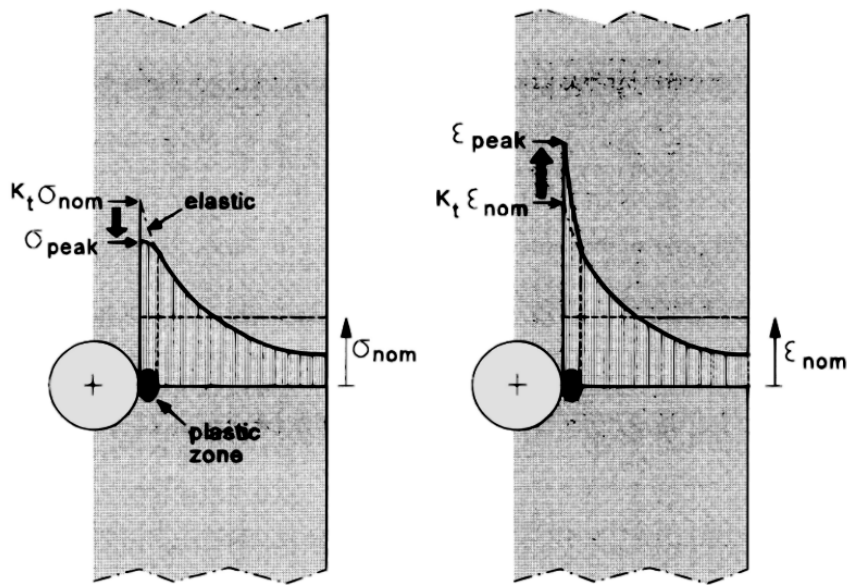


Figure 3.19: Plastic stresses at the root of the notch [22]

3.5 Fatigue life analysis approaches according to notch stress factor evaluation

The notch stress evaluation is one of important part in fatigue life evaluation. Following concepts could be simply explained on bar with rectangular cross-section loaded in tension like in fig. 3.20.

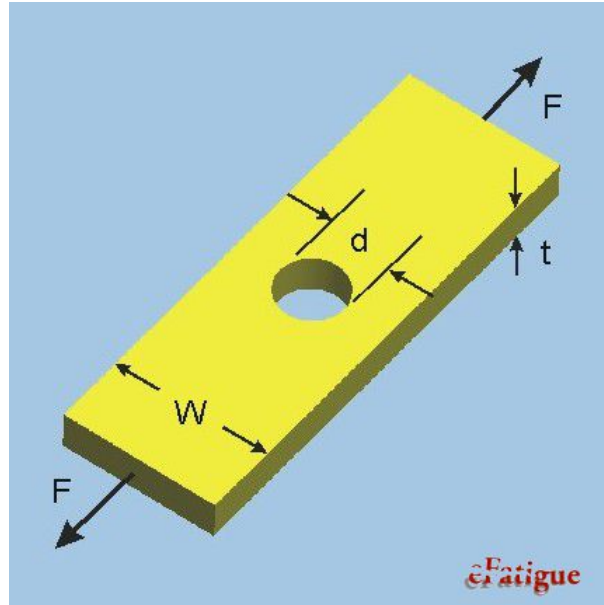


Figure 3.20: Example load case [32]

3.5.1 Concept of nominal stresses

This concept neglects the influence of notches in stress calculation. The nominal stress can be simply calculated using eqn. (3.17).

$$\sigma_{nom} = \frac{F}{(W - D) \cdot t} \quad (3.17)$$

σ_{nom} Nominal stress

F Loading force

W Bar width

D Hole diameter

Visualisation of the nominal stress can be seen in fig. 3.21.

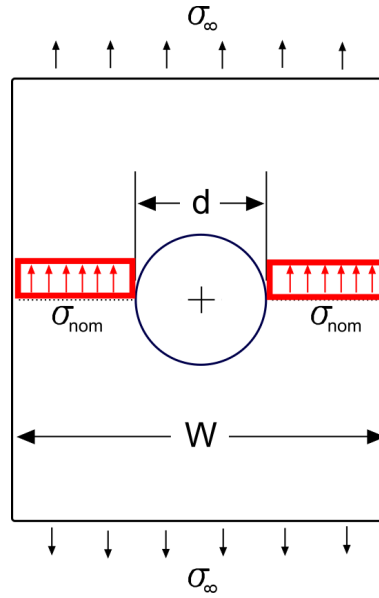


Figure 3.21: Nominal stress distribution (Where: σ_{nom} Nominal stress, F Loading force, W Bar width, D Hole diameter, t Bar thickness)[11]

Calculation procedure continues with calculation of stress concentration factor K_t . The stress concentration factor is then used for fatigue curve choice. Fatigue curves have to be tested on notched specimens with as close K_t value as possible. It is important that this type of fatigue approach demanding on fatigue data, because for each K_t different curve is needed. [32] [23]

In case of eg. bending it is important to use different (rather conservative) approaches to stress calculation. This method extrapolates stress distribution to the edge fiber of cross-section instead of working with CG (centre of gravity) of element cross-section. Principle can be seen in fig. 3.22.

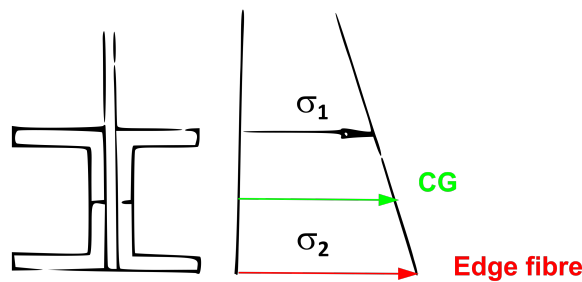


Figure 3.22: Edge fiber stress vs CG stress

3.5.2 Net cross-section stress

The net cross-section is considered to be the section at root of the notch. This can be shown on previous rectangular bar with hole example, the cross-section has less area thus stress calculated is higher according eqn. (3.18). This approach tends to be more conservative. The mentioned cross-section can be seen in fig. 3.23.

$$\sigma = \frac{F}{(W - D) \cdot t} \quad (3.18)$$

σ Cross-section stress

F Loading force

W Bar width

d Hole diameter

t Plate thickness

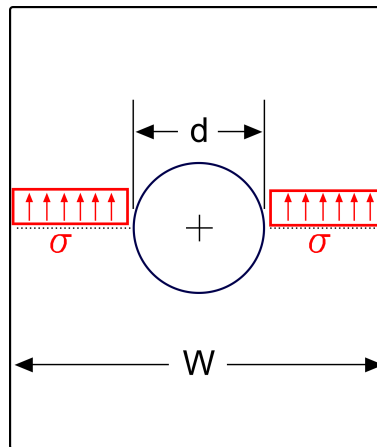


Figure 3.23: Net-section of rectangular bar with hole (σ cross-section stress, F loading force, W bar width, D hole diameter) [11]

3.5.3 Gross cross-section stress

As opposite to net cross-section stress reduction of cross-section area by notch is neglected, in case of gross cross-section approach and stress (eg. rectangular bar with hole) is calculated in eqn. (3.19). Resulting stress distribution can be seen on fig. 3.24.

$$\sigma = \frac{F}{W \cdot t} \quad (3.19)$$

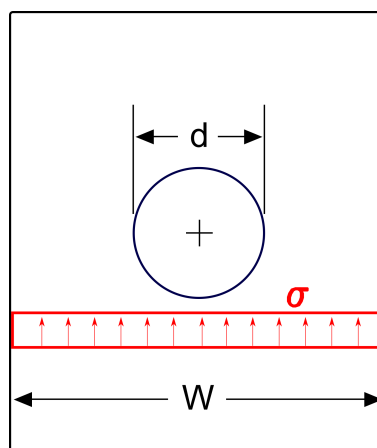


Figure 3.24: Gross-section of rectangular bar with hole[11]

To determine stress which is further analysed we have to perform critical cross-section analysis. One task of such analysis is to find places with stress concentration that are critical for proper operation of aircraft. This approach is suitable for analytic calculation, therefore will be used for purposes of this thesis.

3.5.4 Concept of local stresses

This concept is based on precise knowledge of real stress distribution in the part. The stress maximum can be determined in trivial cases (eq. hole in plate of infinite width) from known solutions. Stress distribution for plate with hole can be seen in fig. 3.25. Stress calculation for method of local stresses is usually performed using net cross-section stress concept (sec. 3.5.2) or gross stress concept (sec. 3.5.3).

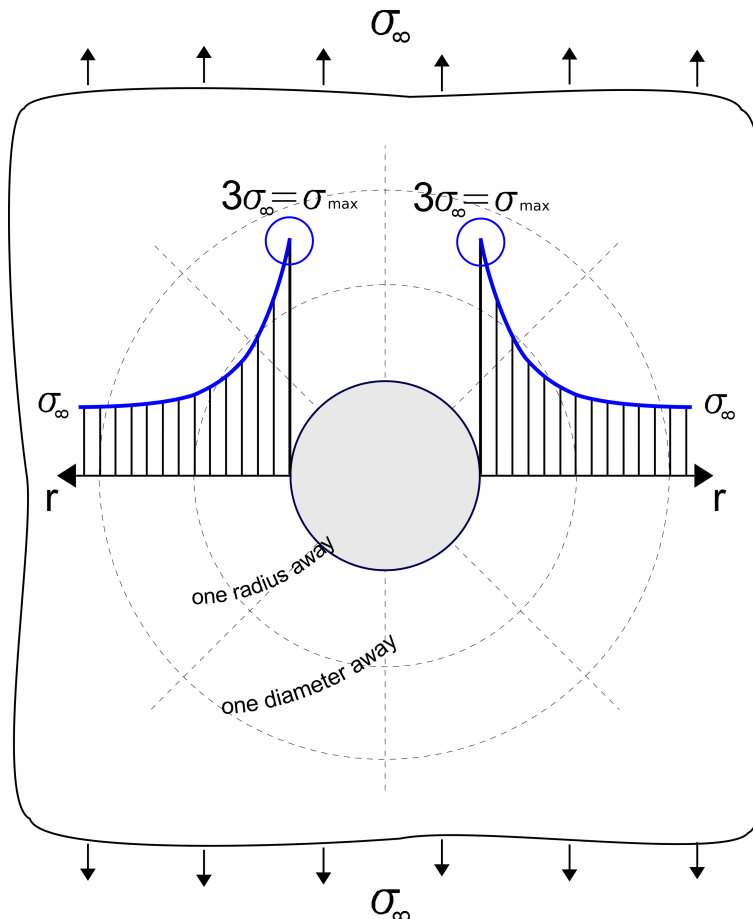


Figure 3.25: Real stress distribution ($3 \cdot \sigma_{\infty}$ maximal stress, σ_{∞} remote stress, r hole radius) [11]

The local stress is 3 times remote stress σ_{∞} , thus stress concentration factor K_t for this notch is equal 3.

For more complex cases we have to use finite element methods or real stresses data from specimen tests for determination of local stress maximum. Better results can be achieved with aid of FEM solver approach. This approach gives accurate results and is not demanding on material testing data. Therefore this approach is cheaper. There is one S-N curve per material for various stress concentrations type needed. It is especially advantageous to use concept of local stresses for cases when nominal cross-section could not be clearly defined. See fig. 3.26 for nominal and real stress distribution comparison. [25]

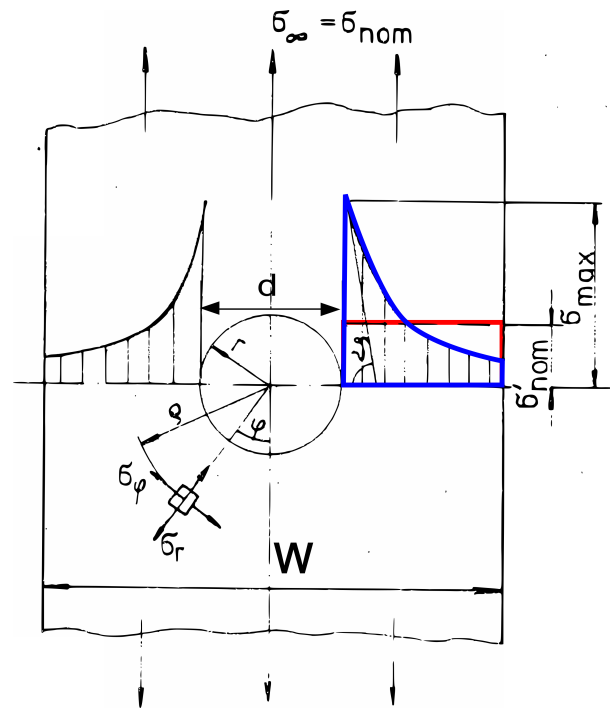


Figure 3.26: Real vs nominal stress distribution (σ_{max} max (local) stress, σ_{nom} nominal stress, F loading force, W bar width, d hole diameter) [23]

4 Fatigue in aerospace engineering

To better understand fatigue approach choice we need to define some widely used approaches and concepts. There are some major differences in terms of part strength utilisation. Main difference is that aerospace industry is focused on light parts. Therefore parts are designed for finite fatigue life. This requires specific fatigue evaluation approach.

4.1 Important aerospace fatigue terms

There are some aerospace fatigue terms and analysis rules which should be mentioned. Understanding of which is essential to meet requirements of standards used for calculation.

Scatter factor can be interpreted as margin of test data variation. Otherwise it could express uncertainties in fatigue analysis. Historically civil and military authorities in Australia and United Kingdom required separate scatter factor for loads and separate scatter factor for structure.[18]

$$L_B = \frac{L_S}{SF_{struc} \cdot SF_{load}} \quad (4.1)$$

Where:

L_B Safe-life

L_S Mean life (obtained by test or analysis)

SF_{load} Scatter factor for loads

SF_{struc} Scatter factor for structure

Scatter factor for loads is here obtained as:

$$SF_{load} = 10^{Z \cdot \sigma} \quad (4.2)$$

Where:

Z normal distribution variate

σ is the standard deviation of the load spectra distribution. Reference 2 states a value for $\sigma = 0.12$.

In contrast FAA interprets the scatter factor concept only for structure. Scatter factor for loads is already included in recommended spectra. Therefore fatigue Safe-life is then calculated as:

$$L_B = \frac{L_S}{SF} \quad (4.3)$$

Where:

L_B Safe-life

L_S Mean life (obtained by test or analysis)

SF Scatter factor for structure

Full scale fatigue test scatter factor is calculated as:

$$SF_{FST} = 10^{Z_p \cdot \sigma \cdot \sqrt{\frac{n_s+1}{n_s}}} \quad (4.4)$$

Where:

Z_p is the normal distribution variate for the specified probability of a detectable crack-free safe-life.

σ standard deviation of the population of fatigue test lives

n_s is the number of fatigue specimens tested

For component testing is scatter factor calculated according to eqn. (4.5).

$$SF_{CT} = 1.5 \cdot SF_{FST} \quad (4.5)$$

Different scatter factors for different applications were summed up according to [30] in tab. 4.1. Scatter factor values are calculated assuming that the structure was manufactures out of aluminium. Analysis scatter factor will be important for further calculation in this thesis.

Table 4.1: Summary of scatter factors for aluminium structures[30] (different applications)

Fatigue certification approach	Symbol	Scatter factor [-]
Full-scale fatigue test	FST	3.54-4.96 (according to number of specimens)
Component testing	CT	$1.5 \cdot scatter\ factor_{FST}$
Fatigue analysis	FA	8

Discrete damage source is primary connected with simulating effect of uncontained rotor burst and loading of structure after major damage.[9] Discrete damage source could be rotor blade elements, which causes eg. damage on wing structure.[30]

Primary structural element is part of assembly which is critical for distributing loads in construction. In case of wing this could be spars, struts which are distributing load.[30]

Primary structure is a structure which has to be capable of distributing both flight and ground loads or internal pressure loads from cabin pressurisation.[30]

Secondary structure is such a structure which is not distributing primary loads. Failure of such structure neither reduces airframe load carrying capacity. Secondary structure also does not impact safe flight and landing. [31]

4.2 Fatigue life analysis approaches according to damage evaluation

There are three main fatigue approaches used in fatigue life estimation. This is specific of aerospace fatigue evaluation. Increasing requirements on reduction of aircraft weight had significant influence on development of such approaches.

4.2.1 Safe-life concept

Approach based on determining number of periodic changes in part loading (expressed in flight hours, landings, take-offs) until first crack occurs. So this approach prevents crack nucleation in part and it doesn't deal with crack propagation. Critical failure of structure is in this case initiation of crack.[30]

4.2.2 Damage tolerant concept

This fatigue life estimation is based on assumption, that safety is ensured by inspection of critical element.[17] Primary structural element has to withstand certain amount of fatigue, corrosion damage or damage from discrete damage source so that the residual strength has to be sufficient for function of element to the next inspection check.[30]

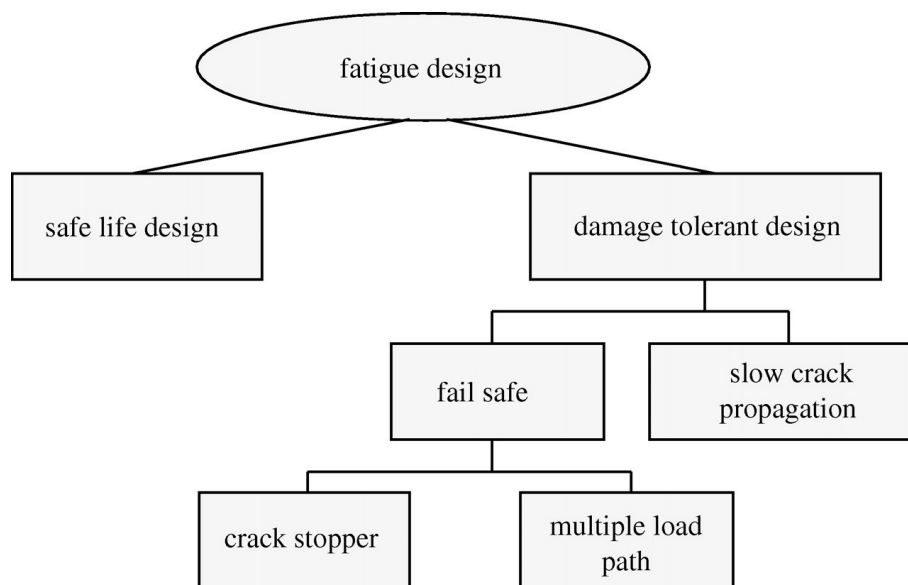


Figure 4.1: Fatigue design strategy [3]

4.2.3 Fail safe concept

Until 1978 Fail safe concept was considered as separate approach. Fail safe design only had to meet criterion that the structure can provide sufficient strength in case of damage or damage from discrete damage source of primary structural element without replacement. There were no conditions or control of crack growth. [20]

Nowadays Fail safe concept concerns strategy of safety ensured by design. This involves combining previously mentioned fail safe with damage tolerance approach. [17]. Security is supplied by usage of construction that can provide sufficient strength in case of damage or damage from discrete damage source of primary structural element without replacement. It handles crack nucleation and growth. Failure of structure is when critical size of crack is achieved. Damaged cross-section is therefore not capable of withstanding the loads [30].

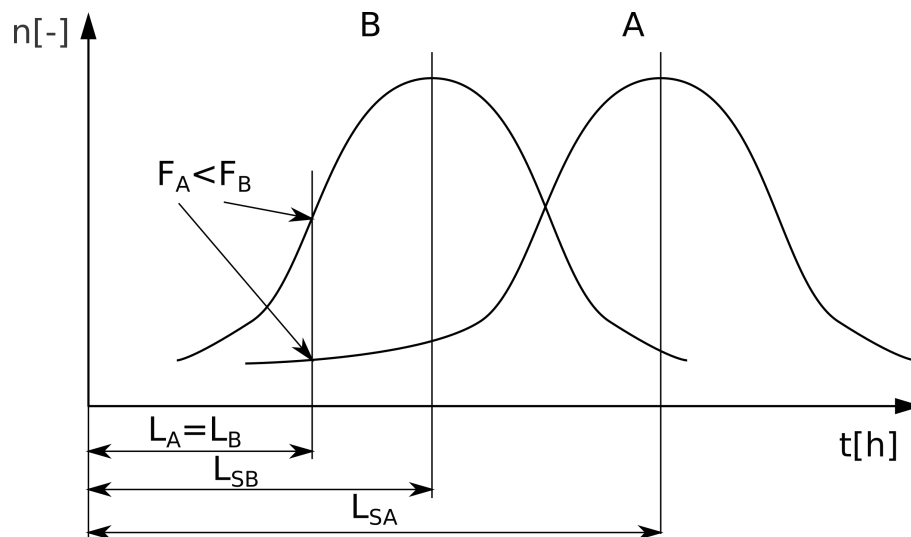


Figure 4.2: Comparison between safe-life and Fail safe concept (curve A represents Damage tolerant approach and curve B represents Safe-life approach) [16]

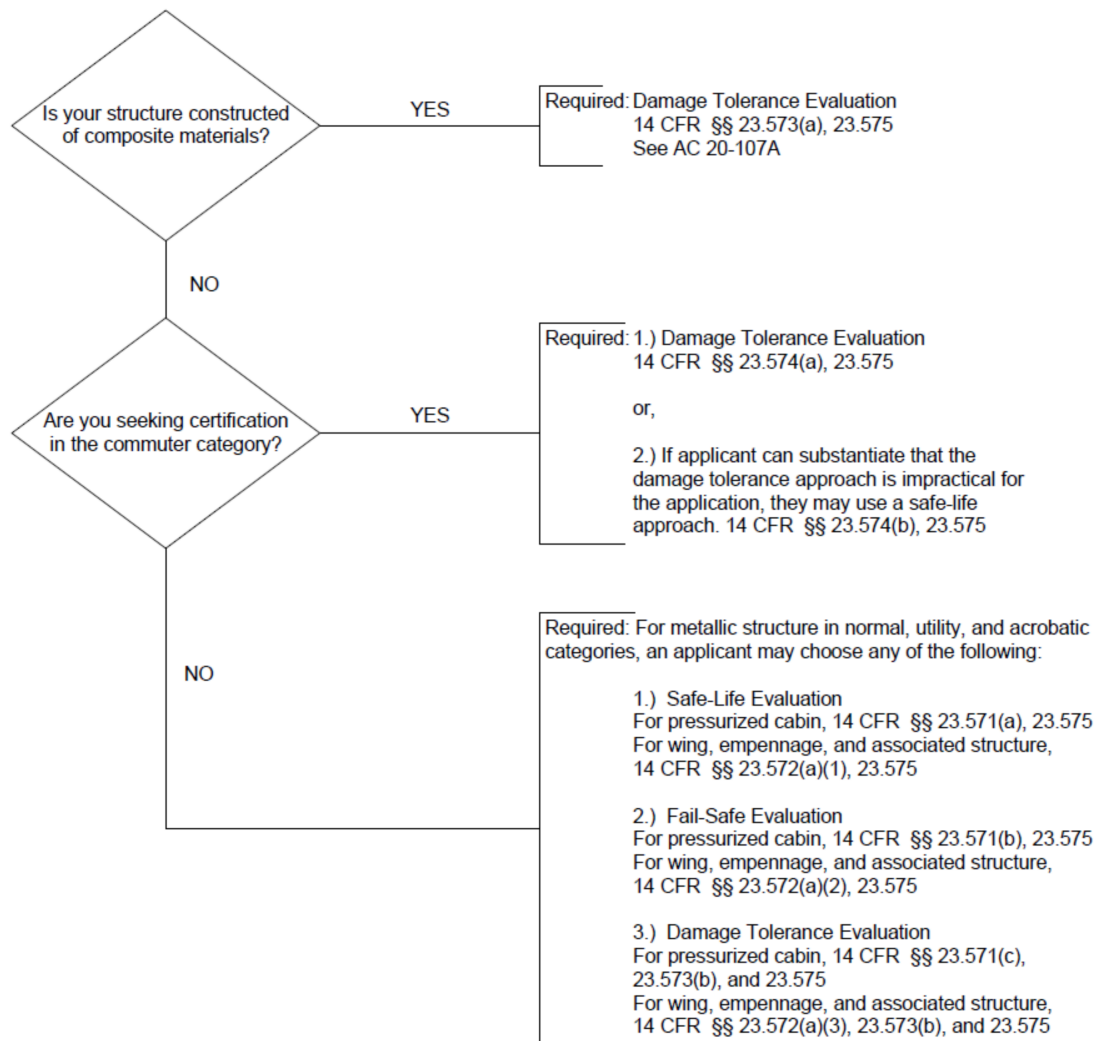


Figure 4.3: Guide to the choice of fatigue life approach [30]

Safe-life approach was chosen for purposes of thesis according to fatigue approach guide in fig. 4.3. This also complies with requirements [28] wing structure (in normal and utility category according to [28]) could be treated as safe-life structure. This approach

does provide usable results and requires lowest calculation complexity and material data requirements. Therefore is perfectly suitable for use in this thesis.

4.3 Safe-life workflow

Determining factor of this method is service time after which should be part taken out of service. Operation point is quantified in service hours to failure. Other way of quantification is number flight cycles until first crack occurs on structure. Failure mode is therefore occurrence of crack on structure. Advisory circular [30] recommends following fatigue safe-life determination methods.

- full-scale testing, see in fig. 4.4
- component testing, see in fig. 4.4
- analysis supported by test evidence

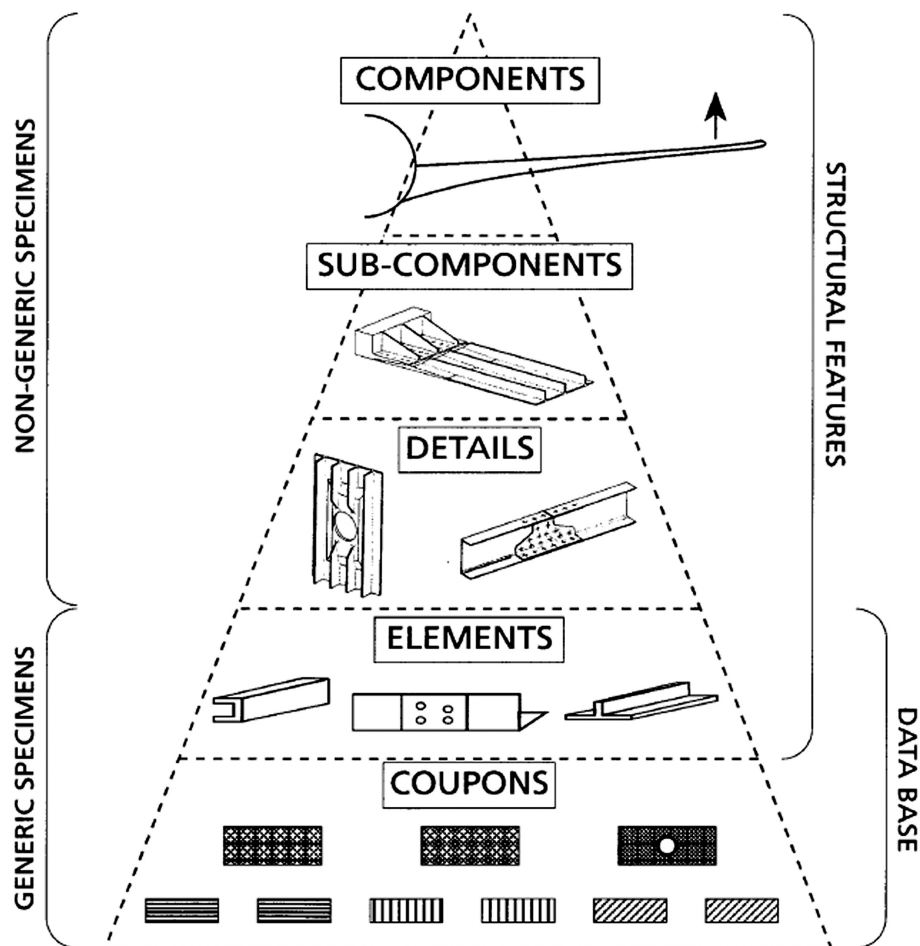


Figure 4.4: Fatigue testing methods [19]

4.4 Load spectra

Load spectra are one of the initial inputs to the fatigue damage calculation. They represent significant loading history per one duty cycle (in this case one flight). Thesis deals for economical and educational reasons only with analysis supported by test evidence. According to [30], flight spectra could be developed on planes similar to calculated plane or

taken from guidance materials. Spectra from [30] were used because they are compatible with all requirements included in this document. Only disadvantage is that they provide rather conservative results.

4.4.1 Classification according to load type

Aircraft flight and ground spectra can further developed in specific load cases. Load cases represent the most significant load from loading history. These load cases can be seen in fig 4.5.

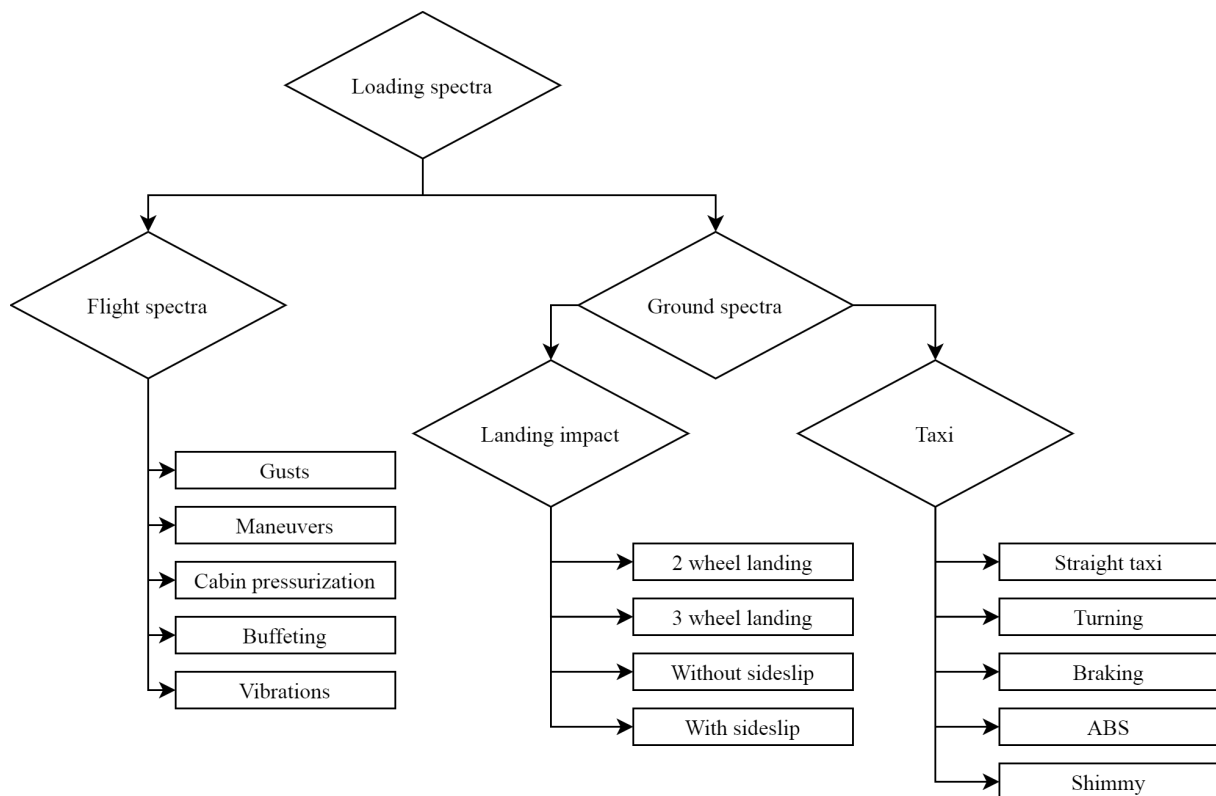


Figure 4.5: Division into specific load cases [1]

Basic parts of fatigue flight spectra are:

1. Maneuvres

This part of spectra represents changes of load factor acting in centre of gravity of aircraft. They are developed on basis of flight measurements with load factor recording device. Typical shape of this spectra can be seen in fig 4.6.[16]

Factors influencing maneuver spectra are:

- aircraft type
- mission profile
- pilot skills
- aircraft employment region

2. Gusts

Gust spectra includes influence of gusts on aircraft loads, main parameters are:

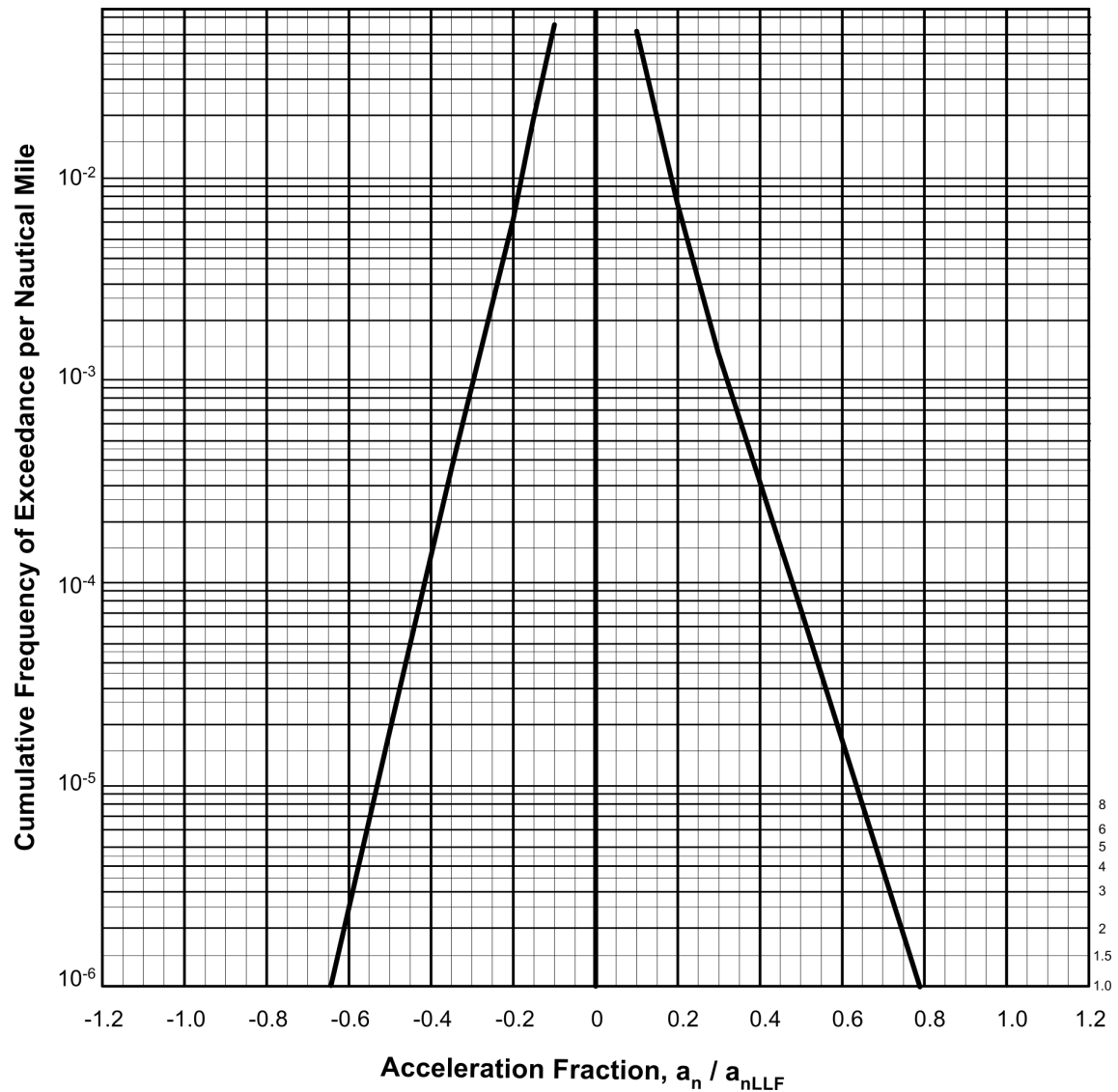


Figure 4.6: Typical shape of maneuver spectra (Single-Engine Executive Usage category according to [30])

- (a) incremental gust load limit load factor according to [30] further calculated according to eqn. (7.1)
- (b) weather conditions, day conditions etc.
- (c) height of flight
- (d) phase of flight (eg. for climb pilot has to hold the course and for cruise phase he can avoid eg. storm)

Gust load spectra are measured similarly to the Manoeuvre load spectra. Results of this measurement are summarised in generalised load spectra. Example shape of this spectra in the fig. 4.7.

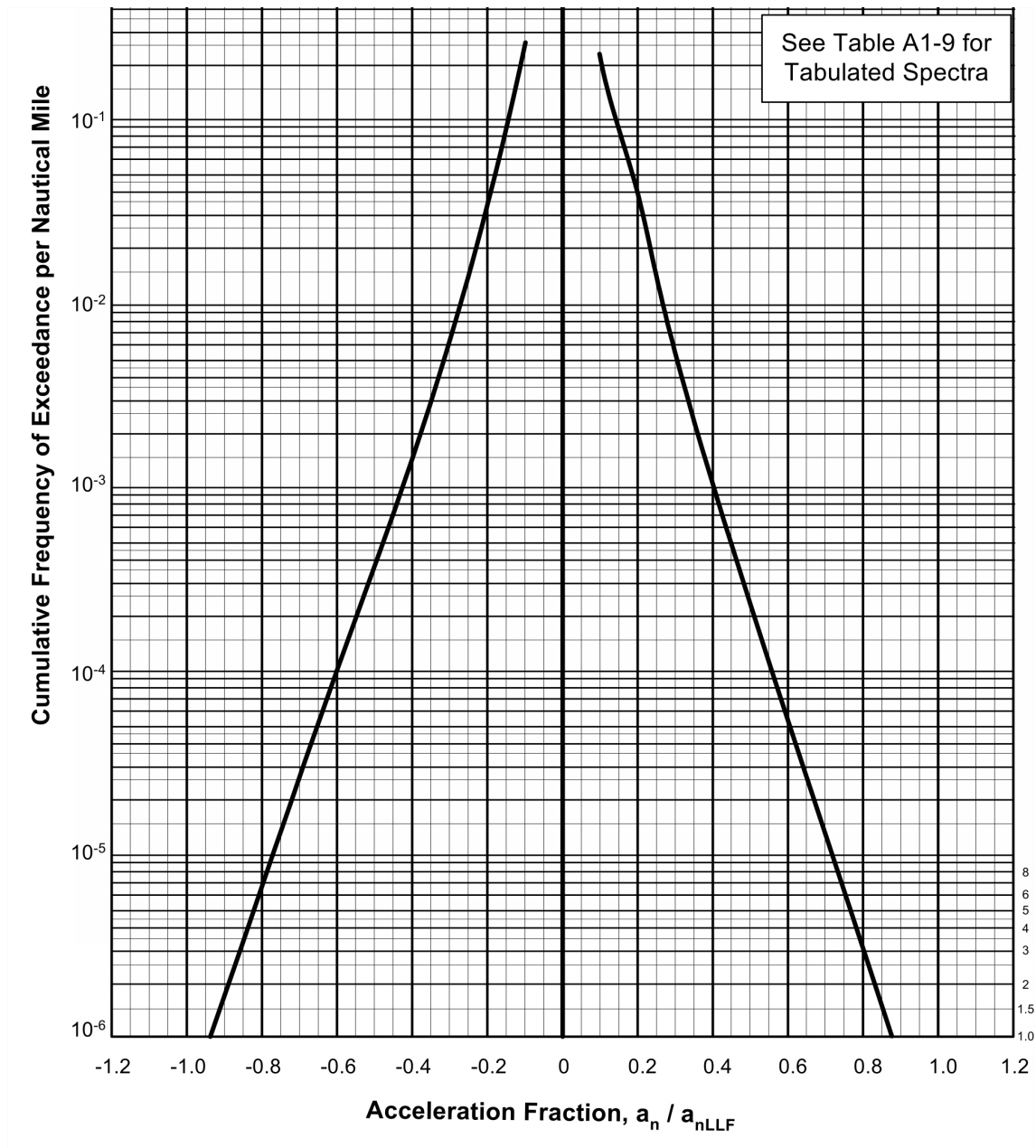


Figure 4.7: Gust spectra (for Single-Engine and Twin-Engine Pressurized Usage categories according to [30])

In development was chosen such approach that after each positive gust load is followed by negative gust load (conservative approach).[2]

3. Landing and Taxi

This part of spectra includes Landing impact (and rebound) damage and movement of airplane on the ground. Landing and Taxi spectra are influenced by:

- runway surface preparation (grass, concrete..)
- landing gear configuration and design

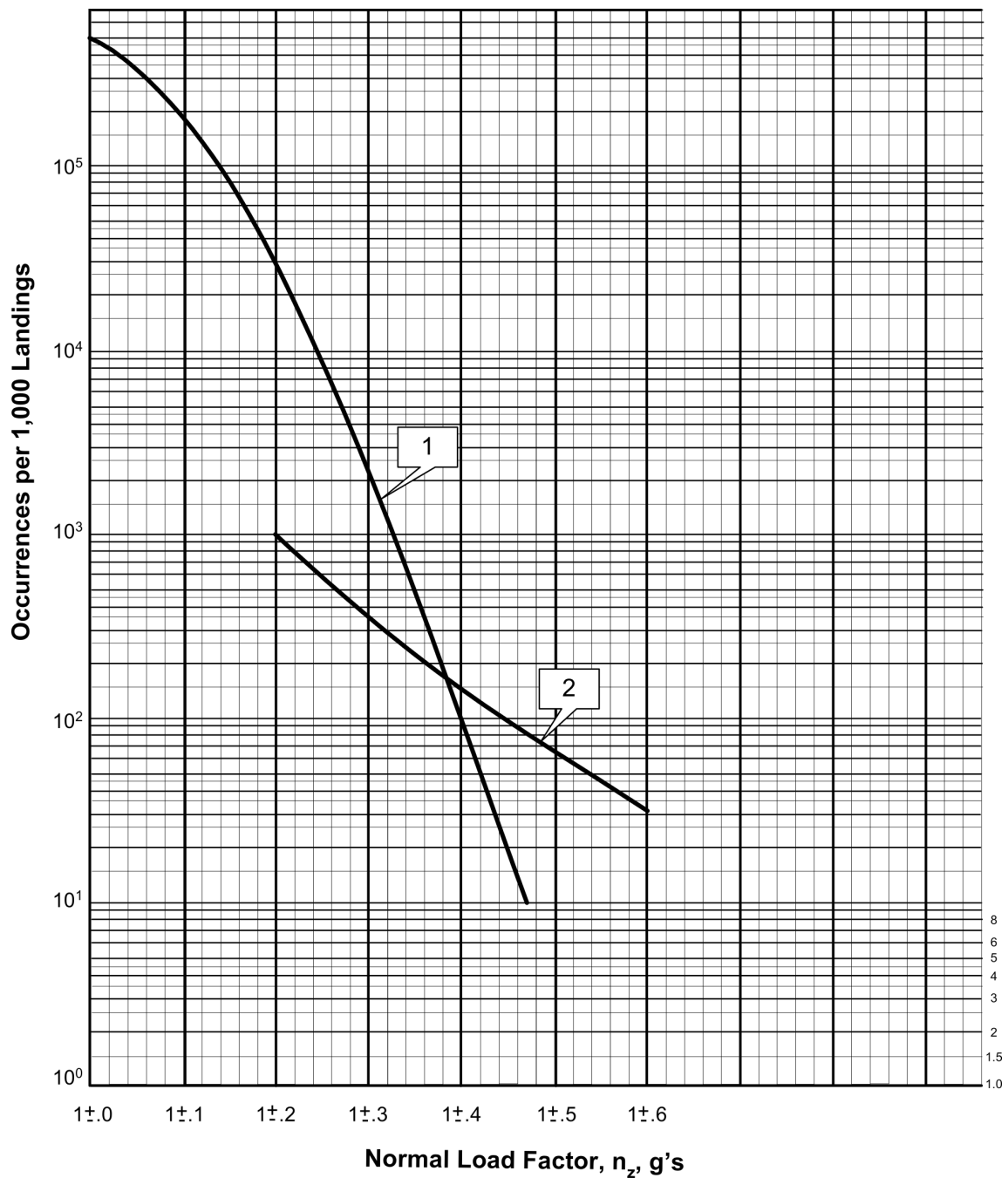


Figure 4.8: Taxi spectra (curves are for 1. All Single-Engine and Twin-Engine Operations, Excluding Aerial Application, 2. Agricultural Usage Aerial Application categories according to [30])

Gathering of such spectra for universal use is difficult because of lack of knowledge about dependencies between impact, side and drag forces acting on tire.[16] Typical spectra included in AC 23-13A [30] can be seen in fig. 4.8 and 4.9.

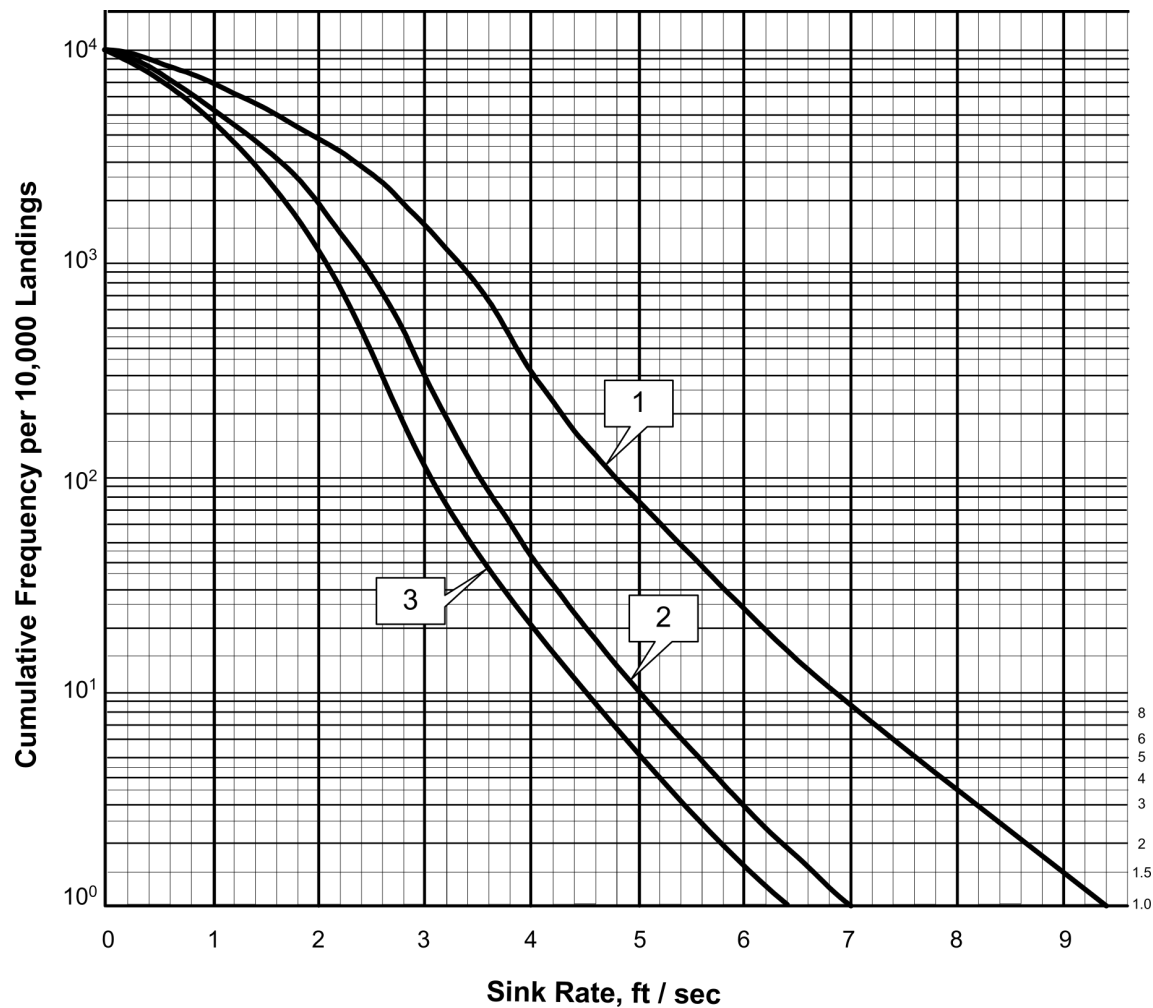


Figure 4.9: Landing impact spectra (curves for 1. Single-Engine Basic Flight Instructional usage, 2. Single-Engine Unpressurized Operations, Including Personal, Executive and Aerobatic Usage, 3. Twin-Engine Unpressurized Usage, Single-Engine and Twin-Engine Pressurized Usage) [30]

4. GAG(Ground-Air-Ground) cycle

Operational loads are connected with mission profile mainly with GAG (Ground-Air-Ground) cycle, which has to be considered as significant part of fatigue damage. In GAG cycle is included influence of:

- flight time in each phase of flight
- velocity in each phase of flight [30]

Serves for purposes of connecting parts of spectra together and is defined as cycle from the minimal stress (ground stress) to the maximal stress (**1g** stress) and back which occurs with frequency per flight:

$$f_{per\ flight} = 1$$

Cycle is visualised in fig. 4.10.[16]

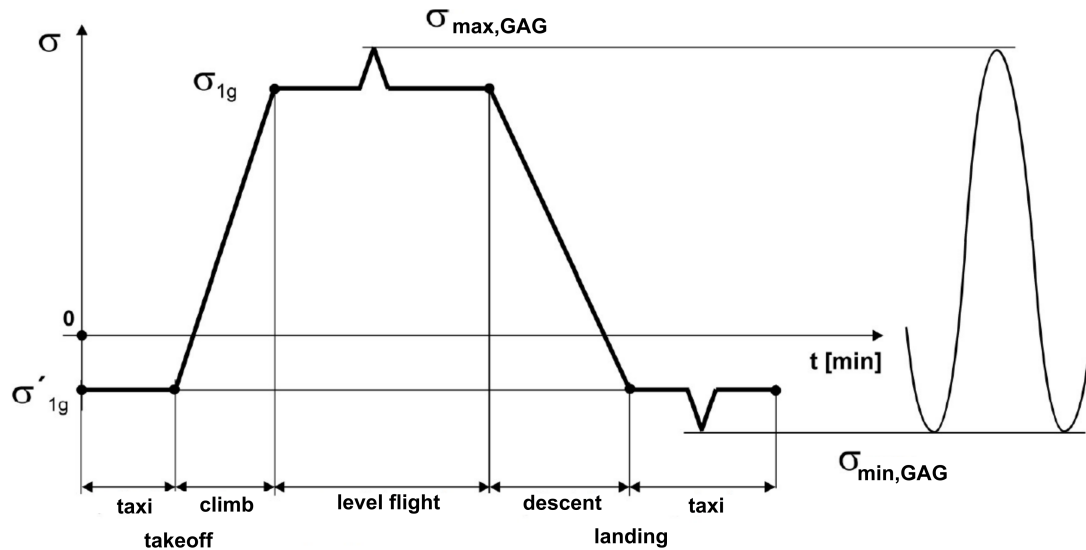


Figure 4.10: GAG cycle visualisation (Where: σ'_{1g} Ground stress level, σ_{1g} 1g load case stress, $\sigma_{max,GAG}$ Maximal stress level of GAG cycle, $\sigma_{min,GAG}$ Minimal stress level of GAG cycle) [16]

Significant factors that are influencing parameters of GAG cycle.

- average flight duration
- aircraft configuration (high-wing, low-wing etc.)
- position of critical cross-section relative to the landing gear
- landing gear configuration

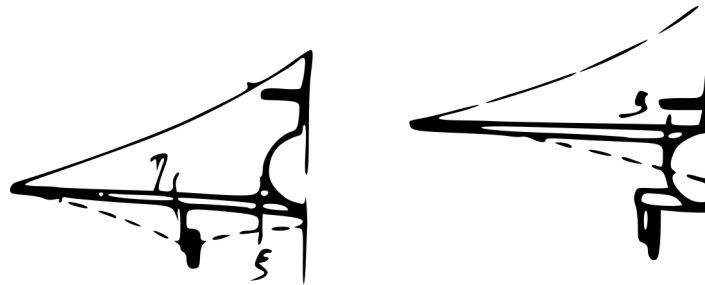


Figure 4.11: Influence of landing gear configuration [16]

5 Inputs for fatigue calculation

In research part were introduced fatigue analysis methods. In following chapters are this methods used in practical calculation to fulfill requirements of standards on analysed structure, in case of this thesis a wing. For such fatigue analysis is important to calculate some prerequisites. Units in computational part will be used both imperial (calculations on basis of [28] and [30]) and metric (for convenience of use).

5.1 Mission profile

Mission profile is important for fatigue calculation because of influence on damage caused by GAG (Ground air ground) cycle. In [30] mission profile needs defined by parameters mentioned in tab. 5.1. As general type of aircraft for spectra choice Single engine executive usage is considered.

Table 5.1: Parameters of mission profile [30]

Parameter	Unit	Recomanded value
Flight time	h	0.65h (Executive usage)
Aircraft Speed	KEAS	$0.9v_{NO}$
Gross weight and load distribution	kg	-

Mission profile can be divided into flight phases. In case of this calculation 5 flight phases were considered. Example of mission profile divided into flight phases can be seen in fig. 5.1. This fig also shows duration of engine operation and flight duration. With inceasing number of flight phases increases also calculation complexity.

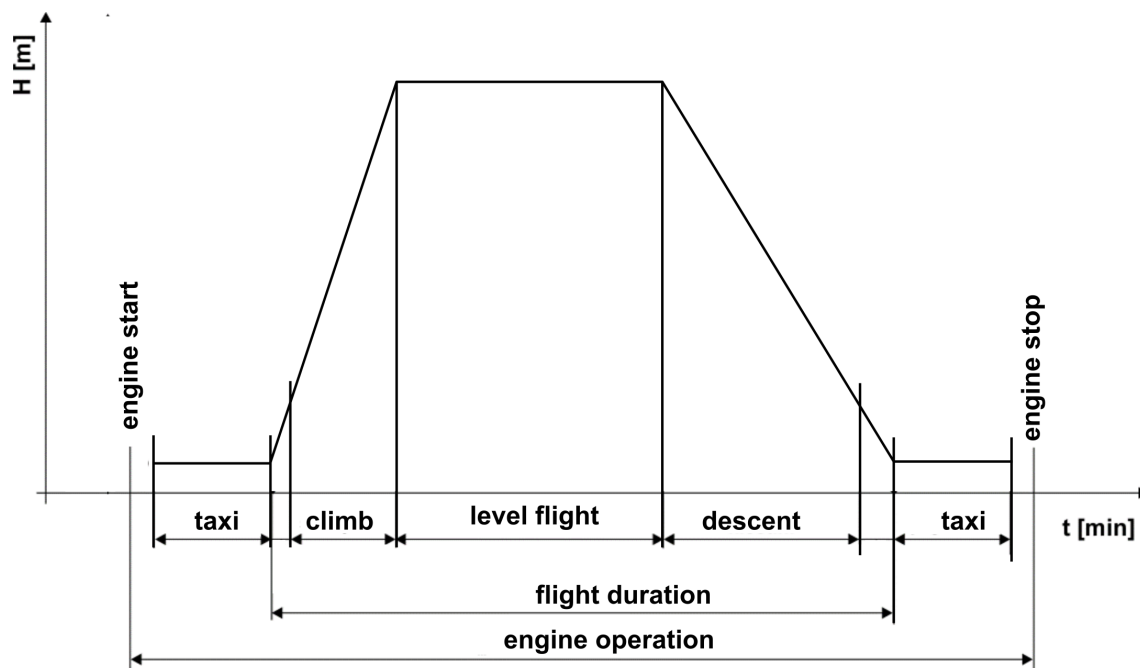


Figure 5.1: Mission profile visualisation [16]

5.1.1 Parachutist dropping

Parachutist dropping mission profile has unique characteristic of short flight time in which should influence on damage distribution. Parameters of mission profile are based on

reference values from flight manual [35] for parachutist dropping operation. Operation is in [35] divided into three "lifts" (short flights) without refueling. In case of fatigue calculation is important second "lift", because it gives the most accurate idea about mean values of monitored parameters from tab. 5.1.

- takeoff with v_{LOF} speed (defined in flight manual)
- climb into FL100 (100000 ft - defined height for parachutist operation) with best climb speed v_{BC}
- level flight parachutist drop with v_{NO} speed
- descent and landing approach with v_{ref}
- landing v_l

Speeds were taken from flight manual as speeds used specifically for parachutist dropping operation:

Table 5.2: Parameters of mission profile

Phase	Speed	Value [KEAS]
takeoff	v_{LOF}	68
climb	v_{BC}	81
level flight	v_{NO}	87
descend	v_{ref}	76
landing	v_l	68

Distances and flight time had determined from flight manual and are obtained from performance section, values can be seen in tab. 5.3.

Weight is considered mean value of weight corresponding to:

- takeoff with total weight corresponding to 2nd lift
- 8 parachutists on board as mean transport capacity
- considering weight of skydiver as: $m_{skydiver} = 80 \text{ kg}$

Actual plane weight (row Aeroplane weight [kg] in tab. 5.3) is calculated as:

$$m_{act(i)} = m_{init(i-1)} - m_{f(i)} - m_{skd(i)} \quad (5.1)$$

m_{act} Corresponding to row Aeroplane weight [kg] in tab. 5.3

m_{init} Weight of aeroplane at the start of phase

m_f Decrement of used fuel weight to row Fuel used [kg] in tab. 5.3

i Index of phase

Table 5.3: Mission profile summary

Phase	Takeoff	Climb	Flight (4000 m)	Descend	Landing
Speed [KEAS]	68	81	87	76	68
Height [ft]	0	6562	13123	6562	0
Distance [km]	0.50	25.00	11.02	32.00	0.40
Distance [NM]	0.27	13.50	5.95	17.28	0.22
Duration [min]	1	14	2	15	1
Fuel used [kg]	10.00	18.00	5.82	10.00	6.00
Parachutist dropped [kg]	0	0	0	720	720
Aircraft mass [kg]	2648	2620	2614	1884	1878
Part of typical flight	0.20	0.36	0.12	0.20	0.12

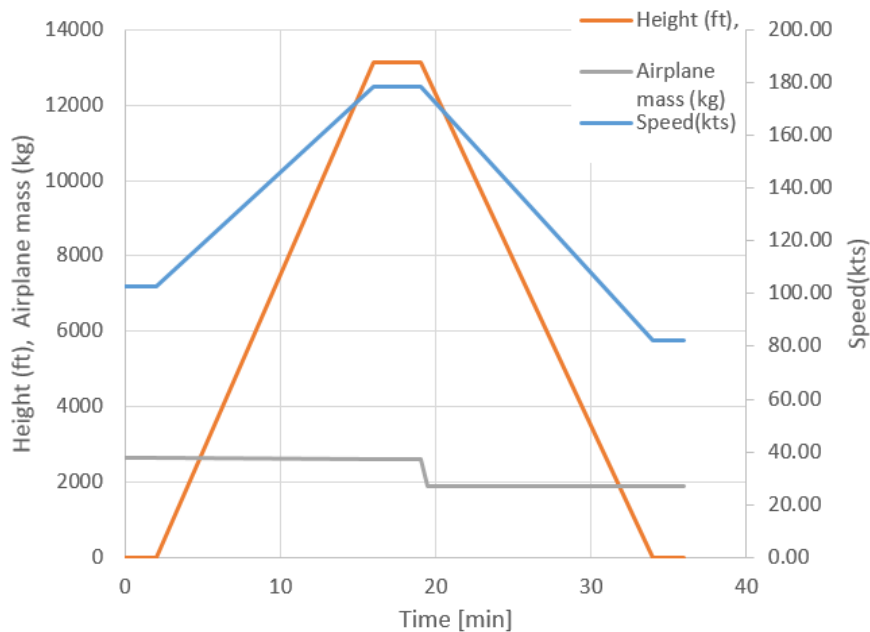


Figure 5.2: Important characteristics of Parachutist dropping mission profile

5.2 V-n diagram calculation

V-n diagram is considered important part of damage calculation input. Three mass configurations were chosen as representative cases :

Table 5.4: Aircraft mass configurations

Configuration		m [kg]
Maximum takeoff weight	m_{TOW}	2700
Zero fuel weight	m_{ZFW}	1800
Minimum takeoff weight	m_{minTOW}	1713

Following calculations were performed assuming Utility category which suits better to parachutist dropping mission profile.

5.2.1 Design speeds

Cruising speed was determined according to [28] Sec. 23.335 (a) wing loading at m_{MTOW} was calculated as:

$$\frac{W}{S} = \frac{2700 \cdot 9.81}{20} = 135 \frac{N}{m^2} = 27 \frac{lb}{ft^2} \quad (5.2)$$

minimum design cruise speed for normal, utility and commuter category was determined as follows:

$$v_c = 33 \cdot \sqrt{\frac{W}{S}} = 33 \cdot \sqrt{27} = 170 \text{ KEAS} \quad (5.3)$$

Other criterion used for v_c was not applicable due to lack of data, therefore minimal cruising speed was conservatively chosen as:

$$v_c = 170 \text{ KEAS}$$

Dive speed was determined from Sec. 23.335 (b) was taken as a conservative assumption for utility category:

$$v_D = 1.5 \cdot V_{Cmin} = 1.5 \cdot 170 = 255 \text{ KEAS} \quad (5.4)$$

Stall speeds were taken from flight manual for reference weight.

$$m_{ref} = 2350 \text{ kg} \quad (5.5)$$

Speeds were recalculated to compensate for weight change between flight manual and actual mass configuration.

Sample calculation is shown below with m_{MTOW} configuration used. Final results are summarized in tab. 5.5.

$$\frac{v_{comp}}{v_{ref}} = \sqrt{\frac{\frac{2 \cdot m_1 \cdot g}{\rho \cdot S \cdot L}}{\frac{2 \cdot m_2 \cdot g}{\rho \cdot S \cdot L}}} = \sqrt{\frac{m_1}{m_2}} \Rightarrow \quad (5.6)$$

$$v_{sMTOW} = v_{ref} \cdot \sqrt{\frac{m_2}{m_1}} = 62 \cdot \sqrt{\frac{2700}{2350}} = 66.46 \text{ KEAS}$$

Following speeds are presented in KEAS.

Table 5.5: Stall speeds at different mass configurations

Speeds		Manual reference m=2350kg	MTOW
Stall speed	v_s	62.00	66.46
Stall speed 20°	v_{s0}	58.32	62.51
Stall speed 40°	v_{s1}	54.00	57.88
Stall speed reversed	v_{sg}	80.61	86.40

Maneuvering speed was determined according to Sec. 23.335 (c) only as minimal maneuvering speed:

$$v_a = v_s \cdot \sqrt{n} = 66 \cdot \sqrt{3.6} = 126 \text{ KEAS} \quad (5.7)$$

where:

- v_s Stall speed with flaps retracted at desired weight
- n Positive limit maneuvering load factor used in design determined in eqn. (5.9) (sec. 5.2.2)

Maneuvering speed reversed was determined according to Sec. 23.335 (c) minimal maneuvering speed reversed was determined as:

$$v_a = v_{sg} \cdot \sqrt{n} = 86 \cdot \sqrt{1.44} = 104 \text{ KEAS} \quad (5.8)$$

where:

- v_s Stall speed with flaps retracted at desired weight
- n Negative limit maneuvering load factor used in design determined in eqn. (5.10)(sec. 5.2.2)

5.2.2 Limit maneuvering load factors

Calculation was performed on basis of [28] Sec. 23.337. Limit load factors were determined from Sec. 23.337 (1) and (2), for positive maneuvering limit factor as follows:

$$n = 2.1 + \frac{24000}{W + 10000} = 3.6 \quad (5.9)$$

W design maximal m_{TOW} in lb

And for negative maneuvering limit factor as:

$$n = -0.4 \cdot n = -0.4 \cdot 4.4 = -1.44 \quad (5.10)$$

5.2.3 Gust load factors

Limit load (n_g) factor for according to [28] Sec. 23.341

$$n_g = 1 \pm \frac{U \cdot K_g \cdot V \cdot a}{498 \cdot W/S} \quad (5.11)$$

where:

U Nominal gust velocity [fps]

W/S Wing loading at max. weight, [lb/ft^2]

$K_g = \frac{0.88 \cdot \mu_g}{5.3 + \mu_g}$ Gust alleviation factor [-]

$\mu_g = \frac{2 \cdot W/S}{\rho \cdot MAC \cdot a \cdot g}$ Aircraft mass ratio [-]

MAC Mean aerodynamic chord [ft]

ρ Air density, [ft/slug³]

g Gravitational acceleration, [ft/s²]

v Structural design speed, KEAS

a Wing lift curve slope, $C_{L\alpha}$, [rad⁻¹]

W design weight [lb]

S wing area from tab. 1.1 [ft²]

Sample calculation is performed for v_C and m_{MTOW} . Wing loading is determined as:

$$\frac{W}{S} = \frac{2700 [kg]}{20 [m^2]} = \frac{5940 [lb]}{215 [ft^2]} = 27 lb/ft^2 \quad (5.12)$$

Wing loading for rest of cases is in tab. 5.6:

Table 5.6: Wing loading of representative configurations

Cofiguartion	m [kg]	G/S [N/m²]	G/S [lb/ft²]
Maximum takeoff weight	2700	135	27
Zero fuel weight	1800	90	18
Minimum takeoff weight-para	1713	86	18

Aircraft wing lift curve slope was about to be determined according to methods listed in [5]. This was caused by lack of aerodynamic measurement data provided by TC holder.

$$a = \frac{a_\infty}{1 + \frac{a_\infty}{\pi \cdot AR}} \quad (5.13)$$

Where:

a_∞ Infinite wing lift curve slope defined as

$$a_\infty = 1.8 \cdot \pi \cdot \left(1 + 0.8 \frac{t}{c}\right) \cdot \cos(\Lambda)$$

AR Wing aspect ratio

t Airfoil max. thickness

Λ Leading edge sweep

Value of wing lift curve slope is after substitution:

$$a_\infty = 1.8 \cdot \pi \cdot \left(1 + 0.8 \frac{t}{c}\right) \cdot \cos(\Lambda) = 1.8 \cdot \pi \cdot (1 + 0.8 \cdot 0.15) \cdot \cos(0) = 7.04$$

$$a = \frac{a_\infty}{1 + \frac{a_\infty}{\pi \cdot AR}} = \frac{7.04}{1 + \frac{7.04}{\pi \cdot 10.8}} = 5.8$$

Aircraft mass ratio is then calculated as:

$$\mu_g = \frac{2 \cdot W/S}{\rho \cdot c_{SAT} \cdot a \cdot g} = \frac{2 \cdot 27}{0.00238 \cdot 4.59 \cdot 5.8 \cdot 32.18} = 24.52 \quad (5.14)$$

Gust alleviation factor is then calculated as:

$$K_g = \frac{0.88 \cdot \mu_g}{5.3 + \mu_g} = \frac{0.88 \cdot 4.59}{5.3 + 4.59} = 0.72 \quad (5.15)$$

Gust limit load factor for normalised gust speed $U = 50 ft$ is then calculated as:

$$n_g = 1 \pm \frac{U \cdot K \cdot V \cdot a}{498 \cdot W/S} = 1 \pm \frac{50 \cdot 0.72 \cdot 170 \cdot 5.8}{498 \cdot 27} = 1 \pm 2.70 \quad (5.16)$$

5.2.4 Service load envelope

V-n diagrams were plotted for every chosen weight configuration. Gust envelopes were plotted for 0 and 4000 m (height of parachute drop) to give better idea of height influence on gust load factor. Plots also include flap envelopes.

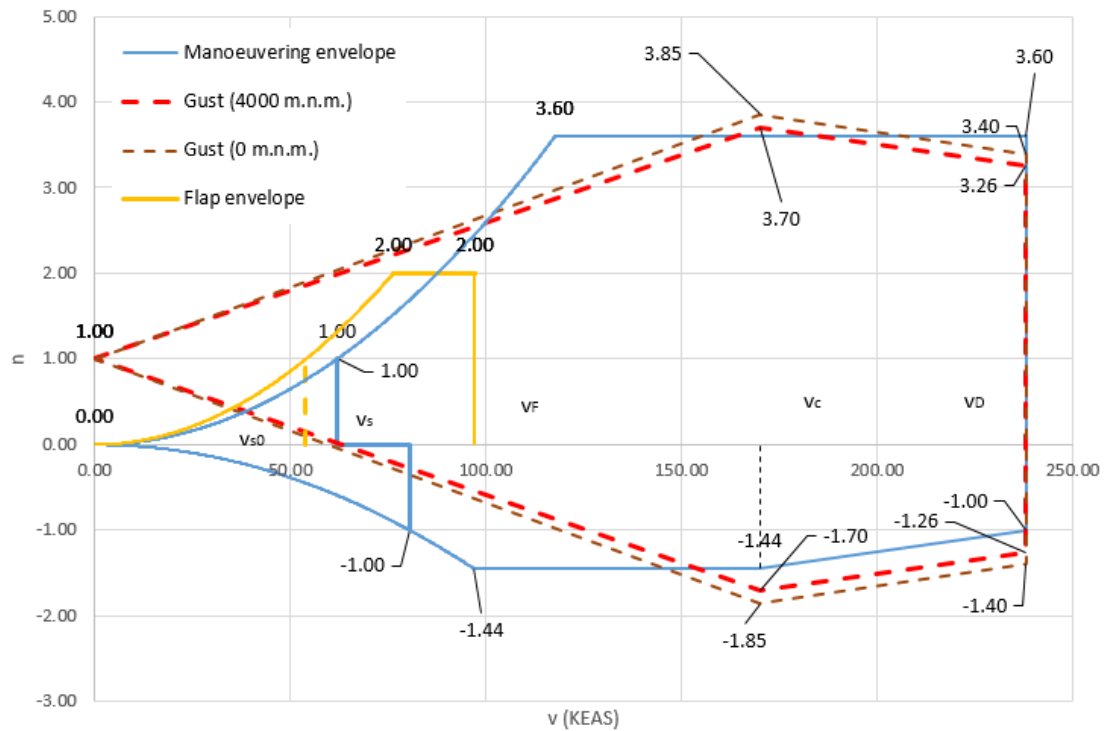


Figure 5.3: V-n diagram for m_{MTOW}

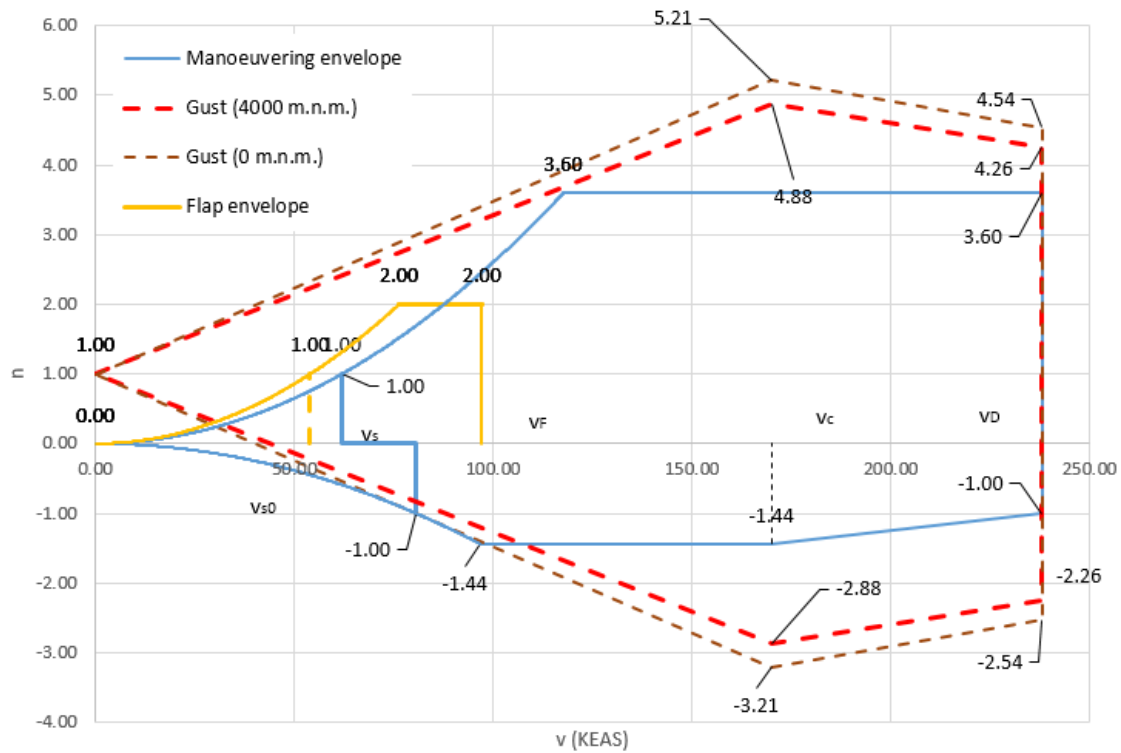


Figure 5.4: V-n diagram for m_{MINTOW}

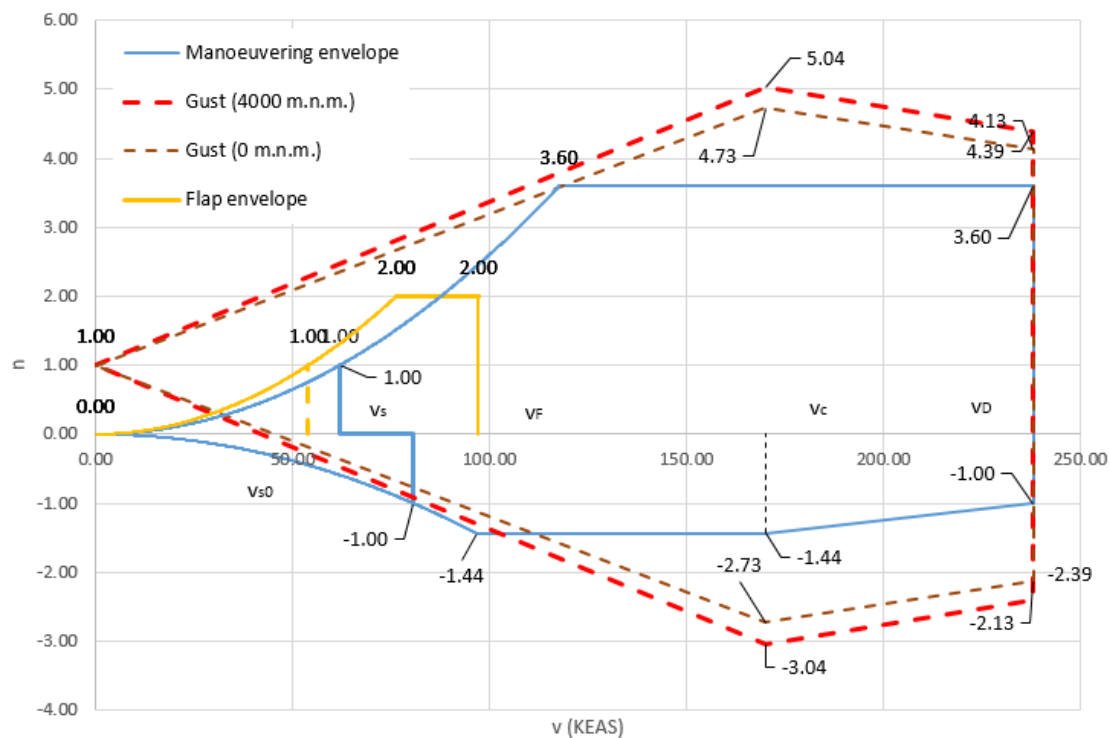


Figure 5.5: V-n diagram for m_{ZFW}

From comparison of m_{MTOW} vs. eg. m_{ZFW} mass configuration can be clearly visible that mass reduction has major influence on gust loads. Mass configurations with higher weight showed also lower sensitivity to change of gust loads with change in height.

5.3 Stress analysis

1g stress is important to determine for safe-life estimation. It is deciding factor for critical cross-section choice. Stress analysis is performed using nominal stress approach. Therefore S-N curves used for further fatigue damage calculation has to be suitable for use with nominal stress approach.

5.3.1 Wing freebody diagram

Because of fatigue orientation of this thesis calculations were made with following assumptions:

- All calculations and notations were done in coordinate system defined according to [16], see fig. 5.6.

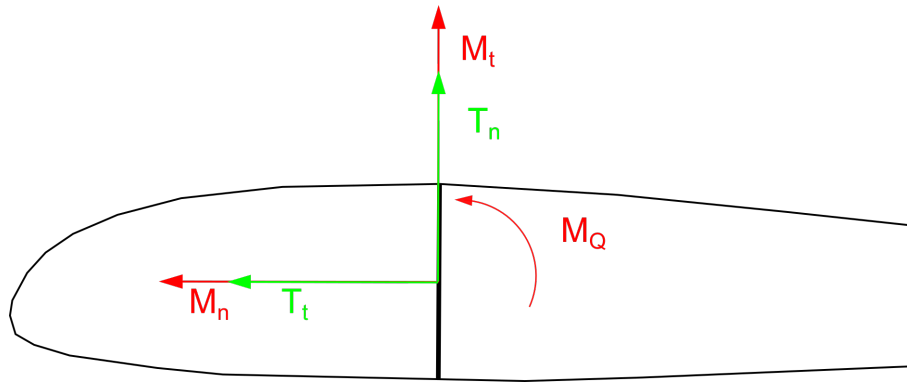


Figure 5.6: Coordinate system used for calculation [16]

- In both of analysed load cases (1g and ground load) tangential shear force T_t influence is considered to be negligible.
- Torsional loading was neglected. It was considered that the influence on longitudinal structure is small. Furthermore spectra for torsional loading are not available for purposes of thesis, therefore calculation of torsional loading is not feasible.
- Calculation includes only 1g and ground load cases (other V-n diagram load cases were skipped due to thesis fatigue specialisation).
- Aircraft mass is estimated as weighted average of mission profile mass values.

Table 5.7: Parachutist dropping input mass values

Description	Symbol	Weight [kg]
Air vehicle mass	m_{op}	2264
Wing mass	m_w	296
Fuel mass	m_f	174

- Wing and fuel mass is assumed linearly distributed.
- Calculation was performed with half of span with hinge supports, see in fig. 5.10.

5.3.2 Load case 1: Flight loads 1g

Flight loads has greatest impact on fatigue damage caused mainly by gust and manoeuvre loads. Flight loads geometrical relations were modified according to simplifications. Simplifications were performed for $\alpha \rightarrow 0$ and $c_D \rightarrow 0$ as:

$$\begin{aligned}
 c_T &= c_L \cdot \cos\alpha + c_D \cdot \sin\alpha \\
 c_N &= c_D \cdot \cos\alpha - c_L \cdot \sin\alpha \\
 n_x &= n \cdot \sin\alpha \\
 n_z &= n \cdot \cos\alpha \\
 &\Rightarrow \\
 c_N &= c_L \\
 c_T &\rightarrow 0 \\
 n_z &= n \\
 n_x &\rightarrow 0
 \end{aligned} \tag{5.17}$$

Where:

c_T Tangential shear force coefficient[-]

c_N Normal shear force coefficient [-]

c_D Drag coefficient [-]

c_L Lift coefficient [-]

α Angle of attack [°]

Wing structure is loaded with distributed lift load. To determine distributed lift load it is important to determine wing lift force. Lift force acting on wing was determined using force and moment equilibrium in fig. 5.7 on basis of methods used in [16].

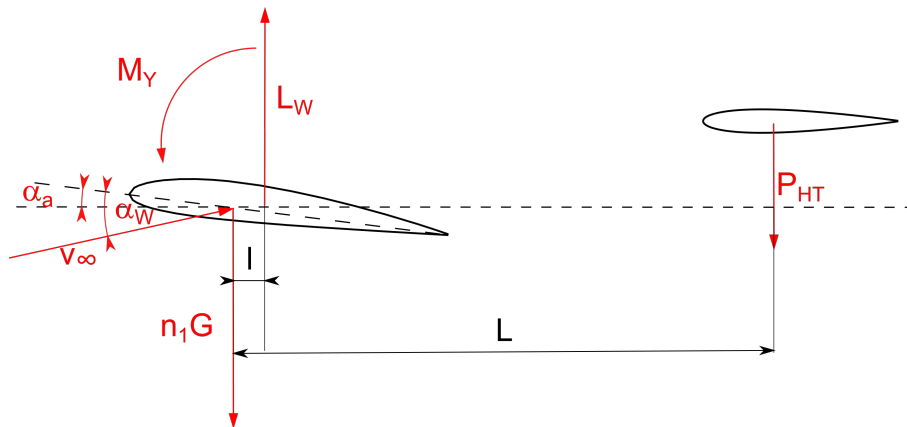


Figure 5.7: Moment and force equilibrium diagram [16]

$$\sum F_z = 0 : L_w - n_1 \cdot G - P_{HT} = 0 \tag{5.18}$$

$$\sum M = 0 : M_Y + L_w \cdot l - P_{HT} \cdot L = 0 \tag{5.19}$$

$$M_y = c_m \cdot q \cdot S \cdot c_{MAC} \quad (5.20)$$

$$G = m \cdot g \quad (5.21)$$

Where:

L_W Wing lift [N]

n_1 Load factor [-]

G Gravitational force acting on aircraft [N]

P_{HT} Horizontal tail trim force [N]

M_Y Wing pitching moment [Nm]

c_m Pitching moment coefficient [-]

l Distance to aerodynamic center [m]

L Distance to horizontal tail [m]

m Aircraft mass [kg]

q Dynamic pressure [MPa]

S Wing area [m^2]

c_{MAC} Mean aerodynamic chord [m]

g Gravitational force [N]

Problem is that the wing pitching moment coefficient is not known (was not supplied by TC holder). Therefore is not possible to determine pitching moment M_Y . Condition from eqn. (5.20) is also not usable. Problem of unknown wing pitching moment coefficient can be solved by simplification from [28] (Sec. A23.7(1)). Horizontal tail trim force is substituted as follows:

$$P_{HT} = 0.05 \cdot m \cdot g \cdot n_1 \quad (5.22)$$

Lift force acting on a wing can be calculated after substitution from force equilibrium (eqn. (5.18)) as follows:

$$\sum F_z = 0 : L_w - n_1 \cdot m \cdot g - 0.05 \cdot m \cdot g = 0 \quad (5.23)$$

Lift force acting on wing is after some of mathematical operations:

$$L_w = 1.05 \cdot (m \cdot g \cdot n_1) \quad (5.24)$$

Calculated wing lift was then normalised into normal lift distribution. Normal lift distribution was calculated according to Lifting line theory in Glauert III software Values and can be seen in fig. 5.8.

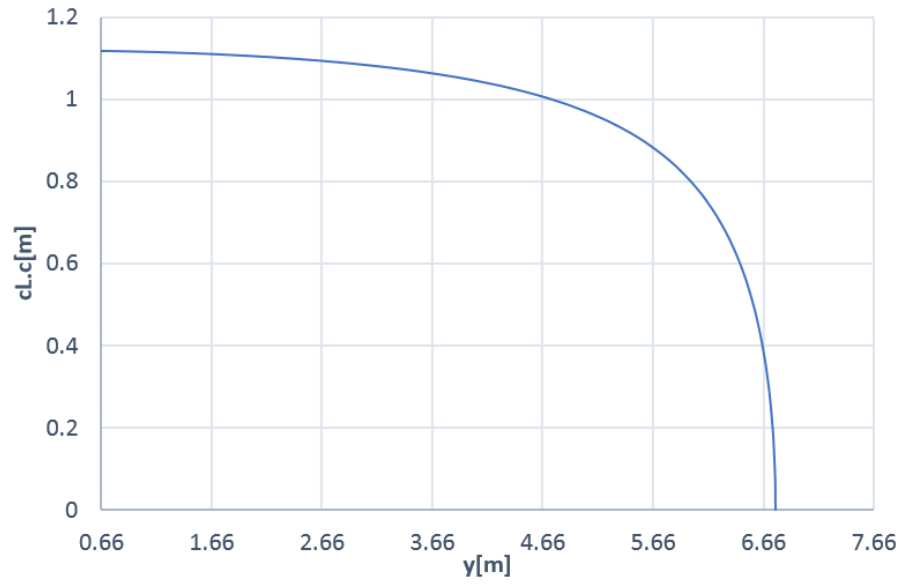


Figure 5.8: Lift distribution from Glauert III

Therefore for distributed load from lift is calculated as:

$$q_L = 1.05 \cdot (m \cdot g \cdot n_1) \cdot c_L(y) \cdot c(y) \quad (5.25)$$

Where:

c_{Lc} Local lift coefficient of normal lift distribution from Lifting line theory [-]

c Local wing chord [m]

Load from wing mass distribution is then calculated as:

$$q_w = n \cdot q_{mw} \cdot g \quad (5.26)$$

Where:

n Load factor

q_{mw} Distributed load from wing mass [kg]

g Gravitational acceleration [m/s^2]

Load from fuel mass distribution is then calculated as:

$$q_f = n \cdot q_{mf} \cdot g \quad (5.27)$$

Where:

q_{mf} Distributed load from fuel mass [kg]

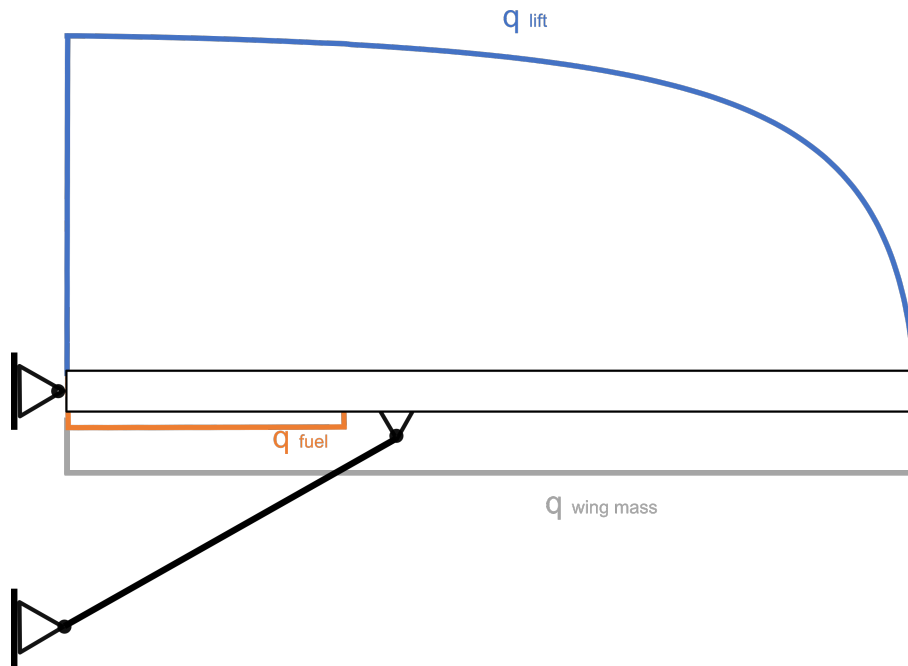


Figure 5.9: Wing loading

Shear force is then calculated according to Schwendler's theorem as:

$$T_n = \int_0^{l/2} (q_L - q_w - q_f) dy \quad (5.28)$$

Where:

$l/2$ Half of wingspan [m]

Bending moment is calculated similarly:

$$M_n = \int_0^{l/2} T_z dy \quad (5.29)$$

Aircraft is equipped with simple strut connected onto main spar. Strut is going to influence shear force and bending moment distribution from strut joint to the wing root. To calculate real shear force and bending moment distribution modifications in freebody diagram has made:

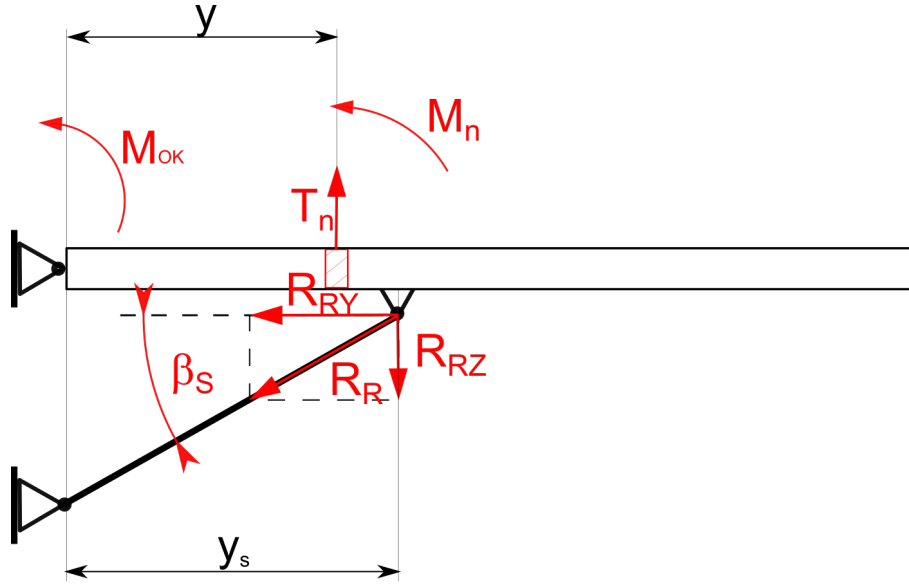


Figure 5.10: Freebody diagram of wing equipped with simple strut

Shear force induced by strut is calculated as:

$$R_{RZ} = \frac{M_{OK}}{y_s} \quad (5.30)$$

Where:

M_{OK} Bending moment from eqn. (5.29) at the wing root

y_s Strut location

Resulting shear force is then calculated as:

$$T_R = T_z - R_{RZ} \quad (5.31)$$

T_z shear force from eqn. (5.28)

Resulting bending moment is calculated as:

$$M_R = M_n - R_{RZ} \cdot (y_s - y) \quad (5.32)$$

Final shear force and bending moment distribution can be seen in fig. 5.11.

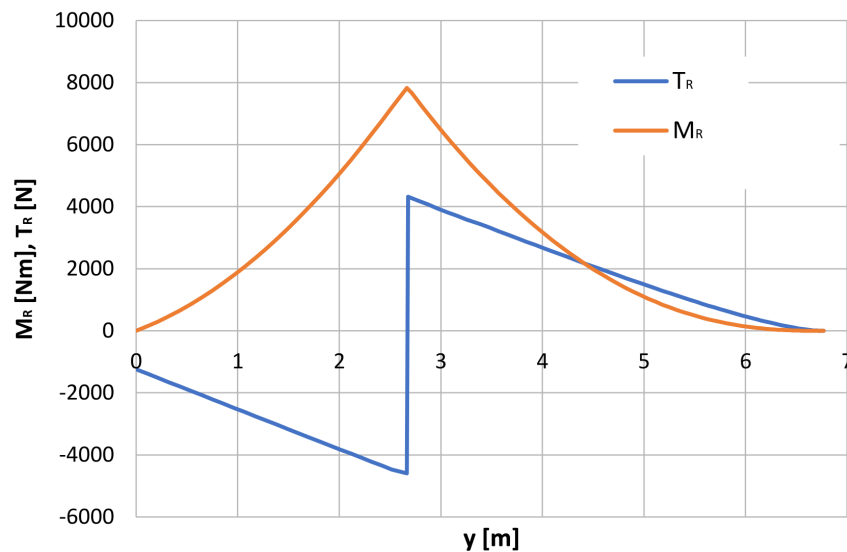


Figure 5.11: Final shear force and bending moment distribution

5.3.3 Load case 2: Ground loads

Ground loading is substantial for calculation of landing and taxi damage. Wing is in this case loaded only with wing and fuel mass. Assumed mass distribution can be seen in fig. 5.12.

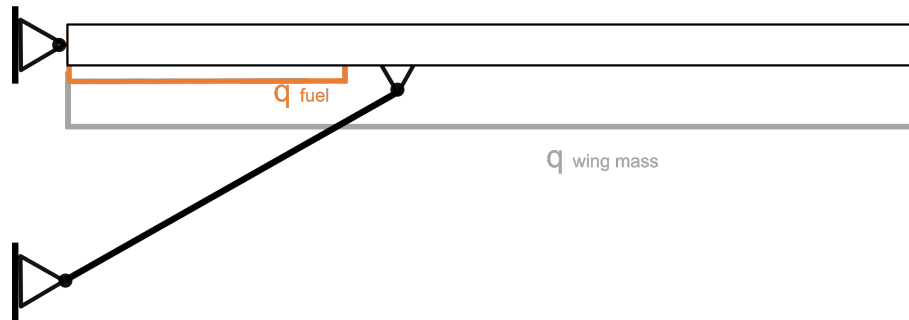


Figure 5.12: Ground load

Rest of calculation is similar to sec. 5.3.2, therefore will be not repeated. Resulting bending moment and shear force distribution can be seen in fig. 5.13

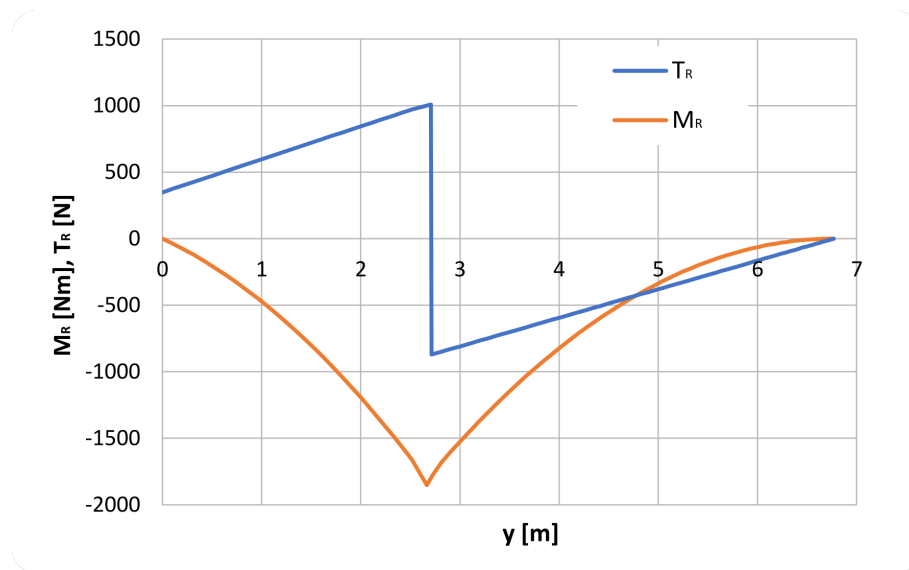


Figure 5.13: Bending moment and shear force results for ground loading

5.3.4 Critical cross-section choice

Selection of critical cross-sections was done according to two criteria:

1. bending moment M_n magnitude (it tends most critical loading of wing structure)
2. change cross-section surface (change of cross-section surface is closely related to change of second moment of inertia therefore is related bending stress)

Bending moment distribution was taken load case 1 from sec. 5.3.2. According to aircraft documentation was performed cross-section surface change analysis in location of maximal bending moment and four most critical cross-sections were determined. Choice of critical cross-section can be seen in fig. 5.14.

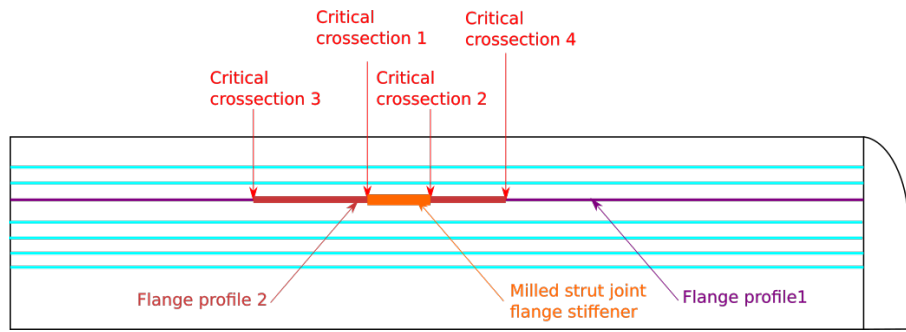


Figure 5.14: Critical cross-section selection

Four most critical locations are:

1. inner end of milled strut joint flange stiffener
2. outer end of milled strut joint flange stiffener
3. inner end of flange profile
4. outer end of flange profile

Bending moment and shear force was determined by linear interpolation.

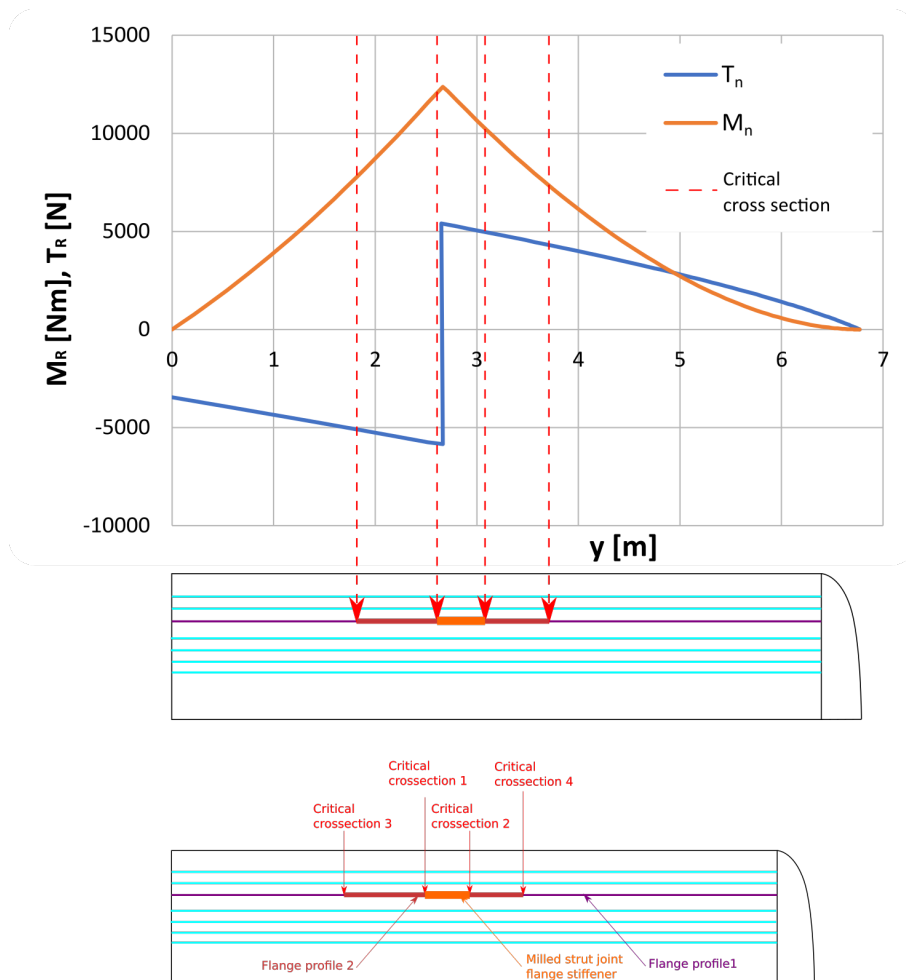


Figure 5.15: Critical correction bending moment and shear force determination

On each of cross-section was performed stress analysis. Detailed calculation will be described only for critical cross-section in load case 1 rest of calculation data is listed in

Appendix 1. For other load cases will be mentioned only final results. Exact dimensions and material characteristics will be not mentioned due to customer data classification.

5.3.5 Critical cross-section 1

Analysed cross-section is localised at the outer end of milled flange stiffener. Analysed cross-section can be seen in fig. 5.16. Important cross-section elements are denoted with arrow, rest of elements are denoted with colour.

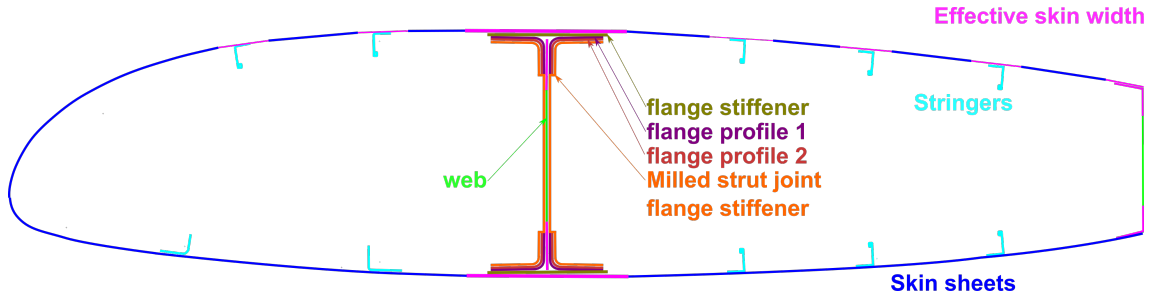


Figure 5.16: Wing spar strut connection location

Further calculation was based on bending stress analysis. Bending moment value was determined by interpolation as:

$$M_R = 9959 \text{ Nm}$$

Material characteristic of every cross-section element were determined:

- compression loaded section of cross-section
 - stringers and flange profiles - critical stress was determined as crippling stress with methods mentioned in [15] averaged with contribution of effective skin width, according to [16] as:

$$w = 30 \cdot t$$

Where t is skin thickness. Critical stress of effective skin width was calculated as inter-rivet buckling stress according to methods from [15].

- rest of skin - critical stress was determined as thin sheet buckling according to methods listed in [4]
- tension loaded section of cross-section - as critical stress was considered ultimate strength of material.

Bending stress of each element was calculated as:

$$\sigma_i = \frac{M_R \cdot z_i}{J_{css1}} \quad (5.33)$$

Where:

M_R Bending moment at the cross-section location [Nm]

z_i z Coordinate CG (Center of gravity) of element i [m]

J_{css1} Second moment of inertia of cross-section [m⁴]

To determine second moment of area first we have to determine CG of every cross-section element. In next step is important to determine CG of entire cross-section as:

$$z_{CG} = \frac{\sum_{i=1}^n z_i \cdot S_i}{\sum_{i=1}^n S_i} \quad (5.34)$$

Where:

z_i Coordinate of CG of every cross-section element[m]

S_i Surface CG of every cross-section element[m²]

Second moment of area is then calculated as:

$$J_{css1} = \sum_{i=1}^n z_i^2 \cdot S_i \quad (5.35)$$

Numbering of elements in critical cross-section is done according to fig. 5.17.

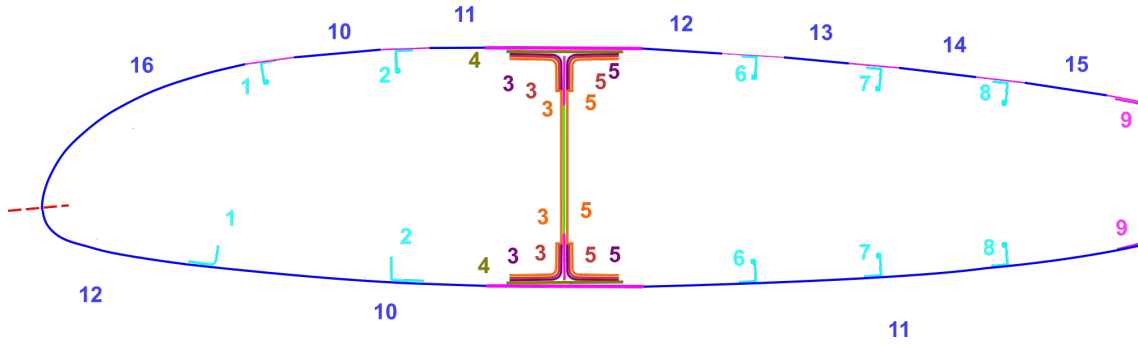


Figure 5.17: Cross-section elements numbering

Results of stresses are plotted in tab. 5.8 for upper and 5.9 lower section.

Table 5.8: Upper section stress analysis

No.	Element	σ_c [MPa]	σ [MPa]
1	Stringer 1	-232	-19
2	Stringer 2	-217	-22
3	Flange 3	-256	-22
4	Stiffening sheet 4	-233	-26
5	Flange 5	-260	-22
6	Stringer 6	-252	-21
7	Stringer 7	-252	-18
8	Stringer 8	-252	-14
9	2nd Flange	-265	-20
10	Skin 1	-48	-25
11	Skin 2	-43	-25
12	Skin 3	-29	-26
13	Skin 4	-42	-23
14	Skin 5	-41	-20
15	Skin 6	-33	-18
16	LE Skin	-91	-7

Table 5.9: Lower section stress results

No.	Element	σ_c [MPa]	σ [MPa]
1	Stringer 1	430	22
2	Stringer 2	430	25
3	Flange 3~	430	25
4	Stiffening sheet 4	430	28
5	Flange 5~	430	25
6	Stringer 6	430	26
7	Stringer 7	430	26
8	Stringer 8	430	25
9	2nd Flange	430	24
10	Skin 1	430	27
11	Skin 2	430	25
12	LE skin	430	16

Fatigue cracks are usually initiated by tension, therefore critical element of the cross-section for fatigue analysis, would be element with highest stress on lower side of cross-section. Element no. 4, flange stiffening sheet is therefore considered as critical cross-section element.

For fatigue calculations is important according to [8] extrapolate stress on edge fibre of element. For such calculation is needed to substitute coordinate of CG of cross-section in eqn. (5.33) with coordinate of edge fibre, recalculated edge fibre stress is:

$$\sigma_{LC1} = 28 \text{ MPa}$$

For fatigue safe-life calculation is also important ground stress result. Calculation was done in same way, only changed parameter was the bending moment. Bending moment was taken from Load case 2. Resulting bending moment was:

$$M_R = -1794 \text{ Nm}$$

Calculated ground stress on Flange stiffening sheet is then:

$$\sigma_{LC2} = -5 \text{ MPa}$$

5.3.6 Critical cross-section 2

Second closest spot to the bending moment maximum with reduction in cross-section surface was considered outer end of milled strut joint flange stiffener. Layout of reduced cross-section can be seen in fig. 5.18.

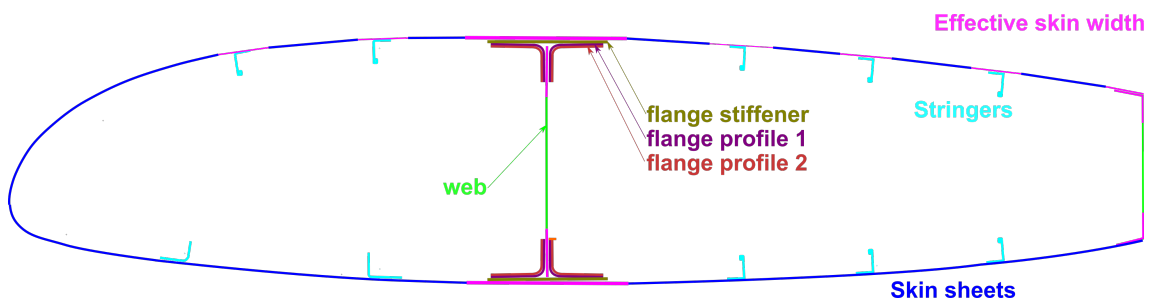


Figure 5.18: Critical cross-section 2

Interpolated moment in location of critical cross-section 2 is:

$$M_R = 7109 \text{ Nm}$$

After stress calculation Element no. 4, flange stiffening sheet is again considered as critical cross-section element because of its position with the biggest effective beam height.

Load case 1 stress is after edge fibre recalculation:

$$\sigma_{LC1} = 20 \text{ MPa}$$

For fatigue safe-life calculation is also important ground stress result. Calculation was done in same way, only changed parameter was the bending moment. Bending moment was taken from Load case 2. Resulting bending moment was:

$$M_R = -1794 \text{ Nm}$$

Calculated ground stress on Flange stiffening sheet is then:

$$\sigma_{LC2} = -4 \text{ MPa}$$

5.3.7 Critical cross-section 3

Third closest spot to the bending moment maximum with reduction in cross-section surface was considered inner end of flange profile. Layout of reduced cross-section can be seen in fig. 5.19.

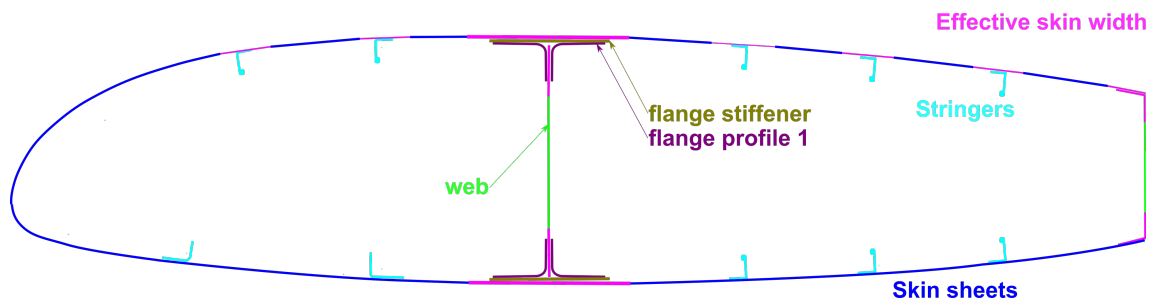


Figure 5.19: Critical cross-section 3

Interpolated moment in location of critical cross-section 3 is:

$$M_R = 6354 \text{ Nm}$$

After stress calculation, flange stiffening sheet is again considered as critical cross-section element.

Load case 1 stress is after edge fibre recalculation:

$$\sigma_{LC1} = 21 \text{ MPa}$$

For fatigue safe-life calculation is also important ground stress result. Calculation was done in same way, only changed parameter was the bending moment. Bending moment was taken from Load case 2. Resulting bending moment was:

$$M_R = -1046 \text{ Nm}$$

Calculated ground stress on Flange stiffening sheet is then:

$$\sigma_{LC2} = -4 \text{ MPa}$$

5.3.8 Critical cross-section 4

Fourth closest spot to the bending moment maximum with reduction in cross-section surface was considered outer end of flange profile. Layout of reduced cross-section can be seen in fig. 5.20.

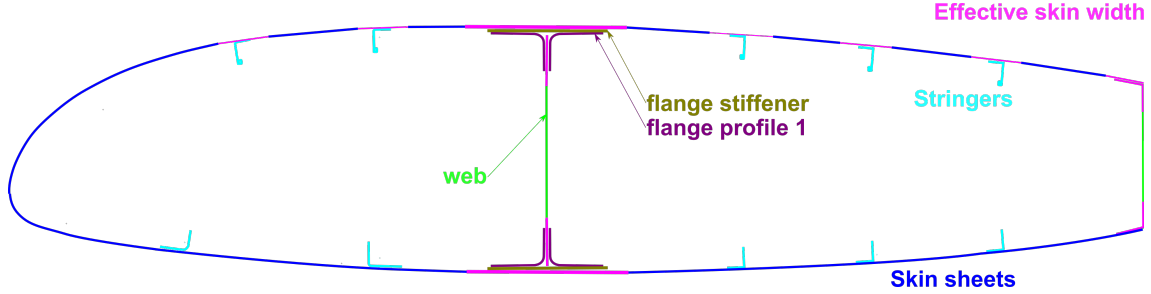


Figure 5.20: Critical cross-section 4

Interpolated moment in location of critical cross-section 4 is:

$$M_R = 5913 \text{ Nm}$$

After stress calculation Element no. 4, flange stiffening sheet is again considered as critical cross-section element.

Load case 1 stress is after edge fibre recalculation:

$$\sigma_{LC1} = 22 \text{ MPa}$$

For fatigue safe-life calculation is also important ground stress result. Calculation was done in same way, only changed parameter was the bending moment. Bending moment was taken from Load case 2. Resulting bending moment was:

$$M_R = -1116 \text{ Nm}$$

Calculated ground stress on Flange stiffening sheet is then:

$$\sigma_{LC2} = -4 \text{ MPa}$$

5.3.9 Stress analysis conclusion

Comparison of Load case 1 (1g) stresses was performed after stress calculation. On basis of this comparison was chosen critical cross-section. As the most critical was the cross-section 1 with the highest stress in element called flange stiffening sheet.

Table 5.10: Stresses summary of all critical cross-sections

Critical cross section no.	σ_{LC1} [MPa]	σ_{LC2} [MPa]
1.	28	-5
2.	20	-4
3.	21	-4
4.	22	-4

Therefore stress used for fatigue safe-life calculation is:

$$\begin{aligned} \sigma_{1g} &= 28 \text{ MPa} \\ \sigma_{min} &= -5 \text{ MPa} \end{aligned} \tag{5.36}$$

Critical cross-section was inspected in TC holder hangar in Hradec Kralove. Critical cross-section spot outside view can be seen in fig. 5.21. Wing structure could not be further disassembled, only more detailed inside view of strut joint can be taken.



Figure 5.21: Critical cross-section detail on spot inspection



Figure 5.22: Strut joint inspection

6 Damage calculation software development

To calculate safe-life of wing structure it was important to have some software tools on hand to automate calculation. Calculation by hand would be unacceptable. Need for development of damage evaluation software caused by the fact, that ACE 100 software could not satisfy all requirements of calculation. These requirements were connected mainly with specific mission profile (mainly changes in aircraft weight). Software had to be capable of dividing mission profile into 5 phases. These phases were presented in sec. 5.1.1. Software development was done on basis of ACE 100 program and its documentation [2]. Development of damage calculation software was done using well known spreadsheet processor MS Excel. Software was upgraded with custom Python and VBA scripts for more intuitive workflow. Results of program ACE 100 [2] will be, from now on, plotted along with calculation results to verify analytic calculation results. ACE 100 would be further stated as program and developed software as analytic calculation.

6.1 Used spectra

Spectra from [30] were chosen for because they are compatible with methods used in [2] and [30]. Spectra are divided according to 8 default plane categories:

1. Single-Engine Executive Usage (non-pressurized, engine size greater than 185 hp)
2. Single-Engine Personal Usage (non-pressurized, engine size less than or equal to 185 hp)
3. Single-Engine Instructional Usage (non-pressurized)
4. Single-Engine Acrobatic Usage (non-pressurized)
5. Twin-Engine General Usage (non-pressurized)
6. Twin-Engine Instructional Usage (non-pressurized)
7. Pressurized Usage
8. Special Usage (including survey and aerial application)

Table 6.1: Excerpt form flight spectra choice guide [30]

Flight Spectra, General Usage, Single-Engine Unpressurized			
Description	Graphic Data	Tabulated Data	Comments
Manoeuvre spectra for single-engine executive usage.	Figure A1-4	Table A1-4	An airplane in the executive usage category has a single, reciprocating engine with more than 185 horsepower. The executive usage category also includes unpressurized, single-engine turboprop airplanes.

Single-engine executive usage profile was chosen on bases of flight spectra choice guide presented in [30] (tab. 6.1). Description of profile which matches best SMG-92 Turbine

Finist. That is in compliance with aircraft power plant power, because it is single engine turboprop powered aircraft with power over 185 hp.

6.2 Used S-N curves

As for material characteristics have been chosen two S-N curve approaches. For sake of comparison one of approaches represents S-N curve obtained by measurements on certain structure and one obtained by measurements of single material. Both curves are suitable for use with nominal stress approach used in sec. 5.3.

6.2.1 Data Sheet E.02.01 S-N curve

For fatigue analysis the VZLU analytic description of E.02.01 S-N Curve was used as the first approach in this thesis. S-N curve shall be used for a wing calculation as well as for horizontal tail lift-surfaces. This S-N curve is represents entire aluminium alloy wing structure not only one material. The S-N curve is (based on VZLU investigation program [14]). This S-N curve is recommended for fatigue analysis by [30].

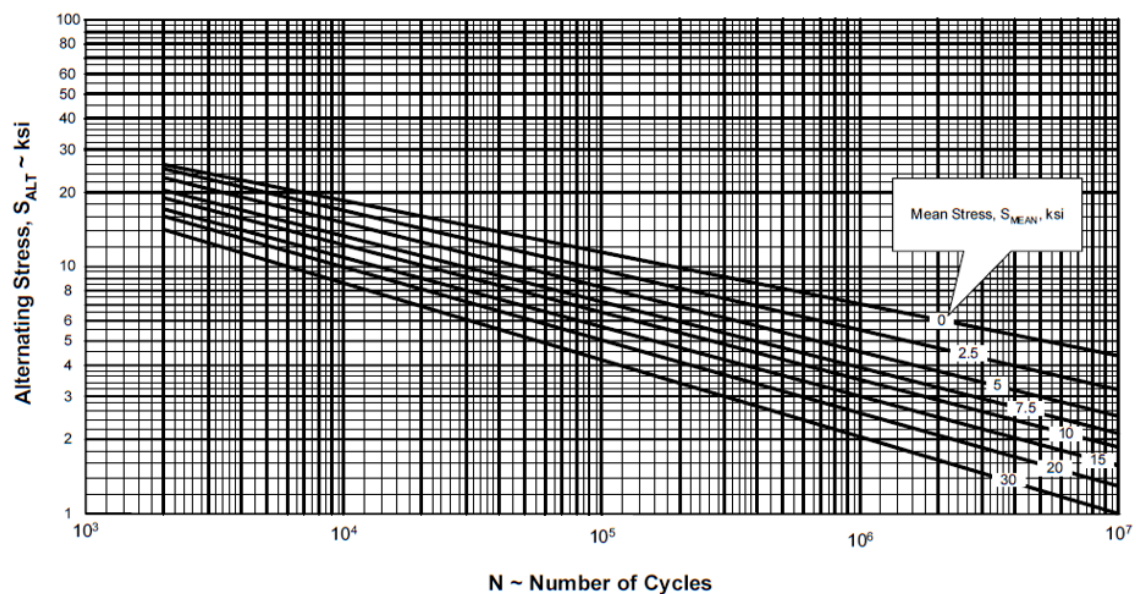


Figure 6.1: SN curve in semi-log scale [30]

6.2.2 Oding S-N curves

S-N curves used in Oding representation are dedicated to one material only. Oding representation is also specific with definition of mean stress influence, mentioned in sec. 2. Curves from [14] represents in contrast to [16] general S-N curve for whole construction. Curves are divided according to constructional zones, see in sec. 3.3.2.

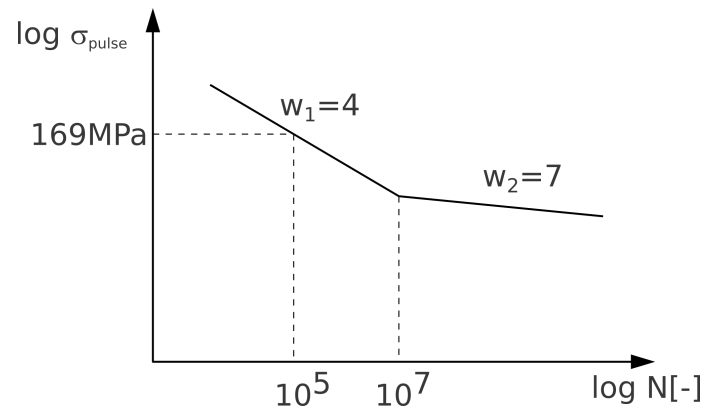


Figure 6.2: SN curve in semi-log scale from [16]

6.3 First iteration

First run was carried out based on ACE 100 program (mentioned in sec. 2.3) sample inputs, to simplify results verification and minimise error occurrence in calculation. Sample input values are taken from [2]. These values are recommended in [2] as values for example calculation. Values are presented in tab. 6.2.

Table 6.2: ACE100 sample input values from [2]

Flight Stress σ_{1g} [MPa]	51.5
Ground Stress σ_{min} [MPa]	-31
Average flight speed [KTAS]	148.5
Positive Gust Limit Load Factor	3.15
Negative Gust Limit Load Factor	-1.15
Positive Maneuver Limit Load Factor	3.80
Negative Maneuver Limit Load Factor	-1.52
Average flight duration	0.65

6.3.1 Spectra interpolation

Spectra used for calculation was taken from [30]. They are tabulated in certain increments acceleration fraction or sink velocity. Therefore they have to be interpolated to obtain exact values. Four methods comes into consideration for spectra interpolation. All methods are then compared in fig. 6.3.

- linear interpolation in Cartesian coordinates
- interpolation in semi-log coordinates
- linear interpolation in log-log coordinates

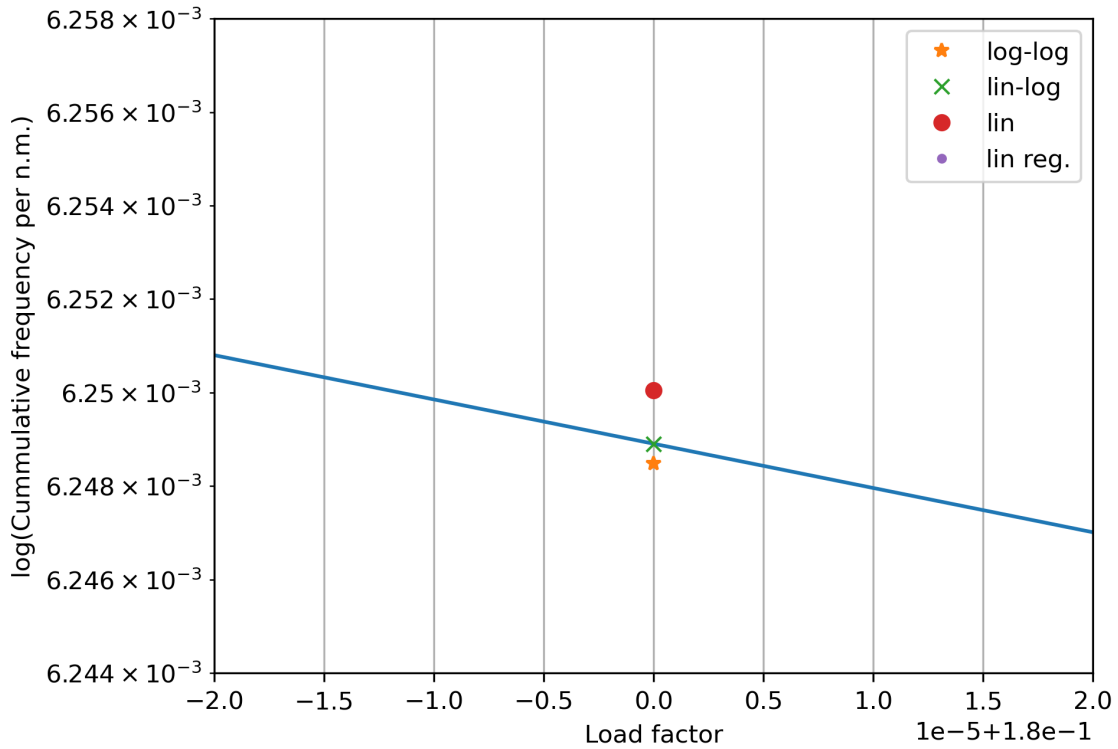


Figure 6.3: Comparison of interpolation methods

Linear interpolation in semi-log scale results in the least error, as can be seen in fig. 6.3. It is caused by the fact that spectra in literature, are mostly given in form of semi-log scale because of plotting convention. For further analysis linear interpolation in semi-log scale is used.

Spectra were divided into segments or blocks defined by increment of load factor or sink speed. Intervals were created according to division of tabulated values in [30].

- Gust, Manoeuvre and Taxi spectra were divided by 0.05 of positive increment of load factor
- Impact and rebound spectra were divided by 0.5 ft/s increment of sink rate

6.3.2 Gust and Maneuver

Gust and Manoeuvre damage evaluation starts with spectra in form of acceleration fraction ($\frac{a_n}{a_{nLLF}}$) values and Cumulative Frequency of Exceedance per Nautical Mile. From positive branch of spectra where taken midpoint of interval border. Load factors as an average of two successive values are showed in fig. 6.4 in red colour as step 1. Corresponding frequency per nautical mile and negative load factors were found using previously explained interpolation method in steps 2-4, because negative and positive values are connected with same cumulative frequency per nautical mile. This frequency is used only for interpolation purposes, due to method of interpolation, real cumulative freq is obtained as increment of cumulative frequency per nautical mile. Difference between midpoint of load factor and midpoint of cumulative freq per nautical mile can be clearly visible on block 1 in fig. 6.4.

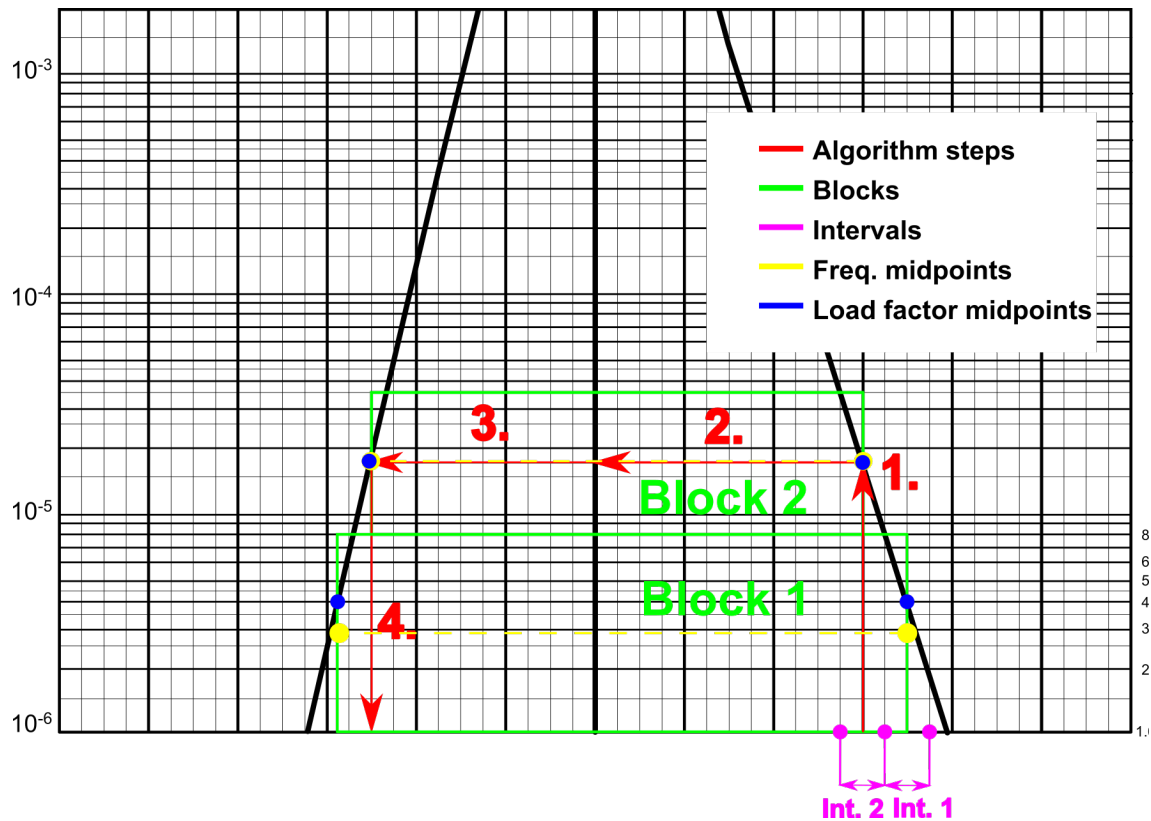


Figure 6.4: Graphical description of spectra processing

Program[2] and analytic calculation results were plotted in fig. 6.5 for gusts and fig. 6.6.

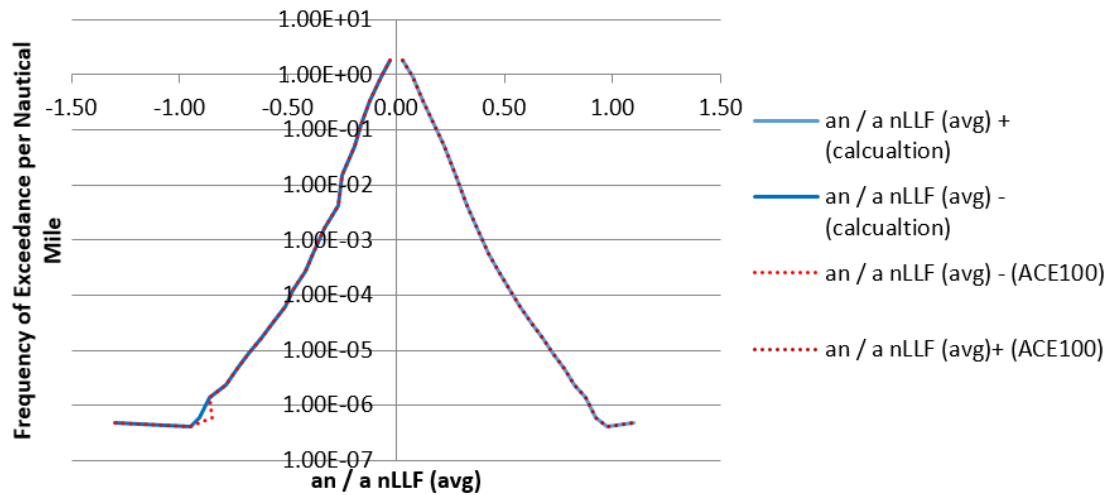


Figure 6.5: Comparison of gust spectra after interpolation

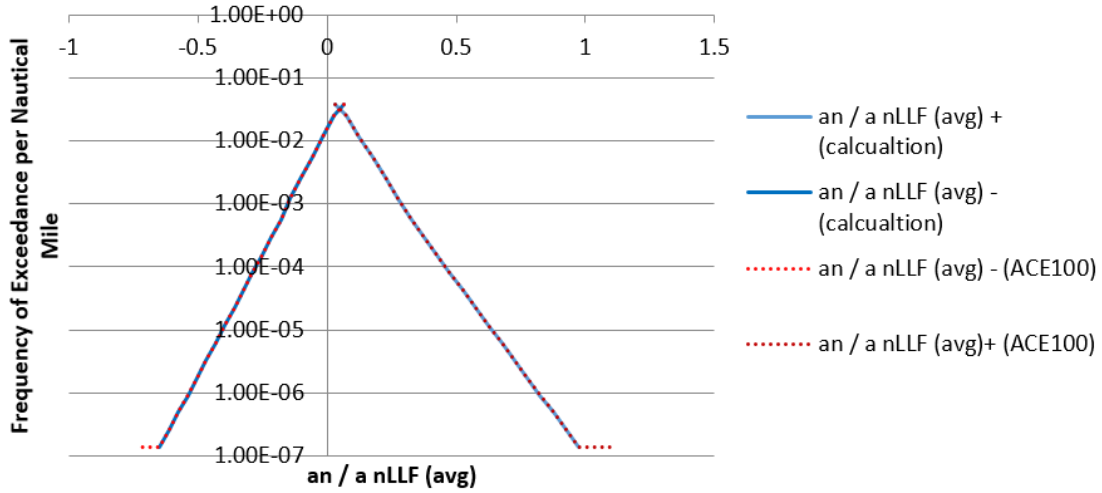


Figure 6.6: Comparison of manoeuvre spectra after interpolation

Goal of this calculation is to get spectra in form of coordinates of load factor and frequency per flight hour. For further calculation is needed:

- Gust limit load factor
- Manoeuvre limit load factor
- Average flight speed

Recalculation of load factor is performed for gusts as:

$$a_{n \text{ actual}} = a_{nLLF} \cdot \frac{\text{Gust Load Factor at Operating Weight}}{\text{Design Limit Gust Load Factor at Maximum Gross Weight}} \quad (6.1)$$

Similarly for manoeuvres:

$$a_{n \text{ actual}} = a_{nLLF} \cdot \frac{\text{Manoeuvre Load Factor at Operating Weight}}{\text{Design Limit Manoeuvre Load Factor at Max. Gross Weight}} \quad (6.2)$$

The comparison of two approaches - analytical and program [2] is shown in following figures.

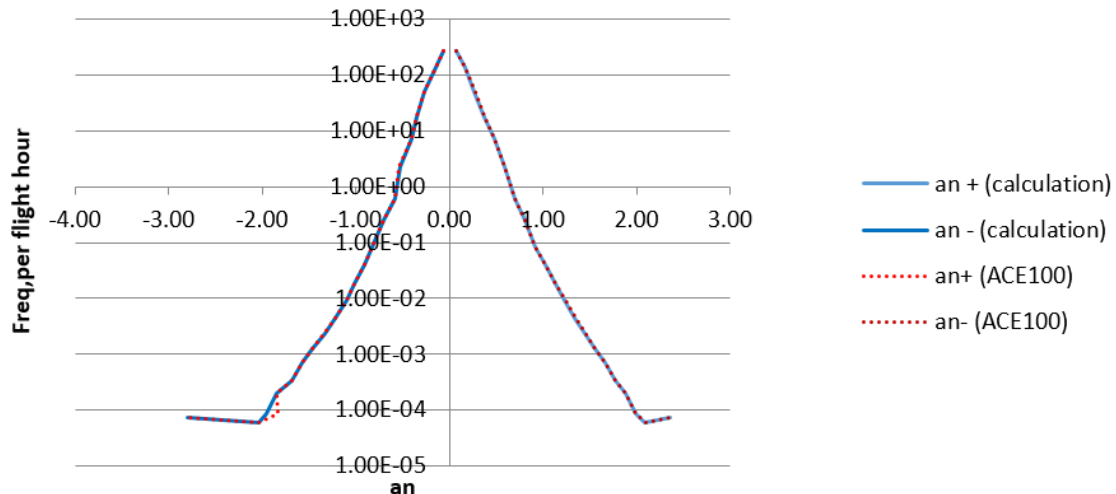


Figure 6.7: Gust load factor spectra benchmark

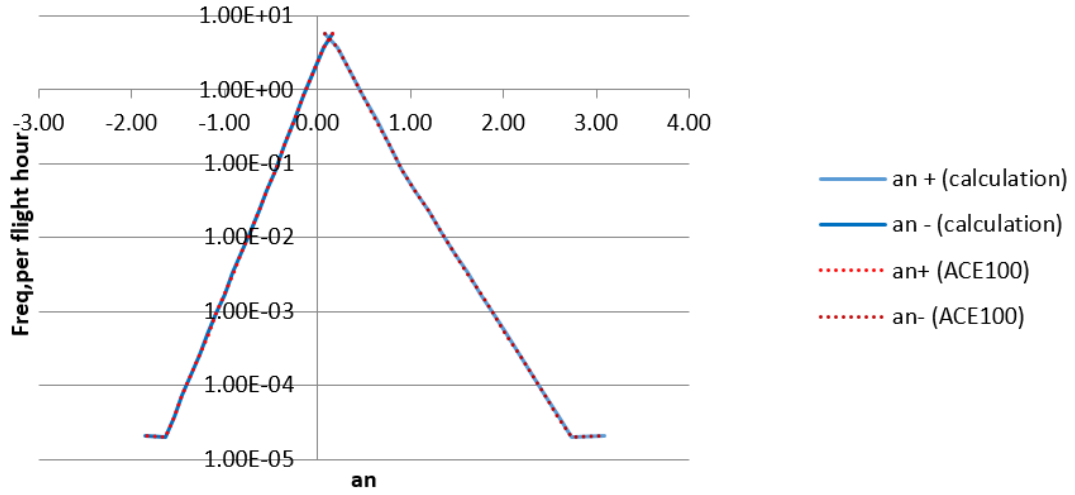


Figure 6.8: Manoeuvre spectra benchmark

Recalculation of frequency per n. m. on freq per flight hour is done using formula:

$$f_{per\ hour} = f_{per\ nautical\ mile} \cdot v_{KTAS} \quad (6.3)$$

Stress was used 1g stress for recalculation of load factors. It is assumed that stress is linear relationship between load factor and stress. Therefore the stress deviation can be calculated ($\Delta\sigma_{actual}$) as:

$$\Delta\sigma_{actual} = \sigma_{1g} \cdot a_{n\ actual} \quad (6.4)$$

σ_{1g} Stress obtained in 1g loading [MPa]

$a_{n\ actual}$ Actual load factor from load spectra [-]

From eqn. (6.4) is obtained negative and positive load has to be recalculated into standard form (cycle characterised with stress amplitude (σ_a) and mean stress (σ_m)) used for damage calculation formulated in eqn. (3.1) and (3.1).

- mean stress is calculated using eqn. (3.1).

$$\sigma_m = \sigma_{1g} + \frac{\Delta\sigma_{pos} + \Delta\sigma_{neg}}{2} \quad (6.5)$$

- stress amplitude is simply calculated using eqn. (3.1).

$$\sigma_a = \frac{\Delta\sigma_{pos} + \Delta\sigma_{neg}}{2} \quad (6.6)$$

Comparison between program [2] and calculation was performed in fig. 6.9 and 6.10.

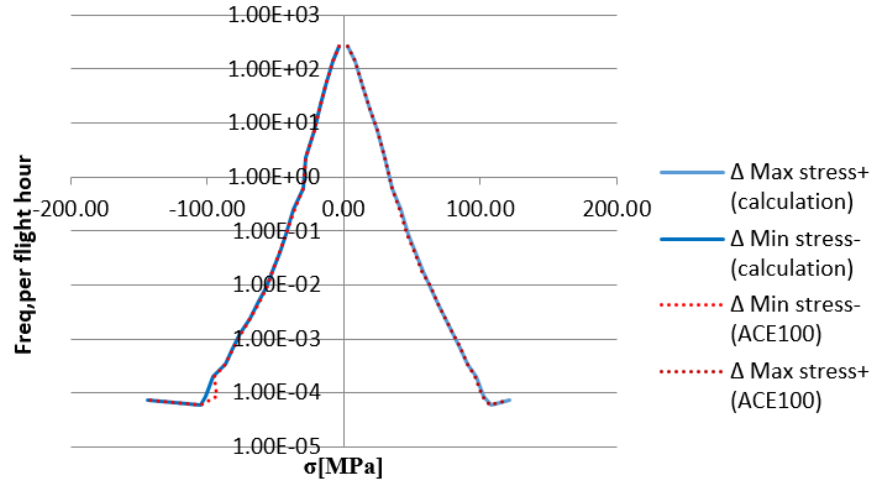


Figure 6.9: Gust spectra benchmark with recalculated stress and frequency per flight

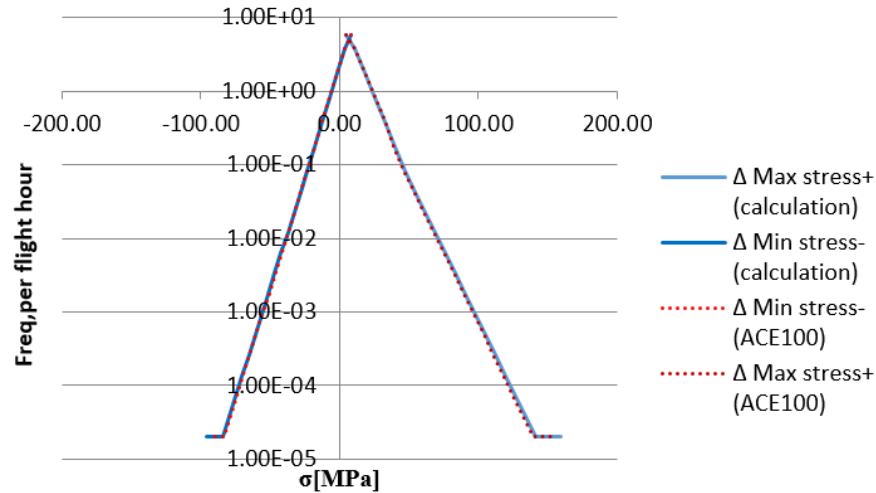


Figure 6.10: Manoeuvre spectra benchmark with recalculated stress and frequency per flight

6.3.3 Taxi

Taxi spectra can be used without interpolation (directly from [30]), only values of load factor and cumulative frequency has to be processed into blocks like in case of gusts in fig. 6.4. Frequency per 10000 landings has to be unified for damage calculation as:

$$f_{per\ hour} = \frac{f_{per\ 10000\ landing}}{flight\ duration} \quad (6.7)$$

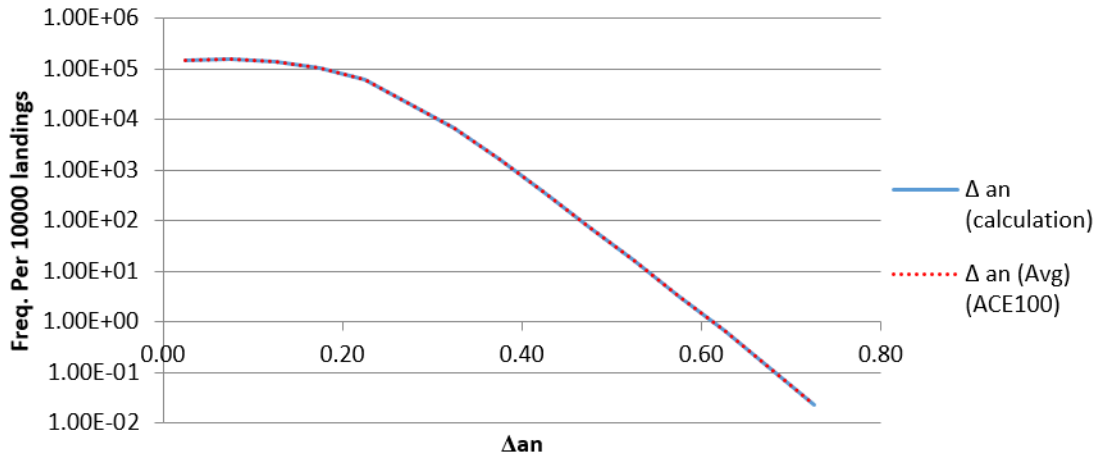


Figure 6.11: Comparison of taxi inputs

Recalculation of stresses is performed with ground stress σ_{min} . Parameters of cycle are calculated as:

$$\sigma_m = \sigma_{min}$$

$$\sigma_a = ABS(\sigma_{min}) \cdot \Delta g$$

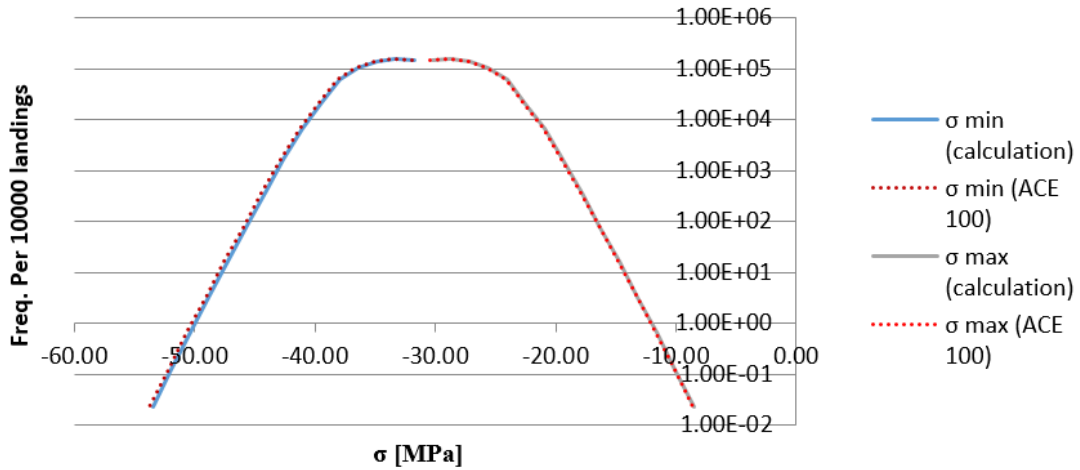


Figure 6.12: Taxi spectra benchmark with recalculated stress and frequency per flight

6.3.4 Impact and rebound

Impact and rebound spectra are expressing loads acting on aircraft during landing. This part of spectra requires different kind of processing. It is given in form of cumulative freq per 10000 landings. That can be simply recalculated as in case of Taxi according to eqn. 6.7. Special is that the load factor values were gained from values of sink rate. Calculation input values were plotted in fig. 6.13.

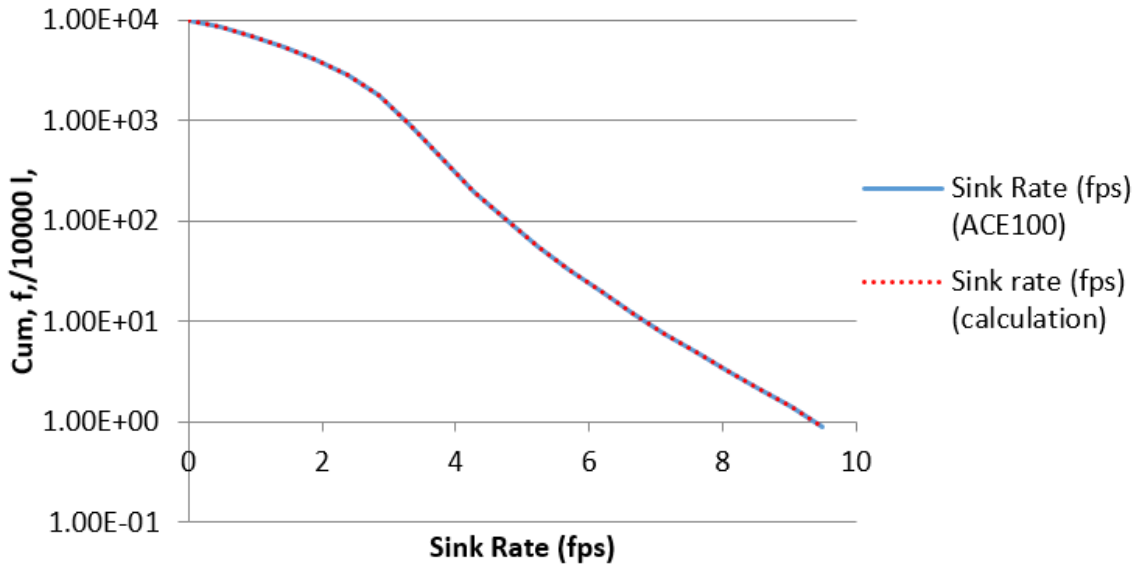


Figure 6.13: Impact and rebound spectra input comparison

FAA recommends using simple linear relationship between sink rate and load factor in form of eqn. 6.8. This approach is therefore used for purposes of thesis.

$$a_n = 1 + 0.3 \cdot v_{sink} \quad (6.8)$$

v_{sink} sink velocity [ft/s]

After this recalculation spectra were compared in fig. 6.14.

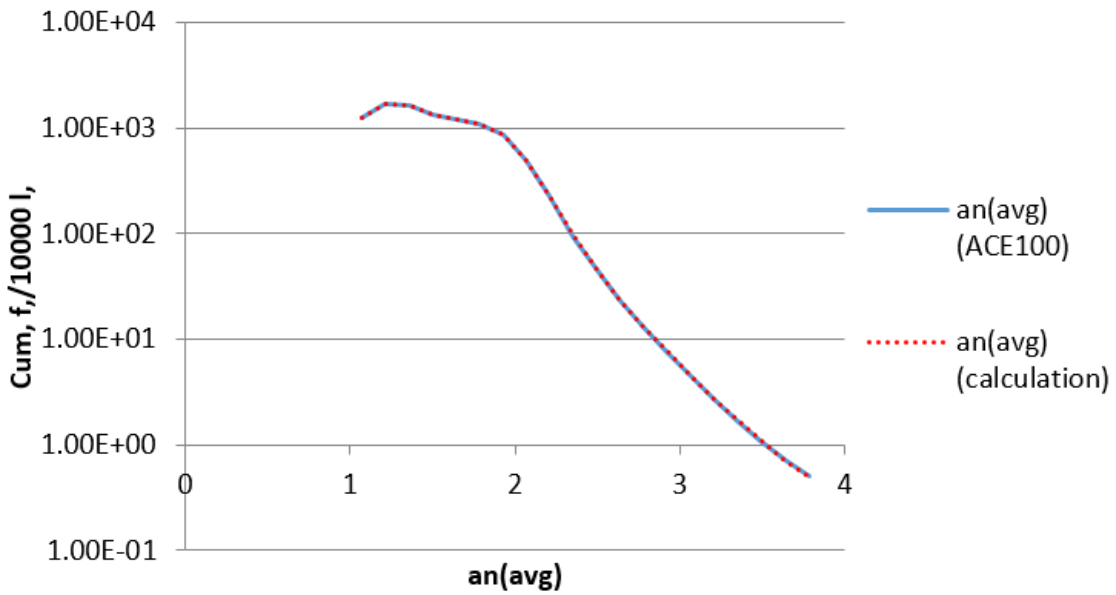


Figure 6.14: Comparison after sink rate recalculation

Division on impact and rebound spectra is performed in recalculation onto stresses. Load factor gained from previous calculation is used for formulation of minimal stresses, there-

fore is necessary to use minimal stress input value (table 6.2) and recalculate stresses according to eqn. 6.9.

$$\sigma_{min \ imp} = a_n \cdot \sigma_{min} \quad (6.9)$$

$\sigma_{min \ imp}$ Actual stress value [MPa]

σ_{min} Max stress value [MPa]

Maximal stress value of impact cycle is considered to be constant and is calculated as:

$$\sigma_{max \ imp} = 2/3 \cdot \sigma_{1g}$$

Where:

σ_{1g} 1g stress value [MPa]

For recalculation on rebound cycle mean stress and stress amplitude has to be determined according to equations (3.1) and (3.1). Rebound spectra is derived from Impact spectra. They have both same mean stress but rebound amplitude is calculated according to eqn. (6.10). Benchmark of analytic calculation and program spectra was performed in fig. 6.15.

$$\sigma_a \ rbnd = 0.6 \cdot \sigma_a \ impact \quad (6.10)$$

Where:

$\sigma_a \ impact$ Value of impact stress amplitude [MPa]

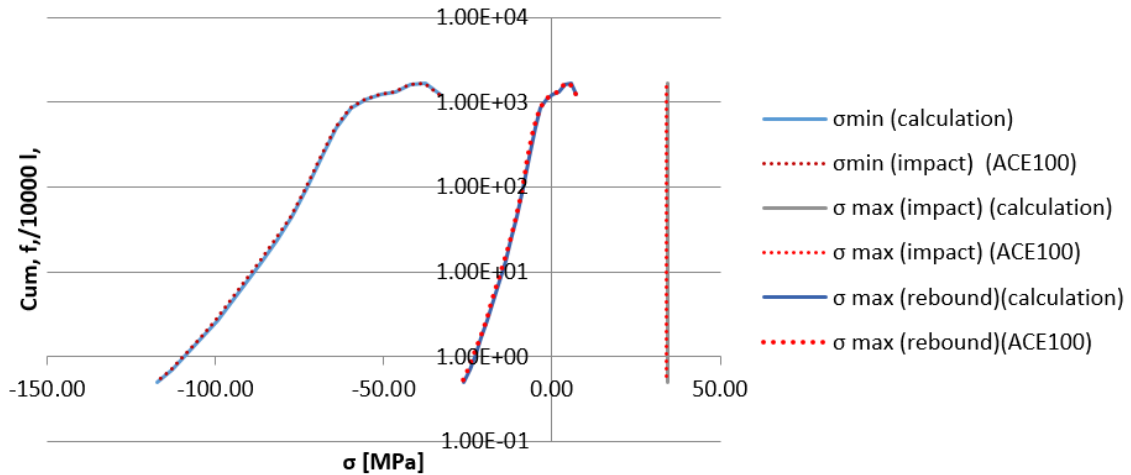


Figure 6.15: Impact and rebound spectra comparison after stress recalculation

6.3.5 GAG cycle

For this calculation is supposed that desired cumulative frequency per flight is equal to 1. Calculation is divided into 2 sections:

- **Max. stress cycle** - that represents superposition of positive stress branch of Manoeuvre and Gust spectra. Spectra are superposed using linear interpolation in semi-log. Interpolation and subsequent summation is showed in fig. 6.16.

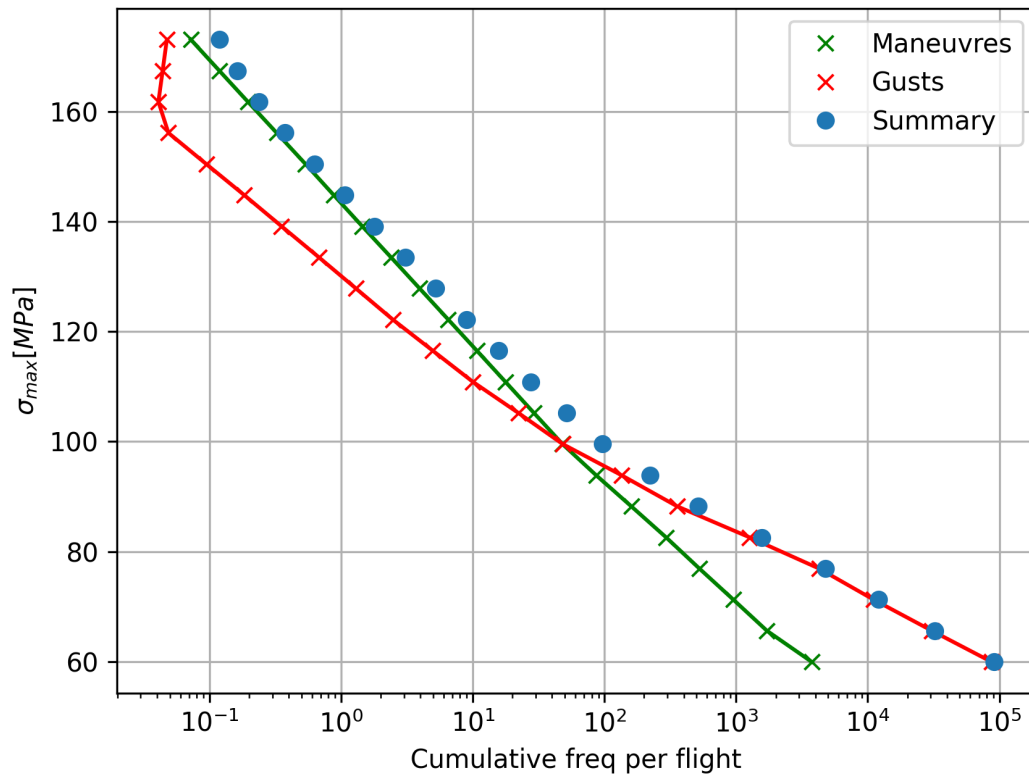


Figure 6.16: Superposition and summation of max stress cycle

- **Min. stress cycle** - which represents superposition of negative stress branch Impact, Rebound and Taxi spectra. Min. stress branch is processed and superposed in fig. 6.17.

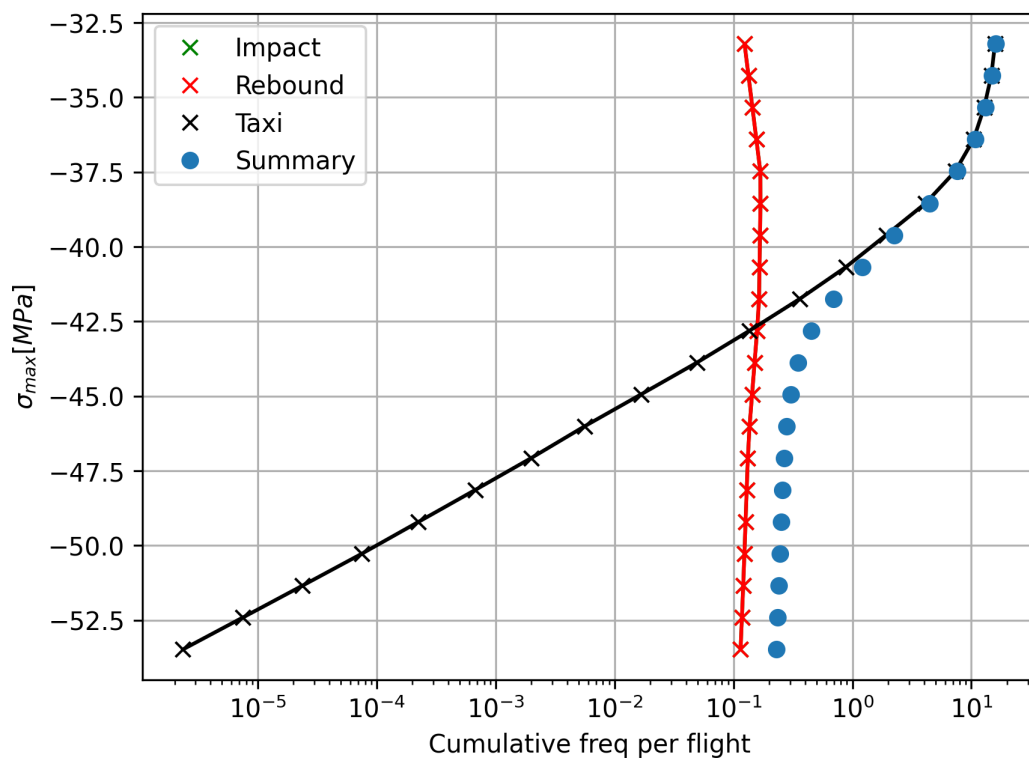


Figure 6.17: Superposition and summation of min stress cycle

From superposed cycle is interpolated each stress corresponding to cumulative frequency per flight $f_{per\ flight} = 1$ which was chosen according to the [30]. Plot of results can be seen in fig 6.18.

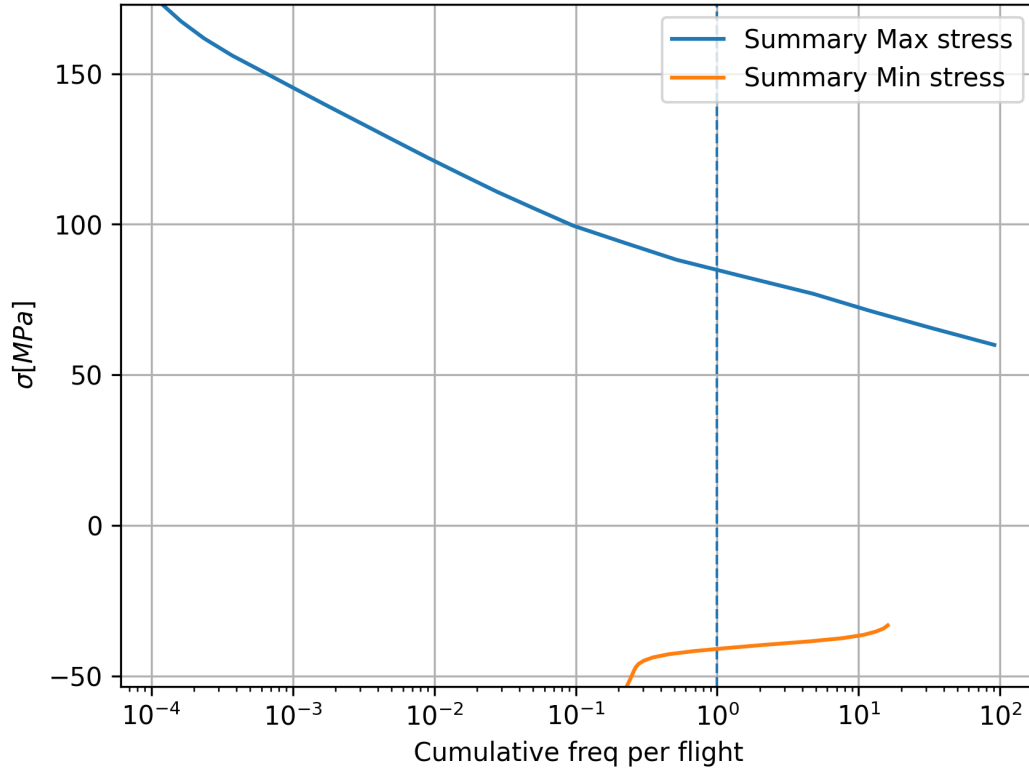


Figure 6.18: Superposed GAG cycle interpolation

Results from ACE 100 program are compared with calculation results in tab. 6.3.

Table 6.3: GAG cycle stress results

Source	$\sigma_{\min\ GAG}$ [MPa]	$\sigma_{\max\ GAG}$ [MPa]
Calculation	-41	85
Program	-42	84

Result are reasonably correlated with program output values.

6.3.6 Damage calculation

From spectra can be calculated damage, after successful preparation in form of stress cycles (σ_a and σ_m) and frequency per flight. Damage is calculated according to Palmgren-Miner rule, see eqn. (3.15).

$$D = \sum_{i=1}^n \frac{n_i}{N_i}$$

Where n_i is substituted with cumulative frequency per flight $f_{per\ flight}$ and N_i is substituted with cycles to failure from S-N curve. Process of damage calculation is visualised in fig 6.19.

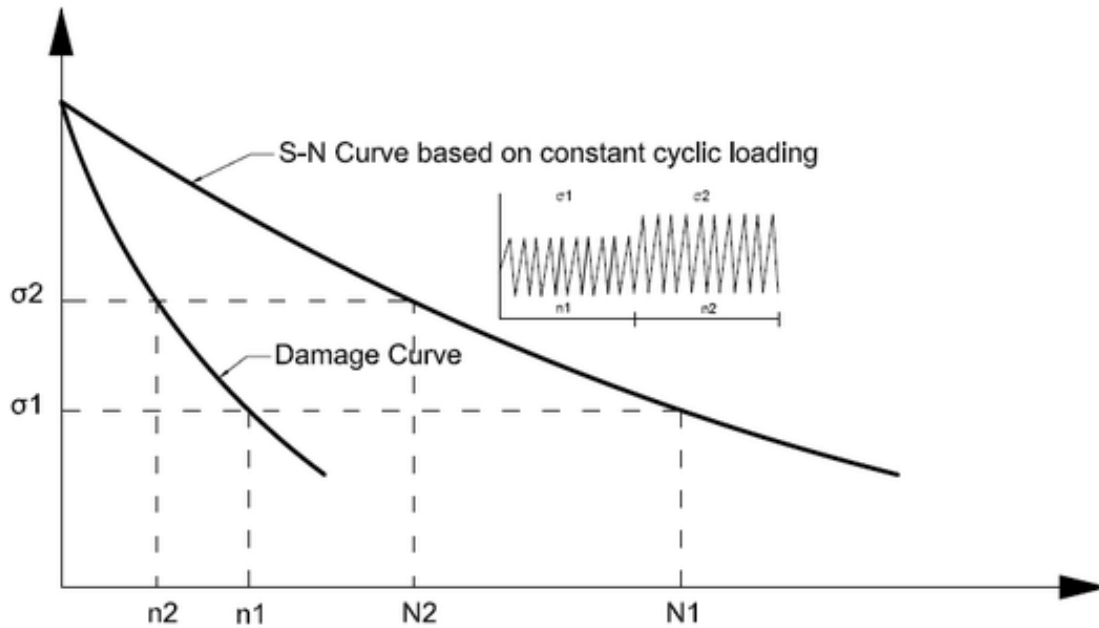


Figure 6.19: Visualisation of Palmgren Miner rule [6]

Damage results comparison with ACE100 values was performed and results were summarized in tab. 6.4. Major components of spectra (Gust, Manouver and GAG) are giving maximal error of 6%. This compliance is great considering that analytic description of Data Sheet E.02.01 S-N curve used in analytic calculation is probably different from ACE 100 program S-N curve description.

Table 6.4: Calculation result summary [2]

	Calculation			ACE 100	
	D[h⁻¹]	D [1000h⁻¹]	D[%]	D [h⁻¹]	D[%]
Gust	2.22E-05	2.22E-02	58.60	2.13E-05	57.55
Maneuver	2.52E-06	2.52E-03	6.66	2.37E-06	6.40
Taxi	1.62E-10	1.62E-07	0.00	7.18E-10	0.00
Impact	3.35E-07	3.35E-04	0.89	2.36E-07	0.64
Rebound	5.06E-09	5.06E-06	0.01	2.94E-09	0.01
GAG	1.28E-05	1.28E-02	33.83	1.31E-05	35.40
Summary	3.78E-05	-	-	3.70E-05	-

6.4 Second iteration

Second iteration of spectra damage calculation development was focused on tuning of calculation algorithm for more accurate results. Only changes in calculation algorithm will be presented, rest of algorithm will stay the same.

First change was connected with source spectra. The source spectra from [2] were substituted with newer more spectra from [30]. Comparison of spectra was performed in fig. 6.20, 6.21, 6.22, 6.23.

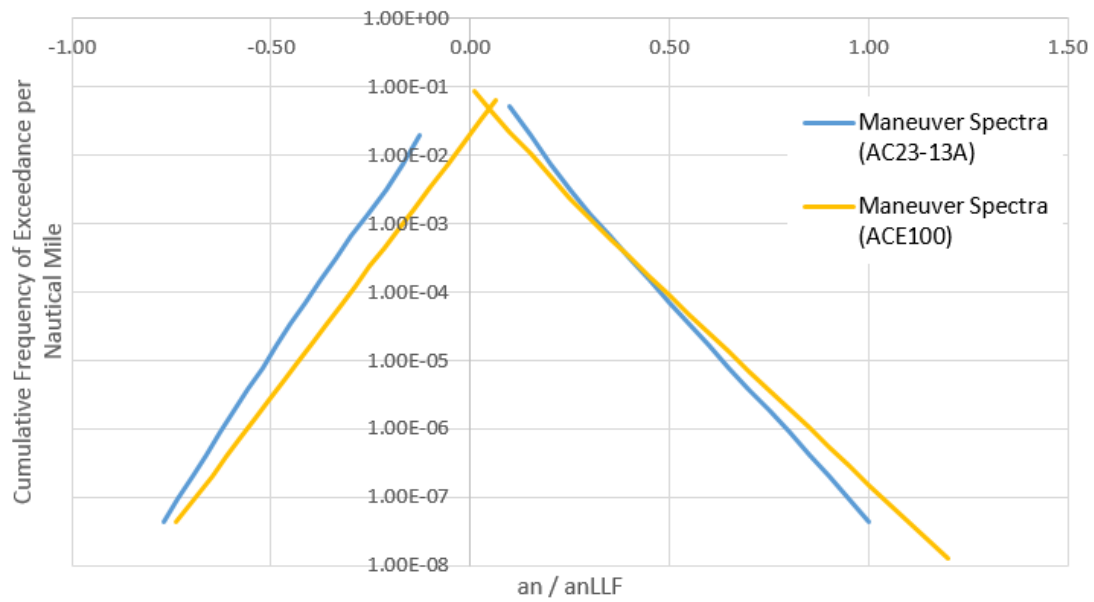


Figure 6.20: Manoeuvre [30] and [2] comparison

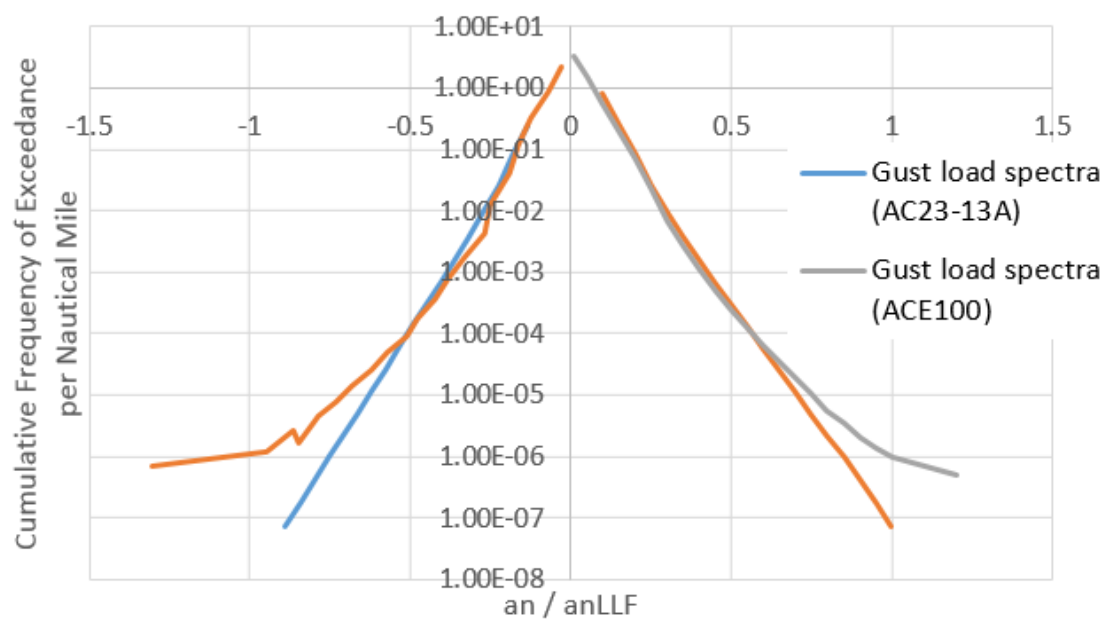


Figure 6.21: Gust [30] and [2] comparison

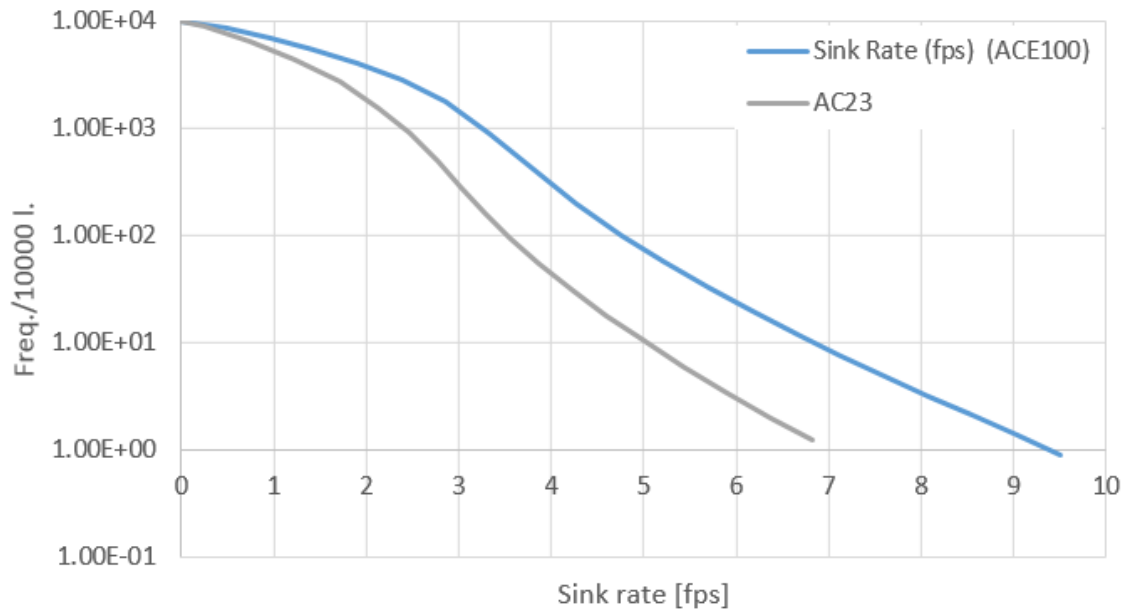


Figure 6.22: Impact and Rebound [30] and [2] comparison

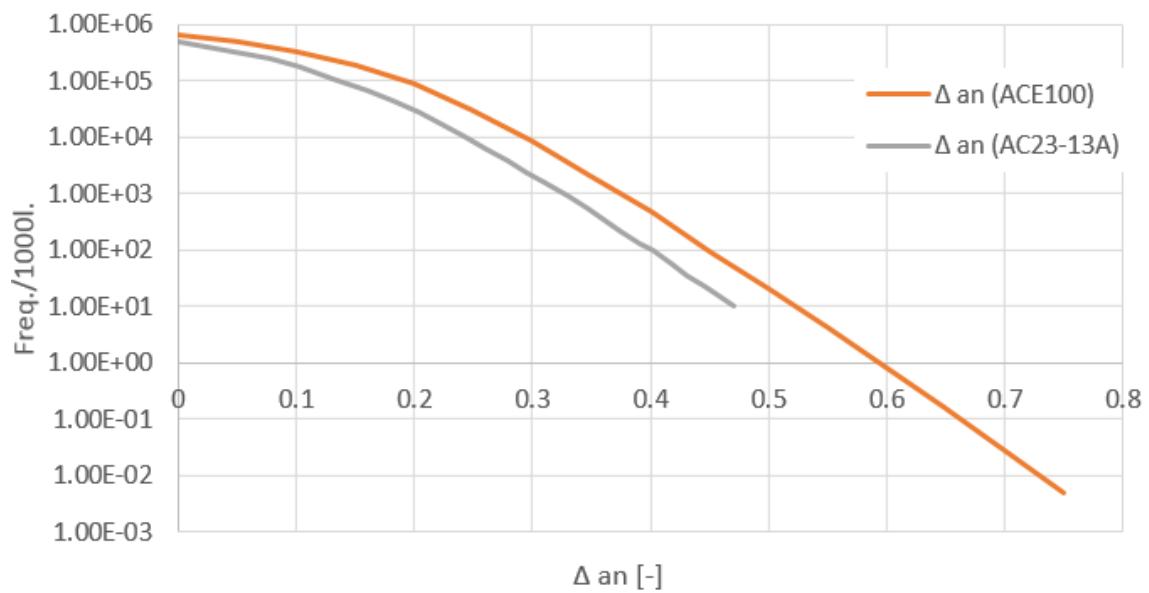


Figure 6.23: Taxi [30] and [2] comparison

Flight phases were divided according to mission profile from fig. 5.1:

- takeoff
- climb
- level flight
- descent
- landing

Phases of flight were adjusted to give weighted average equal to example case presented in tab. 6.2 according to eqn. (6.11).

$$x_{avg} = \frac{\sum_{i=1}^5 x_i \cdot t_i}{\sum_{i=1}^5 t_i} \quad (6.11)$$

Where:

i Index of phase

x_{avg} Averaged quantity (load factor, speed)

x_i Value of quantity in phase i

t_i Duration of flight phase i

Specific values of input quantities are in tab. 6.5.

Table 6.5: Flight phases tuning

Phase	Takeoff	Climb	Flight	Descend	Landing	Average
Speed(kts)	88.41	117.17	168.73	155.46	82.02	147.76
Maneuver positive n	2.50	3.84	3.85	4.03	3.59	3.80
Maneuver negative n	-1.19	-1.55	-1.55	-1.62	-1.09	-1.52
Duration(min)	2.00	7.30	19.50	8.40	2.00	0.65
Gust positive n	3.04	3.05	3.07	3.38	3.38	3.15
Gust negative n	-1.04	-1.05	-1.07	-1.38	-1.38	-1.15

Changes in calculation algorithm were connected mainly with following parts of spectra:

6.4.1 Gusts and Manoeuvres

Division into flight phases is connected with changes flight spectra (manoeuvre and gust spectra). Source spectra from [30] were only multiplied by ratio of flown distance per phase to distance flown per flight.

$$f_{per\ hour\ (phase)} = \frac{s_{phase}}{s_{flight}} \cdot f_{per\ hour} \quad (6.12)$$

Where:

$f_{per\ hour\ (phase)}$ Frequency of exceedance per hour recalculated per phase [h⁻¹]

$f_{per\ hour}$ Frequency of exceedance per hour [h⁻¹]

s_{phase} Flown distance per phase [NM]

s_{flight} Flown distance per flight [NM]

Decomposition of spectra into 5 phases can be seen in fig. 6.24 for Manoeuvres and fig. 6.25 for Gusts.

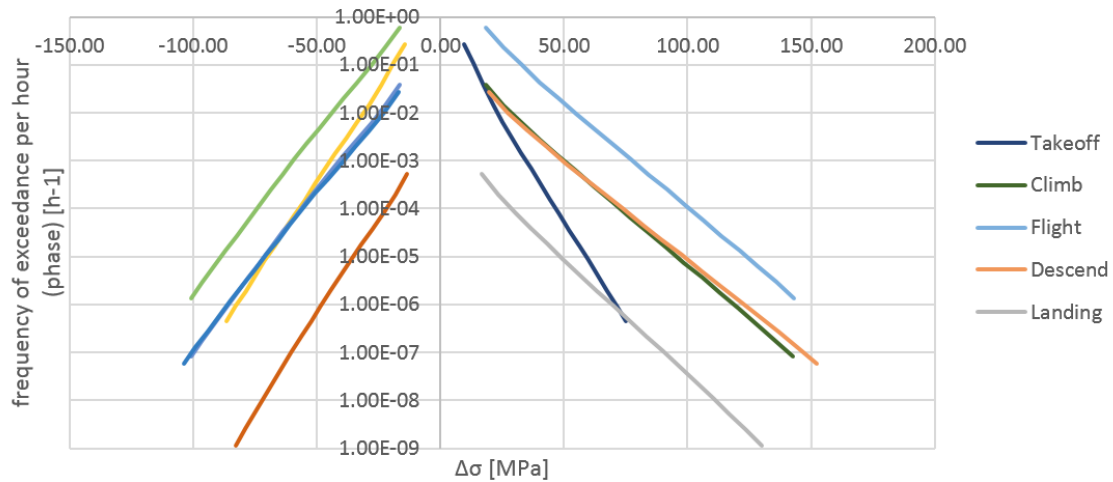


Figure 6.24: Manoeuvre spectra recalculated into 5 phases

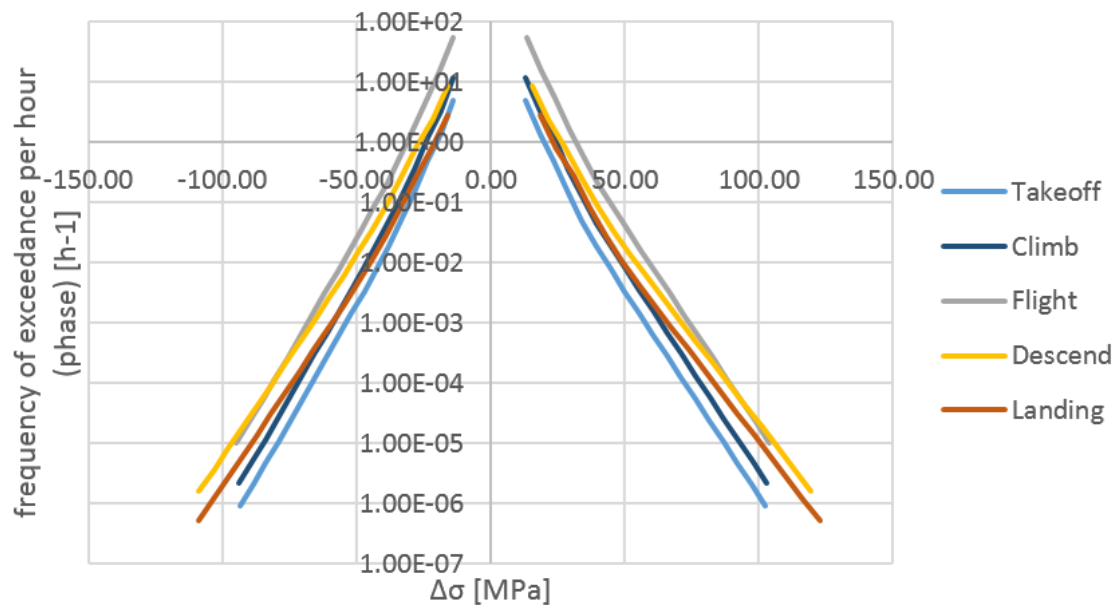


Figure 6.25: Manoeuvre spectra recalculated into 5 phases

From accordingly formatted spectra were recalculated stress according to chapter 6.3.2 and damage according to sec. 6.3.6

6.4.2 Taxi, landing impact and rebound

Taxi, landing impact and rebound calculation was performed according to chapters 6.3.3 and 6.3.4.

6.4.3 GAG cycle

For this part of calculation was used Python scripting language as more suitable tool due to complexity of data manipulation. For data manipulation purposes were used data science libraries Scipy and its core packages Numpy, Matplotlib and Pandas.

Scipy `interpolate.interp1d` function was used due to simplicity of parameter declaration for interpolation with minor modifications to work in semi-log coordinates in following code:

```
1 def log_interp1d(xx, yy, kind='linear'):
2     logx = xx
3     logy = np.log10(yy)
4     lin_interp = sc.interpolate.interp1d(logx, ...
5     ...logy, kind=kind, bounds_error=False)
6     log_interp = lambda zz: np.power(10.0, lin_interp(zz))
7     return log_interp
```

Numpy was used for general array data manipulation

Pandas was used for data streamlined extraction of data form Excel and for clear output of script

Calculation was, like in sec. 6.3.5, divided into.

- **Max. stress cycle** interpolation was performed in coordinates logarithm of frequency of exceedance and load factor due to easier data manipulation and it was feasible due to fact that both maneuver and gust spectra are related to same stress value for recalculation.

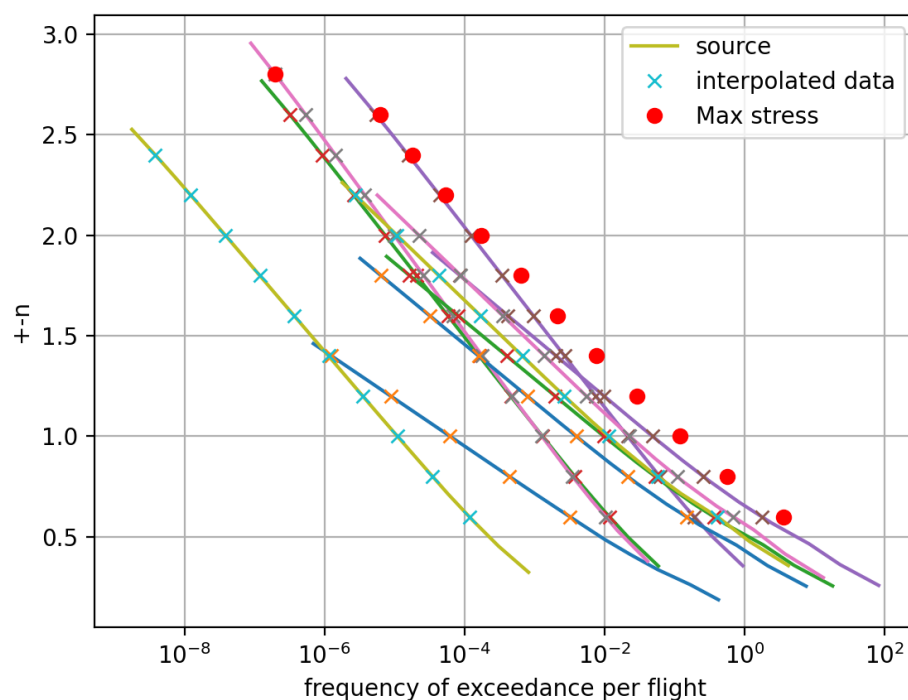


Figure 6.26: Max. stress cycle

- **Min. stress cycle** interpolation was performed in coordinates logarithm of frequency of exceedance and stress like in sec. 6.3.5

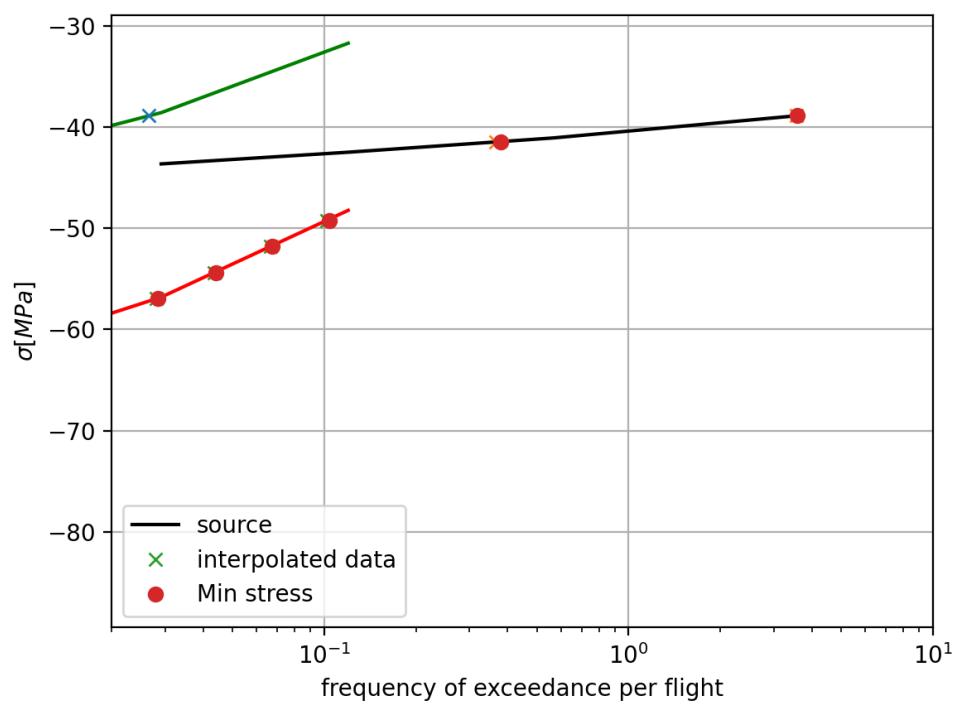


Figure 6.27: Min stress cycle

Interpolation from superposed cycle can be seen in fig. 6.28.

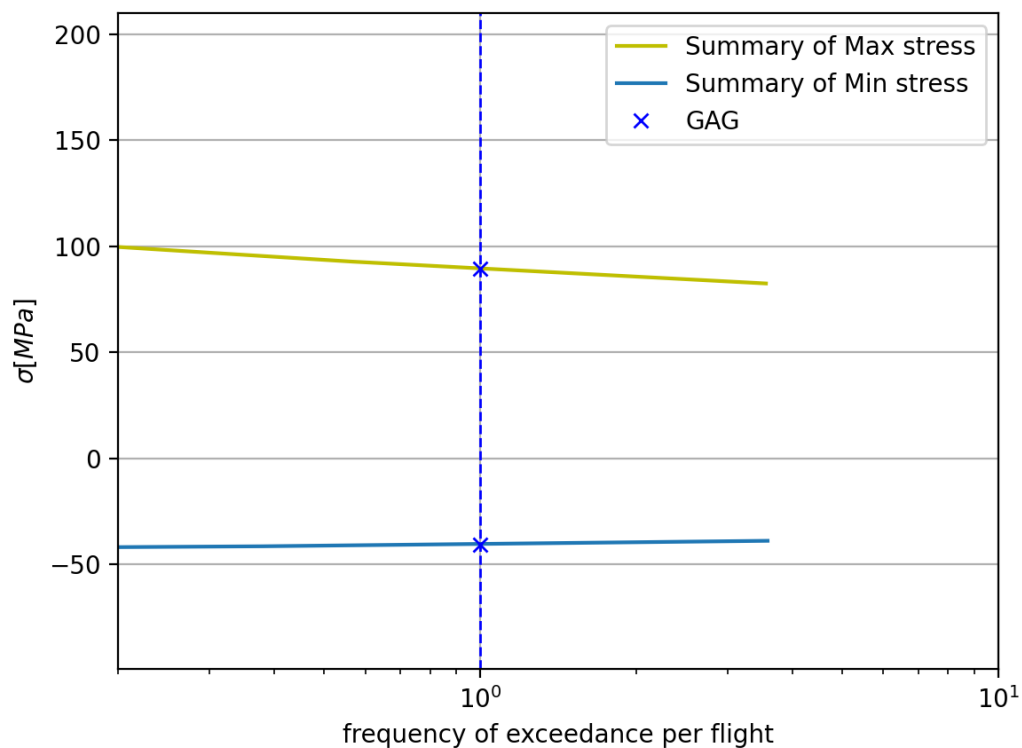


Figure 6.28: Superposed GAG cycle interpolation

Results from GAG cycle were compared with results from previous verification calculations in tab. 6.6.

Table 6.6: GAG cycle stress results with 5 phase spectra

Source	$\sigma_{\min \text{ GAG}}$ [MPa]	$\sigma_{\max \text{ GAG}}$ [MPa]
Calculation	-41	85
Calculation (5 phase spectra)	-41	89
Program	-42	84

Results regarding Min. stress cycle were, as expected, in compliance with previous results because of no change in calculation algorithm. Vice versa Max. stress cycle with 5 phases of flight has showed more conservative tendencies.

6.4.4 Damage calculation

Damage calculation algorithm was the same but results of damage calculation, mainly the percentage distribution of damage across the gives clear comparison of 3 calculation methods.

Table 6.7: Damage results 1 phase, 5 phases calculation and ACE100 comparison

	Calculation 1 phase		Calculation 5 phases		ACE 100	
	D [h^{-1}]	D [%]	D [h^{-1}]	D [%]	D [h^{-1}]	D [%]
Gust	2.22E-05	58.33	2.93E-05	59.08	2.13E-05	57.55
Maneuver	2.52E-06	6.63	1.34E-06	2.71	2.37E-06	6.40
Taxi	2.49E-10	0.00	6.52E-11	0.00	7.18E-10	0.00
Impact	5.13E-07	1.35	4.18E-07	0.84	2.36E-07	0.64
Rebound	7.74E-09	0.02	2.20E-09	0.00	2.94E-09	0.01
GAG	1.28E-05	33.67	1.85E-05	37.36	1.31E-05	35.40
Summary	3.80E-05		4.96E-05		3.70E-05	

Results from 5 phase [30] spectra tends to be more conservative. That trend in newer spectra is caused by increasing requirements on safe-life evaluated structures. Important is that the percentage of the spectra components is reasonably correlated.

Methods and approaches used in software development are therefore validated. Results of both, program and analytic calculation are in compliance with results obtained from ACE 100 program [2]. This could be seen from figures and tables above.

7 SMG-92 Safe-life estimation

Final safe-life evaluation was carried out with use of previously mentioned methods concerning 5 phases of flight. For further calculation was necessary to add some data to each phase of mission profile.

7.1 Gust load factor

First of additional data is gust load factor for each phase. Gust load factor was determined according to [30] similarly to [28] Sec. 23.341 with difference in K factor definition:

$$a_{nLFFg} = \frac{U \cdot K \cdot V \cdot a}{498 \cdot W/S} \quad (7.1)$$

where:

U Nominal gust velocity in feet per second

W/S Wing loading at max. weight, lb/ft^2

$$K = 0.5\left(\frac{W}{S}\right)^{1/4} \text{ for } W/S < 16lb/ft^2$$

$$K = 1.33 - \frac{2.67}{\left(\frac{W}{S}\right)^{3/4}} \text{ for } W/S > 16lb/ft^2$$

V speed of flight [KEAS]

a Wing lift curve slope, $C_{L\alpha}$, rad^{-1}

Difference in K factor definition is caused because spectra from [30] are normalised to gust load formula in use before Amendment 23-7 to 14 CFR Part 23. Therefore use of formula presented in [28] could compromise results. For further example calculation would be used first phase of mission profile, rest of mission profile phases will be calculated in similar manner. K is determined as for condition:

$$26.5 > 16lb/ft^2$$

$$K = 1.33 - \frac{2.67}{\left(\frac{W}{S}\right)^{3/4}} = 1.33 - \frac{2.67}{(26.5)^{3/4}} = 1.1$$

Gust load factor is calculated using eqn. (7.1)

$$a_{nLFFg} = 1 + \frac{U \cdot K \cdot V \cdot a}{498 \cdot W/S} = 1 + \frac{30 \cdot 1.1 \cdot 68 \cdot 5.8}{498 \cdot 26.5} = 1.99 \quad (7.2)$$

7.2 Mission profile completion

Paratrooper mission profile was completed with values of gust and limit load factors in each phase. Gust load factor was determined in eqn. (7.1). Limit load factors were taken from V-n diagram from sec. 5.2.2. Summary with completed values of gust and limit load factors can be seen in tab. 7.1.

Table 7.1: Mission profile summary

Phase	Takeoff	Climb	Flight (4000 m)	Descend	Landing
Speed [KEAS]	68	81	87	76	68
Height [ft]	0	6562	13123	6562	0
Distance [km]	0.50	25.00	11.02	32.00	0.40
Distance [NM]	0.27	13.50	5.95	17.28	0.22
Duration [min]	1	14	2	15	1
Fuel used [kg]	10.00	18.00	5.82	10.00	6.00
Parachutist dropped [kg]	0	0	0	720	720
Aircraft mass [kg]	2648	2620	2614	1884	1878
Part of typical flight	0.20	0.36	0.12	0.20	0.12
Gust positive n	1.99	2.19	2.28	2.46	2.31
Gust negative n	-0.50	-1.44	-1.63	-2.00	-0.58
Manoeuvre positive n	2.69	3.60	3.60	3.60	1.72
Manoeuvre negative n	-1.41	-1.44	-1.44	-1.44	-0.90

7.3 Damage calculation

With previous input values was performed damage calculation. This calculation was performed using methods demonstrated in sec. 6.3 and 6.4. Further damage calculation was performed using stress values from sec. 5.3.9.

$$\sigma_{1g} = 28 \text{ MPa}$$

$$\sigma_{min} = -5 \text{ MPa}$$

Procedure of calculation is the same as in previously mentioned chapters. Only plot of GAG cycle stress determination can be seen in fig. 7.1 for clarity of calculation. Interpolated GAG cycle stress values are in tab. 7.1.

Table 7.2: GAG cycle stress results with 5 phase spectra

$\sigma_{\min \text{ GAG}}$ [MPa]	$\sigma_{\max \text{ GAG}}$ [MPa]
-6.7	53.5

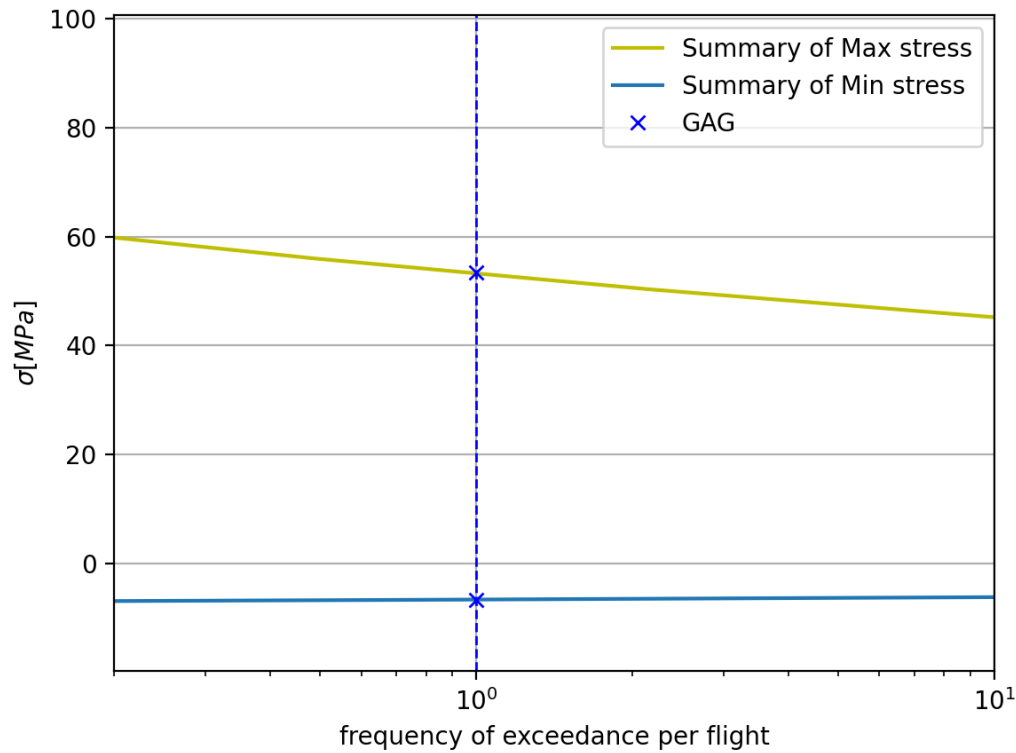


Figure 7.1: GAG cycle of Parachute dropping mission

Damage of all components of spectra was determined according to Data Sheet E.02.01 S-N curve:

Table 7.3: Damage summary according to [14]

	D[h ⁻¹]	D [%]
Gust	9.04E-06	77.13
Maneuver	2.02E-07	1.72
Taxi	4.57E-13	0.00
Impact	6.87E-09	0.06
Rebound	3.07E-10	0.00
GAG	2.47E-06	21.09
Summary	1.17E-05	

Damage of all components of flight and ground spectra was then again calculated using interpretation of S-N curve from [16] according to Oding criteria. Best suitable zone from sec. 3.3.2 is due to location close to the spar and to the bending moment maximum zone 3.

Table 7.4: Damage summary according to Oding [16] zone 3

	D [h ⁻¹]	D [%]
Gust	5.02E-05	88.00
Maneuver	1.00E-06	1.75
Taxi	7.42E-21	0.00
Impact	6.87E-09	0.01
Rebound	2.95E-10	0.00
GAG	5.84E-06	10.24
Summary	5.71E-05	

For better overview of the material data choice influence is damage calculated also using S-N curves for zone 2, which is less suitable for critical element.

Table 7.5: Damage summary according to Oding [16] zone 2

	D [h ⁻¹]	D [%]
Gust	7.76E-06	83.18
Maneuver	1.60E-07	1.72
Taxi	6.15E-22	0.00
Impact	6.87E-09	0.07
Rebound	2.45E-11	0.00
GAG	1.40E-06	15.03
Summary	9.33E-06	

Example safe-life calculation is performed only for Data Sheet E.02.01 S-N curve damage values. Safe-life calculation results are in tab. 7.3. Mean life determined by analysis is:

$$L_S = \frac{1}{D_{1h}} = \frac{1}{1.17 \cdot 10^{-5}} = 85290 \text{ h} \quad (7.3)$$

Where:

D_{1h} Summary damage caused by entire spectra

Safe-life evaluation was performed with scatter factor recommended for analysis in [30]. Safe-life was calculated using eqn. (4.3).

$$L_B = \frac{L_S}{SF} = \frac{85290}{8} = 10661 \text{ h} \quad (7.4)$$

Table 7.6: Comparison of calculated safe-life values

S-N Curve	L_S [h]	$L_B(SF = 8)$ [h]
VZLU	85290	10661
Oding (Zone 3)	4379	2190
Oding (Zone 2)	107217	13402

8 Conclusion

First part of the diploma thesis was dedicated to information about the aircraft. Next few chapters dealt with research of fatigue regulations, advisory materials and methods which came out of them. Chapters were also dedicated to commonly used concepts in the fatigue evaluation (Palmgren Miner rule, concept of nominal and local stresses etc.). There were also mentioned specific methods for fatigue evaluation in aerospace industry (Damage tolerance, Fail safe approaches).

In computational part of the diploma thesis was carried out mission profile estimation. The Mission profile had to include all particular details of parachute dropping mission profile. Then the $1g$ stress analysis was evaluated for parameters of given mission profile (weight, speed etc.). Four critical cross-sections were chosen based on criteria for dominant structure loading (bending loads). The most critical cross-section, evaluated from calculations, is located at inner end of milled strut joint flange stiffener. Analysed $1g$ and *ground* stresses from critical cross-section and mission profile parameters were used as input for fatigue analysis.

Fatigue analysis was performed according to algorithm described in [30]. This algorithm was verified according to [2]. The result of fatigue analysis is expressed in terms of safe-life as follows:

$$L_B = 10661 \text{ h}$$

Such a safe-life is expected for 0.55 hour flight duration and given mission profile. One of the other facts that came into consideration is that the S-N curve is best suitable for such areas. Resulting safe-life value gives the best compliance with advised results in tab. 8.1. Evaluated safe-life was compared with trainer safe-life from tab. 8.1. This mission profile is the most similar to analyzed one.

Table 8.1: Recommended safe-life values from [16]

Airplane type	Recomanded safe-life [h]
Commuters	15000-30000
Airliners	1500-50000
Aerotaxi	10000
Agricultural planes	5000-10000
Trainer	3000-7000
Aerobatic	2000-4000
Gliders	4000-10000

The Project will probably continue with wing full-scale test. This mission profile is one of various mission profiles which can take in account for upcoming full-scale testing. Safe-life results achieved by the testing can be simply predicted using scatter factor calculated from eqn. (4.4). All substituted values are in compliance with [30] recommendations.

$$SF_{FST} = 10^{Z_p \cdot \sigma \cdot \sqrt{\frac{n_s+1}{n_s}}} = 10^{3.511 \cdot 0.14 \cdot \sqrt{\frac{2+1}{2}}} = 4 \quad (8.1)$$

Where:

Z_p Value of the normal distribution $Z_p = 3.511$ (with 99.9777% probability) [-]

σ Value of standard deviation is $\sigma = 0.14$ (Aluminium alloys) [-]

n Number of tested parts $n = 2$ (2 wing halves) [-]

Test scatter factor is valid only assuming for number of tested parts $n = 2$ (2 wing halves) and failure occurring at the flange stiffening sheet. Calculated safe-life values are compared with analysis values (result from eqn. (7.4)) in tab. 8.2.

Table 8.2: Comparison of calculated safe-life values

S-N Curve	$L_S[\text{h}]$	$L_B(SF_{FST} = 4)[\text{h}]$	$L_B(SF = 8)[\text{h}]$
VZLU	85290	21322	10661

Calculated life can be used only for purpose of test preparation and expenses calculation. This estimation is valid only for flight duration of 0.55 hours.

References

- [1] AUGUSTIN, Petr. *Studijní podklady k předmětu Únava a životnost leteckých konstrukcí*. Brno, 2021. VUT Brno.
- [2] BOLLER, Christian a Matthias BUDERATH. *Fatigue evaluation of empennage, forward wing and winglets/tip on Part 23 airplanes: Report No. ACE-100-01*. 800 Independence Avenue, SW Washington, DC 20591 (866) TELL-FAA ((866) 835-5322): Federal Aviation Administration, 1994.
- [3] BOLLER, Christian, Matthias BUDERATH a Christian BOLLER. Fatigue in aerostructures—where structural health monitoring can contribute to a complex subject. *Philosophical transactions. Series A, Mathematical, physical, and engineering sciences* [online]. 2007, **365**(1851), 561-587 [cit. 2021-02-11]. ISSN 1364-503X. Available: doi:10.1098/rsta.2006.1924
- [4] BRUHN, E.F, R. J. H BOLLARD, Lloyd E HACKMAN, George LIANIS, William F MCCOMBS, A. F SCHMITT, Clarence R SMITH a Joseph A. WOLF. *Analysis and design of flight vehicle structures*. Carmel: Jacobs Publishing, 1973, 1 sv. (různé stránkování) : ilustrace, fotografie (černobílé).
- [5] COOK, M.V. *Flight Dynamics Principles*. London: Arnold, 1997, 379 s. ISBN 0-340-63200-3.
- [6] ELJUFOUT, Tamer, Houssam TOUTANJI a Mohammad AL-QARALLEH. Fatigue Stress-Life Model of RC Beams Based on an Accelerated Fatigue Method. *Infrastructures (Basel)* [online]. MDPI, 2019, **4**(2), 16 [cit. 2021-03-27]. Available: doi:10.3390/infrastructures4020016
- [7] IMBERT, JF a D. CAMPASSENS. *Airbus Mts005b Fatigue Manual*. 2, rond-point Emile Dewoitine, 31700 Blagnac, France: Airbus France, 1998. IMBERT, JF a D. CAMPASSENS. *Airbus Mts005b Fatigue Manual*. 2, rond-point Emile Dewoitine, 31700 Blagnac, France: Airbus France, 1998.
- [8] KAHÁNEK, Václav. *Únavová životnost letadlových konstrukcí*. Žilina: Alfa, 1977.
- [9] KRISHNAMURTHY, T. a Brian H. MASON. Equivalent Plate Analysis of Aircraft Wing with Discrete Source Damage. *47th AIAA/ASME/ASCE/AHS/ASC Structures, Structural Dynamics, and Materials Conference* [online]. 2006 [cit. 2021-02-11]. Available: <http://hdl.handle.net/2060/20060017065>
- [10] LOUMAN, Petr. *Porovnání provozních, technických a ekonomických parametrů letounů pro výsadkovou činnost*. Vysoké učení technické v Brně. Fakulta strojního inženýrství, 2010.
- [11] MCGINTY, Bob. Stress Concentrations at Holes. *Fracture Mechanics* [online]. 2021 [cit. 2021-02-11]. Available: <https://www.fracturemechanics.org/hole.html>
- [12] MILITKY, J. a S. IBRAHIM. Effect of textile processing on fatigue. *Fatigue failure of textile fibres* [online]. 2009, , pages 133-168 [cit. 2021-02-11]. Available: <https://www.sciencedirect.com/science/article/pii/B9781845693275500075>

- [13] MOURITZ, Adrian P, Fabio PEGORIN, Mohd Dali ISA a Khomkrit PINGKARAWAT. Fatigue Properties of Aerospace Z-Pinned Composites. In: *Applied Mechanics and Materials* [online]. s. 67-75 [cit. 2021-02-11]. Available: doi:10.4028/www.scientific.net/AMM.828.67
- [14] NEJEDLÝ, Vojtěch. *Analytické vyjádření vlivu napětí pro únavové křivky konstrukce křídel a VOP letounů*. Výzkumný a zkušební letecký ústav, **1976**(R-1705/76), pages 1-7.
- [15] NIU, Michael Chun-Yung. *Airframe structural design*. 2nd ed. Hong Kong: Hong Kong Conmilit Press, 2004, 612 s. ISBN 962-7128-09-0.
- [16] PÍŠTĚK, Antonín, Oldřich GRÉGR a Václav KAHÁNEK. *Pevnost a životnost letadel*. Brno: VUT Brno, 1988, 266 s.
- [17] REDDICK, J. a K. HAROLD. *Safe-life and damage-tolerant design approaches for helicopter structures*. Washington, D.C.: NASA-CP-2278, 1983.
- [18] REYER, Michael. Probability basis of safe-life evaluations in small airplanes. *9th Joint FAA/DoD/NASA Aging Aircraft Conference* [online]. 2009, , 2-4 [cit. 2021-5-12]. Available: <https://www.slideshare.net/Yo/Creo/probability-basis-of-safe-life-evaluation-in-small-airplanes-by-w-michael-reyer>
- [19] ROLFE, Stanley Theodore. Fracture and Fatigue Control in Structures: Applications of Fracture Mechanics. *Mechanical Engineering* [online]. New York: American Society of Mechanical Engineers, 2000, **122**(5), 83 [cit. 2021-5-20]. ISSN 00256501. Available: <http://search.proquest.com/docview/230155371/>
- [20] RŮŽIČKA, Milan a Jiří FIDRANSKÝ. *Pevnost a životnost letadel*. Praha: ČVUT, 2000.
- [21] SHIGLEY, Joseph E. *Standard handbook of machine design*. 3rd ed. New York: McGraw-Hill, 2004, Přer. str. ISBN 0-07-144164-6.
- [22] SCHIJVE, Jaap. *Fatigue of structures and materials*. 2nd ed. S.l.: Springer, 2009, xxi, 621 s. : il. ISBN 978-1-4020-6807-2.
- [23] VLK, Miloš. *Dynamická pevnost a životnost*. 2. vyd. Brno: VUT Brno, 1992, 223 s. ISBN 80-214-0427-2.
- [24] ZHARKOVA, Victoria. *Studie využitelnosti letounu SM-92TE Praga Alfa*. Praha, 2019. Diplomová. ČVUT.
- [25] WÄCHTER, Michael, Christian MÜLLER a Alfons ESDERTS. *Die FKM Richlinie*. VDMA-Verlag.
- [26] Fatigue limit diagram according to Haigh and Smith. *Tec-Science* [online]. tec-science, 2021 [cit. 2021-02-11]. Available: <https://www.tec-science.com/material-science/material-testing/fatigue-limit-diagram-according-to-haigh-and-smith-creation/>
- [27] *CS-23 Normal, Utility, Aerobatic and Commuter Aeroplanes*. Köln am Rhein: European Aviation Safety Agency, 2015.

- [28] *Federal aviation regulation Part 23 Amendment 23-46, Airworthiness Standards: Normal, Utility, Acrobatic, and Commuter Category Airplanes*. 800 Independence Avenue, SW Washington, DC 20591 (866) TELL-FAA ((866) 835-5322): Federal Aviation Administration, 2021.
- [29] SM-92 New Coin fr Russia. *Lantangq4683* [online]. [cit. 2021-02-17]. Available: <https://lantangq4683.blogspot.com/2012/09/sm-92-new-coin-fr-russia.html>
- [30] Advisory Circular (AC) 23-13A, Fatigue, Fail-Safe, and Damage Tolerance Evaluation of Metallic Structure for Normal, Utility, Acrobatic, and Commuter Category Airplanes. *The Federal Register / FIND* [online]. Washington: Federal Information and News Dispatch, 2006, **71**(011), 2981 [cit. 2021-02-11]. ISSN 00976326. Available: <http://search.proquest.com/docview/190238797/>
- [31] Advisory Circular (AC) 23-19A, Airframe Guide for Certification of Part 23 Airplanes. *The Federal Register / FIND* [online]. Washington: Federal Information and News Dispatch, 2006, **71**(011), 2981 [cit. 2021-02-11]. ISSN 00976326. Available: https://www.faa.gov/documentLibrary/media/Advisory_Circular/AC_23-19A.pdf
- [32] EFatigue. <https://www.efatigue.com> [online]. Altair Engineering, Inc.: Nasdaq as ALTR, 2021 [cit. 2021-02-11]. Available: <https://www.efatigue.com/variable/stressconcentration/a>
- [33] Letoun SM-92TE Praga Alfa. *ORBIS AVIA s.r.o.* [online]. Hradec Králové, 2021 [cit. 2021-02-22]. Available: <http://www.orbisavia.cz/sm-92te-praga>
- [34] Technoavia SMG92 Turbo Finist. *The blueprints* [online]. 2021 [cit. 2021-02-22]. Available: https://www.the-blueprints.com/blueprints/modernplanes/modern-t/74193/view/technoavia_smg92_turbo_finist/
- [35] *Airplane flight manual SMG-92 Turbine Finist, reg. HA-YDM, S/N 02-003*. 3rd. Budapest: HgCAA, 2009.
- [36] *New Cessna SE turboprop* [online]. EuroGA Servers Limited, 2016 [cit. 2021-03-01]. Available: <https://www.euroga.org/forums/new-cessna-se-turboprop/6168?page=3>
- [37] EUROPEAN AVIATION SAFETY AGENCY. *Part-21, airworthiness and environmental certification: consolidated version of Part-21 and related Acceptable means of compliance and Guidance material (AMC and GM to Part-21)*. Luxembourg: Publications Office, 2013. ISBN 9789292101480. Available: doi:10.2822/41823

9 List of shortcuts and symbols

<i>EAS</i>	Equivalent Air Speed
<i>EASA</i>	European Union Aviation Safety Agency
<i>FAR</i>	Federal Aviation Regulation
<i>FEM</i>	Finite Element Method
<i>KTAS(KEAS)</i>	knots TAS (EAS)
<i>GAG</i>	Ground Air Ground
<i>HiLo</i>	High Low (sequence of stress cycles)
<i>MTOW</i>	Maximal takeoff weight
<i>MINTOW</i>	Minimal takeoff weight
<i>Min</i>	Minimum
<i>Max</i>	Maximum
<i>R.A.E.</i>	Royal Aircraft Establishment
<i>TAS</i>	True Air Speed
<i>TC</i>	Type Certificate
<i>TCDS</i>	Type Certificate Data Sheet
<i>ZFW</i>	Zero Fuel Weight
<i>Safe-life</i>	Approach or part lifetime to retirement (L_B)

List of Figures

1.1	Military version of SM-92 with radial engine [29]	14
1.2	SM-92T in cargo version[33]	15
1.3	Para version of SMG-92 in operation [36]	16
1.4	3 view drawing of SMG-92 Turbine Finist [34]	17
2.1	Example of ACE100 calculation output	20
3.1	Shape of stress cycle[1]	21
3.2	Cycles sorted according to fatigue ration	22
3.3	Steel S-N curve in semi-log coordinates [12]	23
3.4	Comparison between aluminum alloys and steel S-N curve in cartesian coordinates[1]	23
3.5	Haigh diagram [26]	25
3.6	Example curve material for $D16 T_C$ [16]	26
3.7	Transformation $\sigma_{a,0} \rightarrow \sigma_a$ [1]	27
3.8	Previously mentioned criteria in negative mean stress values[1]	27
3.9	Regular zone	28
3.10	Free holes concentration	28
3.11	Skin connections	28
3.12	Non-regular zone with reinforcement	29
3.13	Influence of shot peening on part made out of 30CHGSNA steel (Curves represent: 1. polishing+shot peening, 2. machining finishing pass, 3. polishing, 4.machining finishing pass)[8]	29
3.14	Influence of anodizing on endurance limit. (Curves represent: 1. machining and polishing 2. 10%NaOH anodisation, 3. $H_2SO_4 + HF$ anodisation, 4. $H_2SO_4 + NaF$ anodisation, 5. $H_3PO_4 + HF$ anodisation,6. 20%NaOH anodisation)[8]	30
3.15	Difference of notch concentration[15]	31
3.16	Influence of notch radius on stress concentration[15]	31
3.17	Nonlinearites included in cumulative damage summation [1]	32
3.18	HiLo and LoHi stress sequence influence [22]	33
3.19	Plastic stresses at the root of the notch [22]	33
3.20	Example load case [32]	34
3.21	Nominal stress distribution (Where: σ_{nom} Nominal stress, F Loading force, W Bar width, D Hole diameter, t Bar thickness)[11]	35
3.22	Edge fiber stress vs CG stress	35
3.23	Net-section of rectangular bar with hole (σ cross-section stress, F loading force, W bar width, D hole diameter) [11]	36
3.24	Gross-section of rectangular bar with hole[11]	36
3.25	Real stress distribution ($3 \cdot \sigma_\infty$ maximal stress, σ_∞ remote stress, r hole radius) [11]	37
3.26	Real vs nominal stress distribution (σ_{max} max (local) stress, σ_{nom} nominal stress, F loading force, W bar width, d hole diameter) [23]	38
4.1	Fatigue design strategy [3]	41
4.2	Comparison between safe-life and Fail safe concept (curve A represents Damage tolerant approach and curve B represents Safe-life approach) [16]	42
4.3	Guide to the choice of fatigue life approach [30]	42

4.4	Fatigue testing methods [19]	43
4.5	Division into specific load cases [1]	44
4.6	Typical shape of maneuver spectra (Single-Engine Executive Usage category according to [30])	45
4.7	Gust spectra (for Single-Engine and Twin-Engine Pressurized Usage categories according to [30])	46
4.8	Taxi spectra (curves are for 1. All Single-Engine and Twin-Engine Operations, Excluding Aerial Application, 2. Agricultural Usage Aerial Application categories according to [30])	47
4.9	Landing impact spectra (curves for 1. Single-Engine Basic Flight Instructional usage, 2. Single-Engine Unpressurized Operations, Including Personal, Executive and Aerobatic Usage, 3. Twin-Engine Unpressurized Usage, Single-Engine and Twin-Engine Pressurized Usage) [30]	48
4.10	GAG cycle visualisation (Where: σ'_{1g} Ground stress level, σ_{1g} 1g load case stress, $\sigma_{max,GAG}$ Maximal stress level of GAG cycle, $\sigma_{min,GAG}$ Minimal stress level of GAG cycle) [16]	49
4.11	Influence of landing gear configuration [16]	49
5.1	Mission profile visualisation [16]	50
5.2	Important characteristics of Parachutist dropping mission profile	52
5.3	V-n diagram for m_{MTOW}	56
5.4	V-n diagram for m_{MINTOW}	57
5.5	V-n diagram for m_{ZFW}	57
5.6	Coordinate system used for calculation [16]	58
5.7	Moment and force equilibrium diagram [16]	59
5.8	Lift distribution from Glauert III	61
5.9	Wing loading	62
5.10	Freebody diagram of wing equipped with simple strut	63
5.11	Final shear force and bending moment distribution	63
5.12	Ground load	64
5.13	Bending moment and shear force results for ground loading	64
5.14	Critical cross-section selection	65
5.15	Critical correction bending moment and shear force determination	65
5.16	Wing spar strut connection location	66
5.17	Cross-section elements numbering	67
5.18	Critical cross-section 2	68
5.19	Critical cross-section 3	69
5.20	Critical cross-section 4	70
5.21	Critical cross-section detail on spot inspection	71
5.22	Strut joint inspection	71
6.1	SN curve in semi-log scale [30]	73
6.2	SN curve in semi-log scale from [16]	74
6.3	Comparison of interpolation methods	75
6.4	Graphical description of spectra processing	76
6.5	Comparison of gust spectra after interpolation	76
6.6	Comparison of manoeuvre spectra after interpolation	77
6.7	Gust load factor spectra benchmark	77
6.8	Manoeuvre spectra benchmark	78
6.9	Gust spectra benchmark with recalculated stress and frequency per flight	79

6.10	Manoeuvre spectra benchmark with recalculated stress and frequency per flight	79
6.11	Comparison of taxi inputs	80
6.12	Taxi spectra benchmark with recalculated stress and frequency per flight .	80
6.13	Impact and rebound spectra input comparison	81
6.14	Comparison after sink rate recalculation	81
6.15	Impact and rebound spectra comparison after stress recalculation	82
6.16	Superposition and summation of max stress cycle	83
6.17	Superposition and summation of min stress cycle	83
6.18	Superposed GAG cycle interpolation	84
6.19	Visualisation of Palmgren Miner rule [6]	85
6.20	Manoeuvre [30] and [2] comparison	86
6.21	Gust [30] and [2] comparison	86
6.22	Impact and Rebound [30] and [2] comparison	87
6.23	Taxi [30] and [2] comparison	87
6.24	Manoeuvre spectra recalculated into 5 phases	89
6.25	Manoeuvre spectra recalculated into 5 phases	89
6.26	Max. stress cycle	90
6.27	Min stress cycle	91
6.28	Superposed GAG cycle interpolation	91
7.1	GAG cycle of Parachute dropping mission	95

List of Tables

1.1	Technical data [24]	17
4.1	Summary of scatter factors for aluminium structures[30] (different applica- tions)	40
5.1	Parameters of mission profile [30]	50
5.2	Parameters of mission profile	51
5.3	Mission profile summary	52
5.4	Aircraft mass configurations	52
5.5	Stall speeds at different mass configurations	53
5.6	Wing loading of representative configurations	55
5.7	Parachutist dropping input mass values	58
5.8	Upper section stress analysis	67
5.9	Lower section stress results	68
5.10	Stresses summary of all critical cross-sections	70
6.1	Excerpt form flight spectra choice guide [30]	72
6.2	ACE100 sample input values from [2]	74
6.3	GAG cycle stress results	84
6.4	Calculation result summary [2]	85
6.5	Flight phases tuning	88
6.6	GAG cycle stress results with 5 phase specra	92
6.7	Damage results 1 phase, 5 phases calculation and ACE100 comparison . . .	92
7.1	Mission profile summary	94
7.2	GAG cycle stress results with 5 phase spectra	94
7.3	Damage summary according to [14]	95
7.4	Damage summary according to Oding [16] zone 3	96
7.5	Damage summary according to Oding [16] zone 2	96
7.6	Comparison of calculated safe-life values	96
8.1	Recommended safe-life values from [16]	97
8.2	Comparison of calculated safe-life values	98